UNIVERSITÀ
DEGLI STUDI
FIRENZE

DOTTORATO DI RICERCA IN SCIENZE CHIMICHE

CICLO XXXI

COORDINATORE Prof. Piero Baglioni

Nanocomposites for the consolidation of stone: novel formulations and a kinetic study

Settore Scientifico Disciplinare CHIM/12

Dottorando
Dott. Camerini Rachel

_____
(firma)

Tutore
Prof. Giorgi Rodorico

_____
(firma)

Coordinatore
Prof. Baglioni Piero

_____
(firma)

Anni 2015/2018

General background and aims

Stone artifacts constitute a wide and rich portion of the world cultural heritage, as the use of stone materials for arts and constructions dates back since ancient times. Furthermore, the variety of materials and features gives place to a manifold panorama, that includes both natural masonry and artificial objects, made of materials like mud, clay, sand, gravel, and cement. Natural aging and a series of environmental and anthropogenic factors, to which outdoor monuments and buildings are continuously exposed, contribute to the heterogeneous forms of degradation affecting the stone patrimony. On the long term, such physical and chemical alterations result in the progressive weakening of the mechanical properties of the substrate, that manifest as detachments, powdering of the surfaces and even crumbling. Of course, the importance of preserving such patrimony for future generations is undeniable. Therefore, a thorough knowledge and an aware compromise between standardized protocols and specific approaches are required to operate properly and ensure the most suitable conservative strategies. As a matter of fact, there are several cases of past conservative interventions that turned out to be ineffective or even harmful for the treated work of art, inducing conservators and restorers to deal with their removal and correction. The issue is controversial and largely debated, with many efforts of the scientific community aiming at covering a multi-variable scenario of cases and contexts (intrinsic properties of the stone, dimensions, state and mechanisms of degradation, conservative methods and application protocols, curing conditions, economic aspects).

The present research focuses on the *consolidation* of stone materials, meaning to apply a product that homogeneously penetrates within the porosities and restores

or improve the substrate cohesion, without affecting its physical, chemical and aesthetical properties. Particularly, two main topics have been here studied and discussed, in the perspective of widening the knowledge and improving the tools to practically intervene in the complex field of consolidation of stone materials.

The first topic addressed the *consolidation of earth*, a substrate that characterized the architecture of many areas of the world since ancient times, and that is still largely in use. Earthen masonry includes a series of techniques that share the employment of unbaked earth, whose many qualities and potential effectiveness are though compromised by its susceptibility to erosive degradation, leading to the progressive loss of surface grains cohesion. Unfortunately, such materials have a scarce background of understandings and expertise, and the choose of the best conservative approach may result challenging. Among earthen materials, 'adobe' represents one of the most common techniques worldwide spread, and consists of sun-dried mud bricks, often stabilized with organic fibers and lime. Here, a promising strategy was developed and tested on adobe, to overcome the drawbacks of traditional consolidating products: a hybrid system based on nanotechnology was formulated using nanosilica, nanolime and a cellulose derivative, to obtain a fully compatible and effective consolidating product for restoring the surface cohesion of a powdery and poorly aggregated material of great archaeological and modern interest.

Secondly, a compared study on the carbonation kinetics of *nanolimes* was conducted. As well as the knowledge of the substrate properties is crucial, understanding the behavior of a consolidating product after application is fundamental to fulfil consolidation. Nanolimes are colloidal dispersions of $Ca(OH)_2$ nanoparticles, that have recently emerged as effective and compatible materials for many conservative operations, and represent a valid alternative to the traditional products for consolidation purposes (organic polymers, alkoxysilanes, inorganic products as lime water), not only for carbonate-based

stone. Despite their diffused adoption, their reaction mechanism is not fully understood yet and little consensus has been reached in the literature. In this work, four different commercial nanolimes were considered for a compared carbonation kinetic study, by means of FTIR and accelerated carbonation under controlled T and RH conditions.

The introduction section of the present dissertation is an overall presentation of the current strategies for the consolidation of stone. The advantages and possible drawbacks of the three main groups of traditional stone consolidants (organic polymers, inorganic materials, and siliceous compounds) are presented, and the new perspectives provided by the recent advancements in colloids and materials science (nanotechnologies and composite materials) are described.
In the two chapters of the fundamentals section, the two research topics addressed in the present research are shown in detail: a knowledge background of the specific issues and the adopted strategies of intervention and investigation are presented.
The chapters of the experimental section describe the used materials and analytical methods and procedures, followed by the discussion of the obtained results concerning the consolidation of earthen masonry using hybrid nanocomposites and the study of the carbonation kinetics of commercial nanolimes for stone consolidation.

PART I

Introduction

Chapter 1 – Consolidation of stone materials

1.1. Introduction

Stone has been largely used as artistic and building material during the centuries, and the stone patrimony includes both natural materials (made of various lithotypes) and artificial materials, obtained from the transformation of the formers (e.g. stucco, mortar, plasters, ceramic products, cement). Since their implementation, lithic materials continuously undergo physical erosion, chemical corrosion and bio-pollution processes, as well as anthropic detrimental interventions, which inevitably alter their original form. Among the variety of degradation causes and mechanisms, one of the most concerning consequences is the loss of the substrate granular cohesion, that progressively affects the exposed layers, leading to the weakening of the mechanical properties and endangering the artifact's integrity. Therefore, many efforts are being done by the scientific community to develop satisfying consolidating strategies. Consolidation, one of the main restoration operations, aims at recovering the conservative status of the degraded object (together with cleaning, protection, gluing, reconstruction etc.), and it consists of applying a product onto the surface which is able to penetrate within the substrate porosities and restore the grains cohesion up to the inner layers. Consolidants are usually applied to the surface of the stone by brush, spray or direct contact. They should be compatible and, hence, durable interventions to prevent, slow down or recover stone materials from degradation.

The aim of this chapter is to introduce the current strategies for the consolidation of stone artefacts, up to the latest technologies, shedding light on their advantages and possible drawbacks.
In this framework, the two research topics of the present dissertation are placed: the development and application of a hybrid nano-composite to address the consolidation of a poorly aggregated earthen material, adobe, and a study on the carbonation kinetics of nanolimes, dispersions on $Ca(OH)_2$ nanoparticles which are commonly used for consolidation purposes.

1.2. Consolidation of stone materials: a brief review

Conservation methods unceasingly evolved over time, thanks to the progress of scientific research and according to specific necessities and happenings. A crucial year was 1966, when the damages caused by the floods of Florence and Venice forced to face the restoration of a considerable number of artworks, promptly. In such situation, the need of deepening the knowledge and techniques for correct conservative interventions was highlighted, and the remarkable research progress defined the birth of modern Conservation Science. In the field of stone consolidation, chemists and material scientists focused on the development of *compatible* materials for *durable* treatments, to address the great diversity of substrates (e.g. chemical composition, porosity and internal structure etc.). Despite carbonate- and silicate-based materials represent the two main categories of stone artefacts for which consolidating methods have being studied and developed, the analysis of the artwork materials is considered a fundamental preliminary step for choosing the most suitable treatment, as universal consolidants do not exist.

In the next paragraphs the principal methods developed and used for stone materials consolidation will be presented, from traditional approaches to nanotechnologies, from organic and inorganic materials to hybrid compounds.

1.2.1. Traditional products

From a general point of view, traditional stone consolidants belong to three main groups, according to their chemistry: organic polymers, inorganic materials, and siliceous compounds.

Organic compounds

Organic compounds are among the first materials used as stone consolidants since the second half of the 20th century, and they are still widely used in conservative practices. They primarily consist of synthetic polymers, such as acrylate, vinyl, silicone, and epoxy polymers, in the form of solutions or dispersions. After the solvent evaporation, continuous films or 3D networks forms within the porous structure, settling the incoherent grains and producing consolidation. Such materials immediately became appealing and competitive on the market thanks to their good consolidating power, high adhesive and elastic properties, water repellency, saturation of colors, easy application and low cost. However, it is now known that these compounds lack physico–chemical compatibility with inorganic porous matrices, producing severe damages on stone artifacts (e.g. yellowing, brittleness, detachments) in a time shorter than 50 years (Giorgi et al. 2010b; Baglioni et al. 2015). Particularly, past treatments with synthetic organic polymers turned out to produce drastic changes in the water capillarity, water vapor permeability, and surface wettability of the substrate. Salt crystallization phenomena, and the consequent reduction of the mechanical properties, are caused by the alteration of the natural breathing of the surface.

Besides, the polymers themselves can undergo degradation, resulting in irreversible and unstable applications. Cross-linking reactions and chain scissions cause molecular weight changes of the polymer, leading to undesired chromatic variations and loss of solubility (Favaro et al. 2006; Giorgi et al. 2010b).

Natural organic compounds have also been used as consolidants, as well as coatings or additives. They include resins, oils and other materials belonging to local traditions, which are easily available and not expensive. An example is given by nopal mucilage (resin suspended in cactus juice), which is widely used in Latin America (Vazquez-negrete et al. 2008; Rodriguez-Navarro et al. 2017). However, a common drawback of natural consolidants is represented by their rapid aging and susceptibility to biodegradation, leading to the need of frequent retreatments.

Inorganic compounds

In 1969, while organic polymers were spreading, the 'Ferroni-Dini method' was developed as a pioneering methodology within the renewed approach arising from recent flood events (Giorgi et al. 2010b; Baglioni et al. 2013; Chelazzi et al. 2013). The method was designed by the physical-chemist Ferroni, after the damaging of the Florence frescoes, as a compatible treatment for wall paintings affected by significant sulfate pollution. It consists of a two-step procedure where aqueous solutions of two different chemicals loaded in cellulose pulp which is applied onto the degraded surface: ammonium carbonate is used to extract gypsum (a typical product of calcium carbonate degradation) by turning it into soluble ammonium sulfate, mainly removed by absorption in the poultices, and then barium hydroxide is used to fix the residual soluble sulfates into insoluble barium sulfate, hence preventing salt migration. Furthermore, the excess of barium hydroxide generates calcium hydroxide in situ, via an exchange reaction

with the powdery calcium carbonate formed in the first step, and gives barium carbonate via reaction with atmospheric CO_2. Calcium hydroxide aqueous solution (lime water) is not used as a direct consolidating compound, given its scarce solubility in water in respect of barium hydroxide. However, the newly formed lime can react with atmospheric CO_2 to obtain a crystalline network of calcium carbonate that consolidates the weakened powdering matrix by renewal of the natural binder. The conservator Dino Dini restored the Beato Angelico wall paintings in Florence using for the first time the described method, in an exemplary interdisciplinary cooperation.

The physico-chemical compatibility between the inorganic barium hydroxide and the mineral matrix made the method a valid alternative to organic treatments, and it has been in fact successfully applied worldwide. Besides, the method served as a precursor for the development of the more recent nanotechnologies, which will be discussed in the next paragraph.

In general, affinity with stone materials and resistance to aging make inorganic compounds interesting materials. They act not only as fillers, but react with H_2O or CO_2 to form new compounds in the porous matrix, which are chemically bound to the substrate.

Among the inorganic compounds, calcium hydroxide is the most eligible for many conservation practices, as it converts into calcium carbonate by reaction with atmospheric CO_2 in presence of water (carbonation process). $CaCO_3$ is the main constituent of mortars and many stone materials, and it is also compatible with cellulosic artistic substrates like paper, wood and canvas. However, the use of both aqueous solutions and dispersions of $Ca(OH)_2$ is not advisable. Because of the low solubility of calcium hydroxide (1.7 g/L at 20°C), saturated aqueous solutions do not guarantee effective consolidation, and the use of considerable amounts of product would introduce high quantities of water in the porous substrate, leading to undesired effects. $Ca(OH)_2$ aqueous dispersions are not

kinetically stable, which results in sedimentation phenomena that cause poor penetration and surface veils. Therefore, the use of nonaqueous media, *i.e.* alcohols, as particles dispersing agents immediately resulted preferable (Chelazzi et al. 2013; Baglioni et al. 2014). The ideal agents in terms of compatibility are alkaline-earth metal hydroxides (calcium, barium and strontium hydroxides), as they react with carbon dioxide to form insoluble carbonates. Nevertheless, when the consolidant size is reduced to nanoscale, better efficacy and penetration of the treatment can be achieved, as described below.

Siliceous compounds

If calcium carbonate shows high compatibility with carbonate-based stone, as well as mortars and wall paintings, siliceous materials are largely applied on silicate-based stones. In general, siliceous compounds represent an important class of consolidants, and can be of both organic and inorganic origin, so they are often discussed separately.

Silica is an inert and stable compound. Degradation of siliceous stone is provoked by the dissolution of the mineral grain binder, hence in situ silica precipitation within the stone pores can regenerate both protection and consolidation.

Alkaline silicates, particularly water solutions of potassium, sodium or ammonium silicates, have been used for stone consolidation, as when exposed to air they precipitate silica inside the porous stone matrix. However, their hydrolysis also leads to the formation of the correspondent hydroxides, with the consequent production of soluble salts, causing mechanical stress and further degradation. The poor penetration ability also limits their use (Wihr and Steenken 1970; Sleater 1973).

The most commonly used compounds are alkoxysilanes: they have been studied for stone preservation since the first decades of the twentieth century, but their greater diffusion took place starting from the 80s, and, not long after, their use

also on carbonate-based stones became frequent. The main reasons of their popularity are linked to their abilities to form siloxane (Si-O-Si) bonds and polymerize to produce materials that mimic the binder of siliceous stone, their low viscosity and easy penetration. They also have lower impact on stone permeability in respect of organic polymers and the siloxane bond is stable and resistant to aging (Clifton 1982; Wheeler 2005; Pinto and Rodrigues 2008). Alkoxysilanes are esters of silicic acid, *i.e.* silanes (SiH_4), where the hydrogens are substituted by alkoxy groups (-OR, where R generally indicates alkyl groups such as methyl, CH_3, or ethyl, CH_3CH_2). Particularly, only four compounds have been regularly used for stone consolidation, as they are tri- or tetra-functional and can form a 3D network, have the correct balance of volatility and reactivity, and are harmful to people and stone: tetraethoxysilane or TEOS, $Si(OCH_2CH_3)_4$; methyltriethoxysilane or MTEOS, $CH_3Si(OCH_2CH_3)_3$; trimethoxysilane or TMOS, $Si(OCH_3)_4$; and methyltrimethoxysilane or MTMOS, $CH_3Si(OCH_3)_3$. These oligomers are applied in solution, with possible addition of catalysts, and, once absorbed by the stone, undergo the sol-gel process: water hydrolyzes the alkoxy groups with the release of alcohols; then the newly formed silanols condensate forming a dispersion of polymer chains (sol); once the solvent evaporates, the chains approach and further condensate, forming a continuous and porous 3D network which still retains the liquid phase (gel) of amorphous silica. Aging involves structural reorganization of the network, variation of the pore diameter and stiffening for further cross-linking. During the last drying phase, residual liquid is removed, and a partial densification occurs.

The sol-gel reactions are shown below (Figure 1.1):

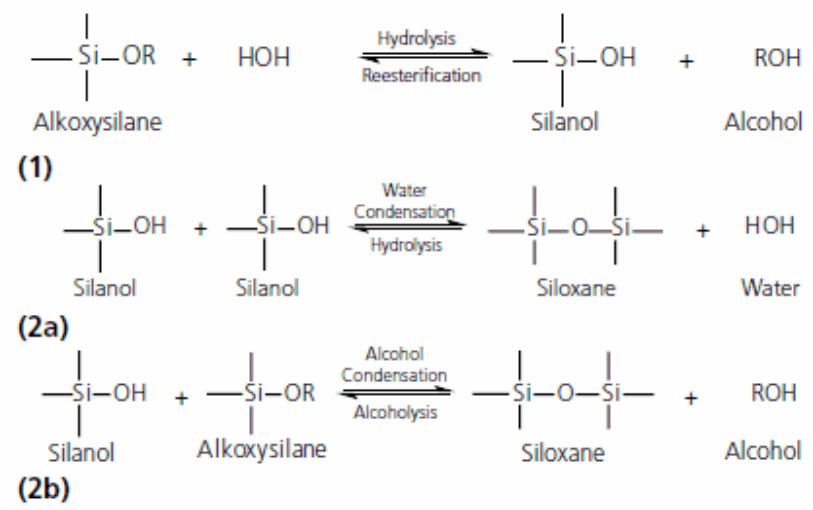

Figure 1.1 - Sol-gel reactions

Alkoxysilanes are hence advantageous due to their penetration properties, chemical, thermal, and light stability owed to their siloxane backbones, and absence of harmful by-products, as water and alcohol are volatile products that evaporate without leaving residues. The formation of silica as a final product makes these products more suitable for silicate-based stones, since the consolidating effect is due to the formation of chemical bonds (condensation) with the substrate hydroxyl groups. If applied on carbonate-based materials they form weaker electrostatic bonds, leading to a simple filling effect rather than a true consolidation. A known drawback of these material is the tendency to form a brittle xerogel that cracks inside the stone, due to the high capillary pressure supported by the gel network during drying, depending on the gel structure and pore size (dense micro-pored gels, typically obtained from TEOS, are known to be susceptible to cracking) (Sakka et al. 2005; Mosquera et al. 2009).

1.2.2. Nanotechnologies

Nanotechnologies have responded to the need of turning attention towards new materials and techniques in many application fields, including Conservation Science: if soft nanomaterials (microemulsions and gels) have been developed for safe surface cleaning operations, hard nanomaterials have been studied to provide alternative consolidants to polymers and inorganic bulk materials.

A colloid is a mixture in which a substance is found in a finely dispersed state, intermediate between the solution and the suspension. This micro-heterogeneous state consists of one dispersed phase of microscopic dimensions (1nm - 1μm diameter) and one continuous dispersing agent. In 2011, the European Commission adopted the following definition of a nanomaterial: "A natural, incidental or manufactured material containing particles, in an unbound state or as an aggregate or as an agglomerate and for 50% or more of the particles in the number size distribution, one or more external dimensions is in the size range 1 nm – 100 nm".

Nanomaterials can be obtained via two main synthetic pathways: break-down and bottom-up methods. In break-down methods, the desired particle size is obtained by grinding or thermal decomposition; in bottom-up methods, the particles are obtained by aggregation of atoms or ions until the desired size, via deposition and growth of crystals starting from liquid or vapor phase or via sintering in the solid state and reaction between nanoparticles (Baglioni and Giorgi 2006).

Nanotechnologies for stone consolidation include both inorganic (mainly dispersions of alkaline-earth hydroxide nanoparticles) and hybrid nanomaterials (*i.e.* organic-inorganic formulations).

1.2.2.1. Inorganic nanomaterials

Many synthetic pathways have been developed in the last 20 years for the preparation of calcium, magnesium, strontium, and barium hydroxide nanoparticles dispersed in short-chain alcohols for different conservation practices, mainly consolidation and deacidification, tailoring the particles' size and shape to obtain enhanced reactivity and higher penetration into the substrate. Here, a general overview of the main synthetic procedures and applications for the consolidation of both wall paintings and lithoid substrates is described, with focus on calcium hydroxide, as it represents one of the most used compounds, and has a central role in the present research.

At the beginning of the 1990s, the Center for Colloid and Surface Science (CSGI, "Consorzio Interuniversitario per lo Sviluppo dei Sistemi a Grande Interfase") was established in Florence and started its research on Colloids and Material Science, focusing on compatible inorganic consolidants, particularly micro- and nano-particles.

Non-aqueous dispersions of calcium hydroxide were initially developed for the consolidation of thin carbonate-based substrates, such as wall paintings, as an improvement of the second step of the Ferroni method. In this way, after desulfation (first step), calcium hydroxide is directly re-introduced into the carbonatic matrix, instead of being obtained from precursors.

As mentioned, the use of non-aqueous methods is preferable, as aqueous solutions lead to particles stacking through hydrogen bonds, favored by adsorbed water molecules (Chelazzi et al. 2018). Instead, the use of low-toxic solvents such as short-chain alcohols and solid submicron-sized particles allows to obtain stable and highly concentrated dispersions, without the need of adding stabilizers, that could leave residues on the porous matrix. In fact, the mentioned hydroxides are not soluble in organic solvents, but if the particle size is very small, stable

dispersions can be obtained, avoiding particle aggregation and subsequent sedimentation and poor penetration.

The first stable lime/alcohol formulation was applied on wall paintings by dispersing slaked lime particles with an average size of 3–4 μm in 1-propanol by vigorous stirring, with a three times higher concentration of calcium hydroxide in respect of limewater (Giorgi et al. 2000a).

Afterwards, the attention was focused on obtaining alcoholic dispersions of nano-sized $Ca(OH)_2$ particles, instead of micron-sized, to enhance the formulation stability, penetration within the porous matrix, and reactivity. Several preparation methods have been developed, taking into account the average particle size, but also the particle size distribution, particle surface area, crystallinity and presence of defects, dispersing agent, as they influence the consolidation process.

Ethanol and propanol are the most commonly employed short-chain alcohols, as they are environmentally friendly and have suitable viscosity and surface tension values to allow a proper application, without hindering particle penetration due to excessively high volatility, or, on the contrary, slowing the consolidation process by protract their permanence in the substrate. Besides allowing for a homogeneous and complete impregnation of the substrate, they also absorb on the particle surface (physisorption), favoring the production of smaller particles 'by slowing down growth on the surface relative to nucleation of separate particles' (Fratini et al. 2007). The adsorption of the hydroxyl group (–OH) of the alcohol molecules to the hydroxide particles surface also inhibits their face-to face sticking (Figure 1.2) and permit to obtain kinetically stable dispersions (Salvadori and Dei 2001).

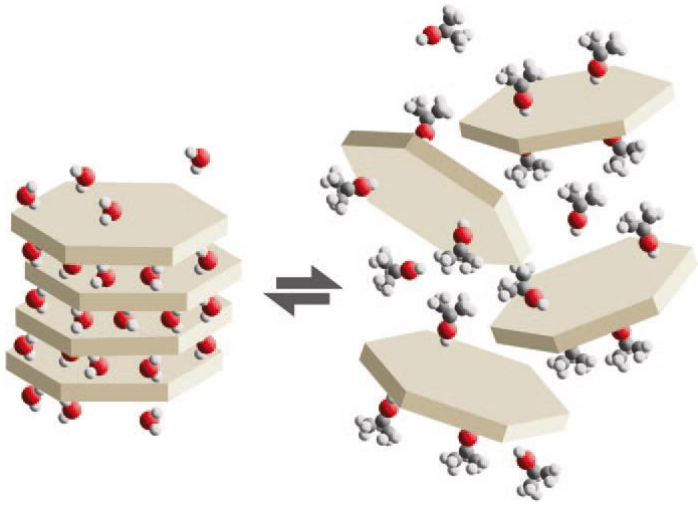

Figure 1.2 - Aggregation of calcium hydroxide nanoparticles in water through bridging driven by hydrogen bonds (left); dispersion stabilization in 2-propanol (right)

It was reported that the stability increases proportionally with the thickness of the hydrophobic layer on the hydroxide particles (that adsorbs alcohol molecules), giving the following order of stability enhancement: 1-propanol > ethanol > 2-propanol (Ambrosi et al. 2001a).

The same authors reported one of the first methods designed for frescoes restoration, *i.e.* a bottom-up synthesis where calcium hydroxide nanoparticles are obtained from aqueous homogeneous phase, by rapidly mixing sodium hydroxide and calcium chloride at 90°C. The product is purified, to remove the by-product NaCl, and dispersed in 1-propanol in an ultrasonic bath. The particles obtained are nanocrystalline hexagonal platelets of $Ca(OH)_2$, namely portlandite, with particle size smaller than 600 nm (Ambrosi et al. 2001b).

The nano-dimensions allow better penetration and kinetic stability in respect of micron-sized calcium hydroxide. The reactivity resulted enhanced by the capacity of portlandite of absorbing water, favoring carbonation. The formulation

was successfully tested both on mortar mock-ups with flaking surface and real historical calcareous stone (Ambrosi et al. 2001a).

Following the described procedure, calcium hydroxide nanoparticles were also synthesized by Daniele et al., and applied for the preservation of stone artworks (Daniele et al. 2008; Daniele and Taglieri 2010), also introducing some modifications (Daniele and Taglieri 2012). Particularly, a non-ionic surfactant, Triton X-100, was used to prevent the aggregation of primary $Ca(OH)_2$ nanoparticles and favor the formation of more reactive $Ca(OH)_2$ nano-crystals. The NaOH drop-wise addition is avoided, but purification is required.

Dispersions of $Ca(OH)_2$ nanoparticles were initially designed to consolidate *fresco* paintings, exploiting the recreation of a $CaCO_3$ crystalline network that provides cohesion and improved mechanical strength to the substrate layers, fixing pulverulent substrates and embedding flaking grains and pigments. However, their use has been extended to *secco* paintings and stone, especially if carbonate-based. In this last case, more factors need to be considered to achieve a homogeneous and satisfactory penetration of the particles, such as substrate pore size distribution, particle size distribution, dispersing agent and curing conditions, especially if targeting mass consolidation (Borsoi et al. 2016).

To further reduce the particle size, a synthesis in diols was then developed for consolidation operations (Salvadori and Dei 2001), as the use of organic solvents allow to reach higher temperatures and hence produce smaller particles. The particles were recovered and dispersed in 2-propanol in an ultrasonic bath, to remove the adsorbed diols. By tuning the reaction parameters, spherical particles of 30-60 nm or hexagonal platelets ranging from 50 to 150 nm can be obtained. The formulation was used for the consolidation of biocalcarenite, calcareous sandstone and limestone (Croveri et al. 2004; Baglioni et al. 2006; Dei and Salvadori 2006).

$Ca(OH)_2$ nanoparticles were then obtained via a water-in-oil (w/o) microemulsions synthesis (Nanni and Dei 2003), by mixing for prolonged time two emulsions containing, respectively, Ca^{2+} and OH^- ions in the dispersed water droplets. The particle obtained have a very small size (2-10 nm), owing to the formation within the nano-sized water droplets dispersed in a nonionic surfactant serving as template, namely cyclohexane (oil phase). The need of selecting the suitable microemulsion composition and the too high reactivity of the obtained particles limit their use for wall painting consolidation purposes. Besides, the described homogeneous phase procedures have low production yields and are time consuming, as the particle purification step is needed, even if they allow to achieve monodispersity and to control the particle size and shape better than heterogeneous phase pathways.

However, these researches allowed to acquire basic notions and background for further developments, like the commercial product Nanorestore®, available on the market since 2008 (produced at CSGI and distributed by CTS Srl (Italy)), and successfully tested in numerous real case studies, comprising mural paintings in harsh environmental conditions, such as Mesoamerican regions, where T and RH conditions fasten the degradation (Baglioni and Giorgi 2006; Giorgi et al. 2010a; Baglioni et al. 2014). Nanorestore® is a dispersion of thin hexagonal portlandite platelets of 300-500 nm (Figure 1.3) in 2-propanol, with a concentration of 5 g/L. It is a simple break-down method, consisting in the fragmentation of slaked lime and subsequent dispersion in alcohol, specifically designed for the consolidation of wall paintings, that produces consistent quantities of particles, avoiding the purification step, with slightly larger size than ones obtained in homogeneous phase. It is possible to obtain also a minor population of about 1 μm, by varying the reaction parameters, which can be useful for substrates with high and varied porosity.

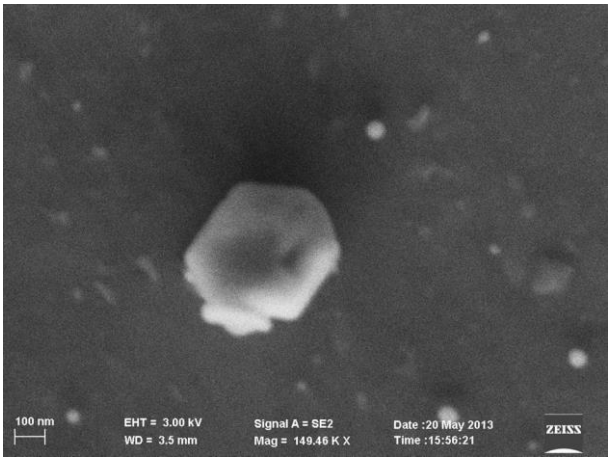

Figure 1.3 - FEG-SEM image of $Ca(OH)_2$ nanoparticles (Nanorestore®)

Nanorestore® was also studied as consolidant for dolostone samples from the Madrid area, which are typically used in historical buildings (López-Arce et al. 2010).

Lime slaking (or hydration) is a typical route for calcium hydroxide production, consisting of a series of heterogeneous phase reactions (the so-called "lime cycle"), involving calcination of carbonate stones at temperatures above 850–900°C, via solid-state reaction, and the hydration of the resulting calcium oxide (or quicklime, CaO) via a highly exothermic process (lime slaking), leading to the formation of portlandite ($Ca(OH)_2$). If a stoichiometric amount of water (or slightly higher) is added to quicklime, dry hydrated lime is produced, which is the standard industrial product; if a higher amount of water is added, an aqueous dispersion of $Ca(OH)_2$ particles, known as lime putty, is obtained, which is the typical binder of lime-based mortars and plaster since ancient times (Rodriguez-Navarro and Ruiz-Agudo 2018). Lime slaking generally produces portlandite particles with bi-modal size distribution, one population consisting of hexagonal primary platelets, with size up to a few hundreds of nanometers, and one population consisting of larger aggregates of micrometric size. This might be

useful for treatments of substrates with high and varied porosity, but their use is limited in many applications. In general, lime slaking allows for high yield of nanoparticles with high surface area, with reduced cost, but monodispersity is hardly achievable. One method for reducing particle size and control crystal shape is the aging of slaked lime putties, by long-term storage under water (also practiced by the Romans to obtain more workable pastes), which allow the production of more stable and effective nanolimes for consolidation.

When calcium oxide on the surface turns into hydroxide during lime slaking, the temperature rapidly increases, and some CaO residues remain within the hydroxide particles core and does not react easily with water due to the passivated surface layer of hydroxide (Chelazzi et al. 2013). The complete hydration of the oxide nucleus can be forced by thermo-mechanical treatments; given the reaction speed and the volume increase, the particle size is reduced by fragmentation.

Other routes commonly adopted for the formulation of $Ca(OH)_2$ nanoparticles' dispersions include sol-gel solvothermal processes (Ziegenbalg 2005; Poggi et al. 2014, 2016), where the alcohol (ethanol or propanol) oxidizes metallic calcium to the corresponding alkoxide, and the subsequent addition of water induces the formation of calcium hydroxide via a hydrolysis reaction. Highly crystalline colloidal calcium hydroxide already dispersed in a suitable solvent for the application is obtained, with portlandite particles of ca. 100-200 nm and thickness of ca. 20–30 nm (Figure 1.4).

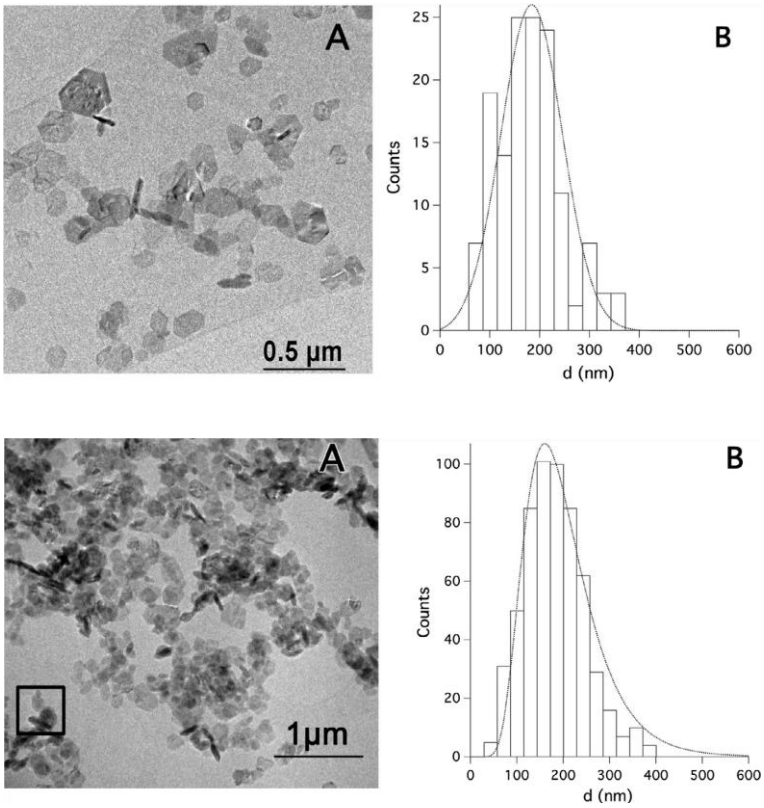

Figure 1.4 - $Ca(OH)_2$ nanoparticles obtained via ethoxide route (top) and 1-propoxide route (bottom): TEM image (8k nominal magnification), and size distribution obtained from TEM images analysis (B)

CaLoSil® is another commonly used product in cultural heritage conservation, commercialized since 2010 by IBZ-Salzchemie GmbH & Co. KG (Germany). It is synthesized via an alkoxide route, directly from alcohol solution, and the obtained particles have dimensions of 50–250 nm. The dispersing agents are ethanol, 1-propanol and 2-propanol, with a concentration range of 5–25 g/L.
CaLoSil® was studied used for stone consolidation with positive results, and more effective consolidation was achieved using the ethanol dispersion in respect of the 2-propanol dispersion (Ziegenbalg 2008; D'Armada and Hirst 2012).

Alternatively, calcium alkoxides in alcohol solution were proposed to impregnate porous substrates, where they can react with atmospheric CO_2 in presence of H_2O (atmospheric or purposely added), to form nanostructured calcium hydroxide in situ (Ziegenbalg 2005; Favaro et al. 2008; De Zorzi et al. 2009). The carbonation process depends on curing conditions and alkoxides particle size, and consolidating efficacy is related to the alkoxides solubility and stability in solution. The low solubility of alkoxides does not allow for concentrated formulations, hence multi-step treatments are needed.

As mentioned, the chemical composition of the substrate should be mirrored by the product applied for its consolidation, to fulfill compatibility criteria. However, good results were obtained also with $Ca(OH)_2$ formulations on siliceous substrates. Particularly, Nanorestore® and carbide lime putty were applied and formed calcite or vaterite, that bind quartz grains, resulting effective for the consolidation of sandstone, with the use of ethanol as dispersing agent producing better consolidation in respect of 2-propanol (Rodriguez-Navarro et al. 2013). This was described as not unexpected by the authors, as calcium carbonate is a common cement for sandstone or quartz sand, and it is also produced by bacterial biomineralization. Moreover, alkaline formulations of calcium hydroxide can react with silica present in the substrate, in the presence of water (e.g. moisture in the pores), and form amorphous or poorly crystalline (gel-like) calcium silicate phases, producing chemical continuity between the carbonate and silicate phases (Armelao et al. 2000). The interaction between silica and lime will be furtherly discussed below.

Colloidal silica is another interesting material for the consolidation of stone, and it was recently explored for its physico-chemical compatibility to silicate-based stones.

Grimaldi et al. evaluated the performances of colloidal silica-based plasters and protective surface coatings over one year of exposure, in the Archaeological Site

of Tajín, Mexico, proving their better durability and compatibility with the sandstone substrate in respect to previously applied plasters, made of synthetic polymers or lime (Grimaldi et al. 2012). Zornoza-Indart and Lopez-Arce studied the influence of relative humidity on the consolidating effectiveness of SiO_2 nanoparticles applied on historical siliceous-carbonate stone. Starting from colloidal nanosilica precursor, they obtained a product acting like a silica gel, upon exposure to lower and higher RH, owing to reversible adsorption and desorption of water. As a consolidant, the product increased the surface hardness and drilling resistance of the stone. (Zornoza-Indart and Lopez-Arce 2016).
Nanosilica was also applied on carbonate-based materials. Calia et al. studied the performance of silica nanoparticles applied on porous substrate like calcarenite, assessing the quantity applied and application method (Angela Calia, Maurizio Masieri, Giovanni Baldi 2012). Falchi et al. investigated the application of nanosilica aqueous dispersions on carbonate rocks, specifically Lecce Stone, in terms of penetration depth, particle dimensions, stone pore radius distribution, and physico-chemical characteristics (Falchi et al. 2013). They reported the necessity of ethanol pre-treatments of the stone, to reduce surface tension and obtain deeper penetration of the particles, which otherwise form a xerogel on the stone surface.

1.2.2.2. Composite nanomaterials

Composite materials are multiphase materials consisting of components with different physical or chemical properties, separated by an interface. Specifically, hybrids materials result from the combination of at least two components, generally organic-inorganic, at a nanoscale or molecular level; therefore, the new material can exhibit improved or even new properties.

Advancements in colloids and materials science have provided candidate materials to improve compatibility and versatility of the products available on the market and optimize existing technologies.

For instance, organic-inorganic nanomaterials are being studied to tackle the challenge of developing crack-free silica materials for application as consolidants, and overcome the practical drawback of traditional products, as mentioned in the previous section. Particularly, silica nanoparticles were added in traditional consolidants like TEOS to obtain a colloid-polymer hybrid that forms mesoporous gels, and hence reduce the capillary forces that develop during drying (Mosquera et al. 2003). Similarly, new TEOS-based consolidants containing flexible (3-glycidoxypropyl) trimethoxysilane and silica nanoparticles of different sizes were synthesized and compared with commercial products, showing good consolidating properties and a crack-free behavior (Kim et al. 2009).

Miliani et al. synthesized particle-modified silica consolidants filled with titania, alumina, and silica particles, obtaining improved properties with respect to unfilled ethyl silicate, comprising reduced risk of cracking and protection of sandstone from salt crystallization damage. In addition, changing the filling particle, the properties of the final composite can be controlled, e.g. color can be tailored to match the stone aspect by choosing a specific starting sol (Miliani et al. 2007).

Alternatively, Mosquera et al. developed a sol - gel process to obtain a silica gel with more coarse and uniform pores, using a neutral surfactant in low concentration, to reduce the capillary pressure during drying (Mosquera et al. 2008). The new surfactant-synthesized nano-consolidant was applied on granite stone and showed no cracking and best results compared with commercial consolidants (an ethyl silicate and an acrylic polymer) (Mosquera et al. 2009).

The same research group also reported the synthesis of an organically modified silicate (ormosil), by the co-condensation of TEOS and hydroxyl-terminated polydimethylsiloxane in the presence of a surfactant, obtaining an organic-inorganic, hydrophobic and crack-free nanomaterial for stone restoration (Mosquera et al. 2010).

Another interesting interaction is the one between silica and calcium hydroxide, yielding CSH phases, which has been widely studied in the past. Greenberg studied the heterogeneous reaction between silica and calcium hydroxide solutions in the temperature range 30 - 85°C, investigating the influence on the reaction rates of temperature, calcium hydroxide concentration, amount and type of silica, and silica surface area. It was concluded that the rate controlling step is the available surface of silica (Greenberg 1961). Mitchell et. al studied the interaction between silica fume and calcium hydroxide (and with cement), leading to the formation of CSH phases via pozzolanic reaction, *i.e.* the reaction of finely dispersed siliceous/aluminous materials with calcium hydroxide in the presence of water, to form compounds with cementitious properties (Mitchell et al. 1998). Baltakys et al. investigated the interaction of $Ca(OH)_2$ with amorphous SiO_2 and crystalline SiO_2 (quartz), and found that, in the $Ca(OH)_2$–amorphous SiO_2–H_2O system, the surface of SiO_2 globules was totally covered with well-crystalline CSH plates, while, in the samples with quartz, only the gaps between quartz crystals were filled with CSH (Baltakys et al. 2007). Lin et al. reported that $Ca(OH)_2$-activated nano-SiO_2 cements show shorter setting times and lower heat liberations than pure C_3S cement using deionized water as the liquid phase (Lin et al. 2010).

The effectiveness of the process could be enhanced when both components are in the form of nanoparticles. In fact, the possibility of preparing dispersions of nanoparticles in different solvents (besides water, short chain alcohols and water-alcohol blends), allows to avoid sedimentation and aggregation of the particles,

and the detrimental effects caused by excessive wetting of the stone with water (freeze-thaw cycles, transport of soluble salts, growth of microorganisms (Baglioni et al. 2013). Moreover, particles with high surface area have higher reactivity, as opposed to bulk materials, in the formation of CSH phases.

Recently, Daniele et al. investigated the interaction of silica fume with $Ca(OH)_2$ aqueous suspensions stabilized by a non-ionic surfactant (Triton X-100) (Daniele et al. 2013), reporting on the formation of CSH phases. However, it is to be noted that the use of purely aqueous systems involves the aforementioned drawbacks in practical applications on stone, and the use of surfactants as stabilizers is discouraged, as the long-term behavior of these additives on the stone substrate has not yet been investigated.

PART II

Fundamentals

Chapter 2 – Consolidation of earthen masonry

2.1. Introduction

Siliceous stone materials represent a wide and important class of global artistic and architectural heritage. These materials share a silicate-based matrix, but have extremely diversified compositions and structures, including both natural lithoids (from granite to sandstone), and artificial materials like ceramic products and cement. Among the latters, earthen masonry (*i.e.* building materials obtained with an unfired mixture of soil and water) has been used since ancient times because of its cheapness and availability, simple manufacturing process, good thermal and acoustic properties and eco-friendliness, and it is now spreading in many industrialized countries (sustainable architecture). Currently, over half of the world's population lives in unbaked earth houses, as estimated by the United States Department of Energy (Avrami et al. 2008). The earthen architectural heritage includes immovable patrimony ranging from archaeological sites to modern buildings. However, the typical outdoors location of these artifacts makes them continuously exposed to various physico-chemical alteration phenomena, leading to the need of developing conservation interventions specifically addressed to the type of substrate and degradation, granting compatibility and long-term effectiveness.

2.2. Definitions: adobe

Adobe is one of the most popular earthen masonry techniques, of great archaeological and architectural interest (Brown and Clifton 1978; Adorni et al.

2013; Caporale et al. 2014). The term adobe generally indicates sun-dried bricks, but also includes adobe mortar and cast adobe (Figure 2.1).

Figure 2.1 - Typical peruvian adobe house (top left); the largest adobe city on earth: Chan Chan, Peru (top right); Fort Union National Monument, Mora County, New Mexico, USA

Adobe bricks are obtained handmade by mixing earth and water to a plastic consistency, shaping it in molds, and letting the water evaporate by sun drying. Recipes and mineralogical composition of soils are various, according to local traditions and availability. Cohesive soils (clay and silt) represent the binding fraction, responsible of the mechanical strength of the material. Particularly, the active phase is represented by the clay fraction, mainly consisting of alumino-silica, carbonates, sulfates, oxides. Granular soils (sand and gravel) represent the inert fraction and play an important role in controlling the mixture workability and shrinkage. Figure 2.2 shows the granulometric distributions of soil particles.

Soil group	Particle size fractions (symbol)	Range of particle sizes mm
Very coarse soil	Large boulder (lBo)	>630
	Boulder (Bo)	>200 to ≤630
	Cobble (Co)	>63 to ≤200
Coarse soil	Gravel (Gr)	>2,0 to ≤63
	Coarse gravel (cGr)	>20 to ≤63
	Medium gravel (mGr)	>6,3 to ≤20
	Fine gravel (fGr)	>2,0 to ≤6,3
	Sand (Sa)	>0,063 to ≤2,0
	Coarse sand (cSa)	>0,63 to ≤2,0
	Medium sand (mSa)	>0,20 to ≤0,63
	Fine sand (fSa)	>0,063 to ≤0,20
Fine soil	Silt (Si)	>0,002 to ≤0,063
	Coarse silt (cSi)	>0,02 to ≤0,063
	Medium silt (mSi)	>0,006 3 to ≤0,02
	Fine silt (fSi)	>0,002 to ≤0,006 3
	Clay (Cl)	≤0,002

Figure 2.2 - Particle size fractions (ISO 14688-1:2017(E))

In order to avoid cracking during drying and optimize the bricks' strength, the mixture can be adjusted by re-proportioning the soil fractions, or by adding stabilizers (Figure 2.3), especially natural organic fibers (straw, dry grass) (Galán-Marín et al. 2010; Quagliarini and Lenci 2010) or artificial products, often including lime in small percentages (Guerrero Baca 2007; Maskell et al. 2014).

Figure 2.3 - Adobe bricks manufacturing (left);
soil with fibers from an adobe brick (right)

2.3. Earthen masonry consolidation

A major issue regards the degradation processes of adobe, which is particularly susceptible to wind and water erosion (Clifton 1977; Brown et al. 1979; Illampas et al. 2013). Reportedly, adobe bricks are porous substrates with pore size of micrometric scale, up to a few mm, and porosity values of 20-40% (Brown et al. 1979; Hamiane et al. 2016). The prolonged circulation of water in the adobe pores induces washouts, freeze-thaw cycles, and swelling-shrinkage cycles of the clay fraction, leading to the progressive reduction of cohesion of the grains, the loss of mechanical properties, and eventually crumbling (Figures 2.4 and 2.5).

Figure 2.4 - Wind and water erosion: Santa Cruz Papalutla, Oaxaca (left); Nuestra Señora del Pilar and Santiago de Cocóspera Temple, Mexico (right)

Figure 2.5 - An adobe brick from the Morelos state (Mexico): crumbling and loss of grains by touch

Figure 2.6 schematizes three of the main processes by which water affects adobe structures: action of rain water on the top of walls, resulting in the formation of cracks; slow erosion of the vertical surfaces, and spalling at the wall base due to the accumulation of water containing salts.

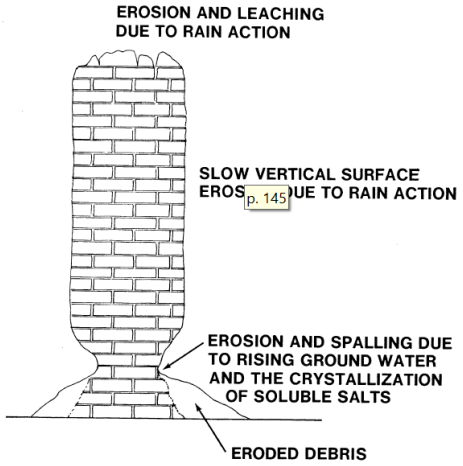

Figure 2.6 - Major effects of moisture on adobe walls

The preservation of earthen masonry is a relevant and widely discussed topic in cultural heritage conservation, as testified by the number of international

conferences carried out with the aim of promoting research and improving interdisciplinary knowledge (2000, 2008). A deep understanding of the various building types, components proportion and composition is required, and many strategies have been proposed so far for renewing the cohesion of adobe artefacts. It is to be noted that a complete penetration of the consolidating product along the whole depth of a stone substrate is a hardly achievable in many cases, especially if dealing with thick substrates, limiting the possibilities of fulfilling a real structural/mass consolidation. However, general pathologies tend to manifest at the top of the adobe wall, where erosion occurs if adequate protection lacks, and at the bottom, if water penetrates from the ground, carrying damp and salts (Clifton 1977; Doat and CRATerre 1983). Under this point of view, maximizing the consolidation treatment penetration and protecting the surface layers from further weathering is a fundamental goal.

2.3.1. Traditional conservation methods

Inorganic consolidants for earthen masonry restoration mainly include alkaline silicates (sodium and potassium), owing to their availability, easiness of application and ability to reproduce the inorganic matrix. However, a careful control of molar ratios and application is necessary to obtain good results (Warren 1999). Organic resins and oils have also been used, starting from the 1980s. Different materials belonging to local traditions have been applied as consolidants, surface coatings, or additives to new earthen materials, thanks to their availability, relatively low cost and potential effectiveness. The nopal mucilage (resin suspended in cactus juice) is commonly used in Meso-american regions (Figure 2.7), frequent treatments are needed due to its rapid aging (Martínez-Camacho et al. 2008; Kita 2013).

Figure 2.7 - Restoration with nopal mucilage: Nuestra Señora del Pilar and Santiago de Cocóspera temple, Mexico

Other traditional consolidants are synthetic products, including alkoxysilanes, acrylic resins, vinyl polymers, epoxy resins and polyurethanes, but they often produce little and superficial hardening (Avrami et al. 2008), or significant changes in the substrate properties (Figure 2.8).

Figure 2.8 - Impregnation with synthetic polymers: Adobe cannot breathe and 'explodes'. Santa María el Tule, Oaxaca

The use of alkoxysilanes on earthen materials, particularly TEOS and TMOS, dates back to the 1960s, mainly due to their proven effectiveness on a wide range of silicate-based substrates, and the ability of providing water repellency. However, they have poor consolidating power on grains larger than sand and hardly produce high weather-resistance on soils. They have also been studied in combination with acrylic polymer and alkaline silicates. Similar consolidating effect is obtained with diisocyanates, but their use is limited to specific clay mineralogies and methods of application. Polyvinyl alcohol and polyacrylamide, as well as acrylic resins like Primal AC-33 and Rhoplex E-330 are more commonly used as admixtures for new materials rather than in situ consolidants. Acrylic resins like Paraloid B-72 and Paraloid B-67 have been used, but their application is limited to dilute solutions, in order to obtain sufficient penetration, and limit properties changes in the substrate.

2.3.2. Innovative strategies: composite nanomaterials

Currently, valid alternatives to traditional products for adobe consolidation are still lacking, but advancements in colloids and materials science could provide candidate materials to fill this gap. For instance, sols have been obtained using silica oligomers and surfactants, and applied to stone consolidation (De Rosario et al. 2015), and aqueous solutions of colloidal silica nanoparticles have been investigated as consolidants, inquiring the effect of relative humidity on the treatment of siliceous-carbonate stone (Zornoza-Indart and Lopez-Arce 2016). Besides, nanoparticles of $Ca(OH)_2$ have been successfully used for the consolidation of wall paintings, plaster and stone (not only carbonate); and several approaches have been proposed in the last decades concerning the production of stable dispersions in short chain alcohols up to high concentrations (Chelazzi et al. 2013; Rodriguez-Navarro et al. 2013; Lanzón et al. 2017;

Rodriguez-Navarro and Ruiz-Agudo 2018). As mentioned above, lime has been used as a stabilizer since ancient times, and evidence of the cementing phases can be found in antique samples (Lanzón et al. 2017).

In the present research work, we aimed at obtaining the consolidation of adobe by exploiting the chemistry of cement, namely the *in situ* formation of calcium silicate hydrate (CSH), responsible for the cement hardening. As mentioned in Chapter 1, the interaction of silica with calcium hydroxide, yielding CSH phases, has been widely studied in the past, and preliminary studies on the combination of both silica and lime in the form of nanoparticles have also been conducted. Moreover, the alkaline activation of bulk silica with aqueous solutions of hydroxides was considered for the restoration of adobe, by reducing the swelling capacity of clays by turning them into non-expandable binding materials, such as calcium silicate hydrate, using alkaline activators like $Ca(OH)_2$ (Oti et al. 2009; Elert et al. 2015). In fact, nanosilica is a pozzolanic material, a broad class of siliceous materials which, in themselves, possess little or no cementitious value but which will, in finely divided form and in the presence of water, react chemically with calcium hydroxide at ordinary temperature to form compounds possessing cementitious properties.

In this perspective, hybrid nano-composites were here proposed for surface consolidation treatments of adobe, whose complexity lies in its composite nature. The combination of three components such as nanosilica, nanolime and a cellulose derivative (namely, hydroxypropyl cellulose, *Klucel*®-*G*) was exploited to obtain a formulation that could show high compatibility both with the earth matrix and additives, and allow consolidation of a powdery and poorly aggregated substrate by the *in situ* formation of a cementing phase like CSH. Silica and $Ca(OH)_2$, two major components of the cement chemistry, are in the form of nanoparticles to burst their reactivity. Moreover, cellulose ethers (CEs) constitute an important class of organic polymers used in cement formulations.

They are used in the cement industry as anti-washout or water-proofing admixtures, for adhesive mortars production, as a viscosity-modifiers, and to control the workability of cement (e.g. drying time). In the present case, *Klucel* performs three main actions: i) acts as a viscosity-modifier; ii) cellulose based materials are typically used in adobe preparation to provide flexural strength and reduce hygrometric shrinkage during drying, and are commonly used in restoration practices as adhesives, densifiers, and additives for earthen grouts (Bouhicha et al. 2005; Quagliarini and Lenci 2010; Chan 2011); iii) cellulose additives act as regulators of water release during the whole hydration, reaction increasing the hydration efficiency, and promoting the formation of CSH (Ridi et al. 2011, 2013).

Ethanol/water blends were investigated as dispersing agent, exploiting the presence of the cellulose derivative to achieve the system stability without using surfactants. The amount of water was reduced but maintained sufficient for the setting of CSH phases. Ethanol was selected as it is an optimal solvent in terms of volatility, surface tension, and boiling point, for the application of nanoparticles to mortars and stone (Baglioni et al. 2015)**.** Nanoparticles can be dispersed in different solvents (besides water, short chain alcohols and water-alcohol blends), allowing to avoid aggregation and sedimentation phenomena, and detrimental effects caused by excessive wetting of the stone with water (freeze-thaw cycles, transport of soluble salts, growth of microorganisms (Baglioni et al. 2013)); moreover, the high surface area provides enhanced reactivity, as opposed to bulk materials, in the formation of CSH phases.

Chapter 3 – Nanolimes for stone consolidation: the reaction mechanism

3.1. Introduction

Nanolimes are colloidal dispersions of calcium hydroxide nanoparticles which have emerged as a compatible and effective strategy for the consolidation of immovable artworks.

As described in Chapter 1, the use of calcium hydroxide grants durability, effectiveness and compatibility. Indeed, the carbonation process results the main responsible for the strengthening and the consolidation of degraded lime-based materials, such as wall paintings and carbonate stones, as calcium hydroxide reacts with atmospheric carbon dioxide in presence of water, and forms a new network of crystalline calcium carbonate, which fills the cracks but also binds loose grains. (Giorgi et al. 2000a; Rodriguez-Navarro et al. 2016b). Moreover, their use was also experimented for the consolidation of silicate-based substrates (Dei and Salvadori 2006; Rodriguez-Navarro et al. 2013).

The particle nano-size (ideally < 300 nm) and the use of short-chain alcohols as dispersing agents (e.g. ethanol and propanol) allow to obtain concentrated stable dispersions and good penetration within the substrate porosities. Besides, high reactivity is granted by the high surface area and crystalline hexagonal plate-like shape of portlandite, which enhance the capacity of absorbing water, favoring carbonation.

Different synthetic processes have been developed over the last decades to tailor the particles' shape and size, crystallinity, and adsorbed additives (Yura et al. 1990; Pérez-Maqueda et al. 1998; Salvadori and Dei 2001; Nanni and Dei 2003; Xu et al. 2004; Sequeira et al. 2006; Stefanis and Panayiotou 2007; Daniele et al.

2008; Daniele and Taglieri 2010; Giorgi et al. 2010a), which in turn are known to affect the carbonation process, and hence the efficacy of the consolidation treatment. However, while both the carbonation of bulk $Ca(OH)_2$ and the carbonation in solution have been addressed in the literature (Yagi et al. 1984; García-Carmona et al. 2003; Montes-Hernandez et al. 2007, 2010; Rodriguez-Navarro et al. 2015), less studies have so far focused on the carbonation mechanism of nano-sized $Ca(OH)_2$ particles in air. The process is affected by several factors, mainly including the particles' size, surface area, and impurities, as well as environmental parameters such as temperature, relative humidity (RH), and CO_2 concentration (Beruto and Botter 2000; Dheilly et al. 2002; Rodriguez-Navarro et al. 2016b).

In this chapter, a general overview on the state of the art concerning the carbonation process of $Ca(OH)_2$ nanoparticles is provided.

A systematic study on four different nanolimes was carried out within the present research project, aiming at improving the knowledge on the subject and comparing the performances of four commercial products typically used for consolidation operations.

3.2. On the carbonation of nanolimes

The carbonation process can be outlined in two main steps: the dissolution of the reactants, and the reaction of the ions in presence of water. Specifically, when lime is applied to a porous substrate and the alcohol has evaporated, carbonation starts with the diffusion of CO_2 in the gas/water interface and dissolution in water (Eq. 3.1), forming carbonic acid (H_2CO_3) (Eq. 3.2), which dissociates into carbonate ion (CO_3^{2-}) (Eq. 3.3) and bicarbonate ion (HCO_3^-) (Eq. 3.4); $Ca(OH)_2$ dissolves and dissociates into calcium ion (Ca^{2+}) and hydroxyl ion (OH^-) (Eq. 3.5); then calcium ions and carbonate ions react, leading to the precipitation of

solid calcium carbonate ($CaCO_3$) (Eq. 3.6) (Cizer et al. 2012a, b; Pesce 2014; Pesce et al. 2017; Rodriguez-Navarro and Ruiz-Agudo 2018).

- Dissolution of reactants in water:

  - Carbon dioxide

$$CO_{2(g)} \leftrightarrow CO_{2(aq)} \quad \text{Eq. 3.1}$$

$$CO_{2(aq)} + H_2O_{(l)} \leftrightarrow H_2CO_{3(aq)} \quad \text{Eq. 3.2}$$

$$H_2CO_{3(aq)} \leftrightarrow HCO^-_{3(aq)} + H^+_{(aq)} \quad \text{Eq. 3.3}$$

$$HCO^-_{3(aq)} \leftrightarrow CO^{2-}_{3(aq)} + H^+_{(aq)} \quad \text{Eq. 3.4}$$

  - Calcium hydroxide

$$Ca(OH)_{2(aq)} + H_2O_{(l)} \leftrightarrow Ca^{2+}_{(aq)} + 2(OH)^-_{(aq)} + H_2O_{(l)} \quad \text{Eq. 3.5}$$

- Reaction of calcium ions and carbonate ions in presence of water:

$$Ca^{2+}_{(aq)} + CO^{2-}_{3(aq)} + H_2O_{(l)} \leftrightarrow CaCO_{3(s)} + H_2O_{(l)} \quad \text{Eq. 3.6}$$

The reaction in Eq. 3.3 is favored at high pH, which is achieved by the dissolution of portlandite. The dissolution and hydrolysis of CO_2 is considered a rate

controlling step in the overall process: under high pH conditions, the hydration of CO_2 can also take place at a significantly higher rate via the reaction in Eq. 3.2a followed by the production of carbonate ions according to Eq. 3.4.

$$CO_2 + OH^- \leftrightarrow HCO_3^- \qquad \text{Eq. 3.2a}$$

The overall process is usually schematized as follows (Eq. 3.7):

$$Ca(OH)_2 + CO_2 \leftrightarrow CaCO_3 + H_2O \qquad \text{Eq. 3.7}$$

Eq. 3.7 shows that one mole of $CaCO_3$ (and one mole of H_2O) is produced by one mole of $Ca(OH)_2$ and one mole of atmospheric CO_2. The new carbonate phase, whose molar volume is 12.6% higher than portlandite, will fill pores more effectively and will bind the grains producing consolidation (Rodriguez-Navarro and Ruiz-Agudo 2018).

It has been reported that the carbonation process takes place with a rate depending on the formation of an interface of water molecules or OH-ions, at the solid interface not covered by $CaCO_3$. The reaction rate increases with temperature (with a peak at 450°C, after which $CaCO_3$-decomposition is thermodynamically favored) and with addition of water vapor (a nine times the rate of dry carbonation of $Ca(OH)_2$ is reported) (Nikulshina et al. 2007).

Another study demonstrated that gas-solid carbonation of calcium hydroxide is activated at low temperature (< 30°C) and low CO_2 pressure (<1.5 atm) by the absorption of free molecular water on the surface of the reacting particles. If adsorbed water is absent, a dry route can occur at temperatures higher than 300 °C and CO_2 pressure lower than 1 atm. The authors hypothesized that the production of carbonate around the grains core is owed to the atomic excitation of oxygen

atoms, which migrate from the solid towards adsorbed CO_2 (Montes-Hernandez et al. 2010).

At room temperature, water is necessary, either in bulk or as an adsorbed film, as it allows for the dissolution of reactants (Rodriguez-Navarro et al. 2016b). The released H_2O during carbonation can subsequently autocatalyze the reaction itself until completion, or until the formation of a passivating $CaCO_3$ layer, which prevents further carbonation.

It is generally reported that, at room T, $CaCO_3$ precipitates on the surface of portlandite crystals if RH is higher than 30% (Beruto and Botter 2000; Dheilly et al. 2002; Yang et al. 2003). Beruto and Botter also concluded that the formation of an adsorbed (liquid-like) water film on $Ca(OH)_2$ particles is critical for carbonation to progress, and that the process accelerates at RH values > 75%, when multilayer water adsorption occurs. The gas-solid reaction is in fact considered a gas–liquid–solid reaction. In saturation conditions (RH ≥ 98%) a macroscopic film of water over the $Ca(OH)_2$ layer is produced, and carbonation is delayed due to Le Chatelier principle (water is a product of the reaction of calcium hydroxide and carbon dioxide, besides calcium carbonate).

The role of RH is crucial in that it affects not only the carbonation rate, but also the production yield (fractional conversion of calcium hydroxide into calcium carbonate), the calcium carbonate polymorphs selection and ratio, as well as the effectiveness of consolidation treatments involving the use of nanolimes on porous substrates (Giorgi et al. 2010a). It has to be noted that a total conversion of calcium hydroxide (yield = 100%) is achievable in air only at relatively high RH, in a time scale of weeks or months, and with strong dependence on other factors like temperature, reactants concentrations and surface area. Alcoholic dispersions of $Ca(OH)_2$ nanoparticles consisting of thick portlandite particles (with thickness measured along {001} basal face ≥ 30 nm, typical value for coarse slaked lime putty particles (Ruiz-Agudo and Rodriguez-Navarro 2010)),

left in air for two months at RH = 80 % and T= 20°C, were shown to reach carbonate yields higher than 40%, while nanolimes consisting of thin (ca. 25 nm) portlandite particles can reach yields close to 100% (Rodriguez-Navarro and Ruiz-Agudo 2018). Therefore, best consolidating performances can be obtained by using $Ca(OH)_2$ particles synthesized limiting crystal growth along basal face, for instance by adding alcohols during synthesis, whose chemi- or physi-sorption limits the nuclei aggregation, besides enabling high colloidal stabilization of the nanoparticles, via hydrophobic interactions (Salvadori and Dei 2001).

Calcium carbonate polymorphs

An important aspect of the carbonation process is the evolution of the carbonate polymorphs (*i.e.* the transformation of $CaCO_3$ crystal structure), namely: amorphous calcium carbonate hydrate (ACC, with a general formula $CaCO_3 \cdot nH_2O$); three anhydrous crystalline forms, calcite, aragonite and vaterite; two crystalline hydrated forms, monohydrate (or monohydrocalcite, $CaCO_3 \cdot H_2O$) and hexahydrate (ikaite, $CaCO_3 \cdot 6(H_2O)$).

Calcite is the only stable polymorph at 1 atm and T between 0 and 40°C (Pesce 2014). Depending on RH conditions, amorphous calcium carbonate, monohydrocalcite, vaterite and aragonite were reported to form, in different amounts, prior to or along with calcite, as metastable precursors phases with different stability and crystalline structure (Gomez-Villalba et al. 2011, 2012; López-Arce et al. 2011; Rodriguez-Navarro et al. 2013; Baglioni et al. 2014). For instance, metastable vaterite consists of polycrystalline spherulites and is more soluble than calcite, with possible affects the bond formation with the calcite-based substrate and the treatment performances. Nevertheless, vaterite is reported to produce some effectiveness in consolidating stone (Rodriguez-Navarro et al. 2013). Moreover, the formation of vaterite can result in positive effects in the long-term, as it eventually transforms into stable calcite.

Recently, Navarro et al. studied the commercial product Calosil® in ethanol and reported that the carbonation in humid air at room T follows the Ostwald's step rule, where amorphous calcium carbonate (ACC) is firstly formed, followed by metastable phases (ACC → vaterite → aragonite → calcite) (Rodriguez-Navarro et al. 2016b). ACC is the dominant phase during early stages of carbonation, accounting for up to 24 wt% of the carbonate phases in the first 24 hours at RH = 80 ± 5%. ACC pseudomorphs formation after $Ca(OH)_2$ involves multilayer adsorption of water onto the hydroxide crystals, followed by a dissolution-precipitation mechanism (Beruto and Botter 2000; Rodriguez-Navarro et al. 2016b). Capillary condensation into the mesoporous structure, formed upon drying of the $Ca(OH)_2$ nanoparticles' dispersions, and the release of water during carbonation, favor the ACC formation in the aqueous solution film (where a very high supersaturation is reached during the early stages) (Montes-Hernandez et al. 2010; Rodriguez-Navarro et al. 2016b). In addition, these authors observed ACC nanoparticles with no spatial connection with the ACC pseudomorphs; thus, they suggested that these particles might form through homogeneous nucleation in the aqueous solution film (Rodriguez-Navarro et al. 2016b). The authors detected vaterite, calcite, and traces of aragonite immediately after ACC formation (after 6 hours of carbonation) and observed an increase of vaterite (and aragonite) within the first 24 hours followed by a decrease, while calcite continuously increased. They concluded the metastable phases form after dissolution of ACC and independently transform into the stable phase, as also reported by Nielsen et al. (Nielsen et al. 2014). According to Navarro et al., ACC grows and transform into vaterite (more abundantly, up to 35%) and aragonite (up to 5 wt%), via a dissolution–precipitation process, followed by nonclassical nanoparticle-mediated crystal growth. Building units of vaterite presumably form via heterogeneous nucleation onto ACC, and then aggregate by mesoscale assembly into nearly iso-oriented structures resembling mesocrystals. A solid-

state ACC-to-vaterite transformation was excluded as no crystalline phases were experimentally observed if water was absent. Aragonite spindle-like structures likely form after heterogeneous nucleation onto ACC; then aragonite dissolves and transforms either into calcite or into large prisms (by Ostwald ripening), and its presence is overall scarce. Vaterite also dissolves and reprecipitates as calcite, the stable phase. Therefore, calcite can directly nucleate and grow after dissolution of ACC/vaterite/aragonite, or nucleate on vaterite/aragonite and grow via non-classical particle-mediated aggregation or a classical ion-mediated mechanism (Nielsen et al. 2014; De Yoreo et al. 2015; Rodriguez-Navarro et al. 2016a, b).

The role of alcohol

Alcohol seems to have no significant effect on ACC formation, but several studies demonstrated that organic additives favor the stabilization of vaterite and aragonite at room T, probably delaying their dissolution-mediated transformation into calcite by surface adsorption (Seo et al. 2005; Zhang et al. 2008; Sand et al. 2012).

Chen et al. (Chen et al. 2006) related the observed polymorphism with different ethanol/water ratios at high temperature: if ethanol predominates, vaterite with traces of aragonite is obtained; if water predominates, pure aragonite is obtained; when the ethanol/water ratio is 1:1, aragonite with vaterite traces is obtained.

Rodriguez-Navarro et. al (Rodriguez-Navarro et al. 2013, 2016c) also observed that alcohol, besides providing high colloidal stability to $Ca(OH)_2$ nanoparticles dispersions, affects the kinetics of carbonation and $CaCO_3$ polymorph selection. According to the authors, the contact of particles with alcohol (e.g. during the storage of dispersions) results in the pseudomorphic replacement of $Ca(OH)_2$ by calcium alkoxides (*i.e.* calcium ethoxide or calcium 2-propoxide, if the involved alcohols are ethanol or 2-propanol, respectively), as the original hexagonal

portlandite platelets maintain their external shape. They observed that alkoxides yield depends on reactivity of $Ca(OH)_2$ particles (surface area and lattice defects) and contact time with alcohol, and that their formation affects the carbonation rate and yield. The authors also reported that the formation of alkoxides in humid environments favors the stabilization of metastable vaterite and aragonite, probably due to the alcohol molecules released during the alkoxides hydrolysis.
López-Arce and Gomez-Villalba (López-Arce et al. 2010, 2011) studied the product Nanorestore® (calcium hydroxide nanoparticles dispersion in 2-propanol) and applied it on dolostone, demonstrating the strong influence of RH conditions on the carbonation rate and polymorphs ratios. At RH 75-90%, the carbonation process is faster, and hydroxide–carbonate conversion is completed within 7 days. Water catalyzes the formation of ACC and its quick conversion into vaterite, aragonite and/or calcite. Moreover, the authors observed that, at high RH, the alcohol evaporation is delayed, leading to a stabilizing effect for vaterite and aragonite. They found similar results for CaLoSil® in 2-propanol (Gomez-Villalba et al. 2011, 2012). The authors also indicate that changes in the water content modify the concentration of the precursor solution and the local water/alcohol ratios, affecting the precipitation/dissolution of anhydrous and hydrated polymorphs, which is mirrored in crystal growth and lattice parameters.

3.3. Kinetic models

The study of the carbonation kinetics of nanolimes is crucial in view of predicting the performances of consolidating interventions.
Different models have been proposed in the past years to fit the experimental data describing the transformation of calcium hydroxide into $CaCO_3$ phases. Some authors used deceleratory models with no induction time (Shih et al. 1999; Dheilly et al. 2002; Montes-Hernandez et al. 2007, 2010), while it was found that

a sigmoidal-type Avrami-Erofeev kinetic model provided a good fitting of the carbonation kinetics when the formation of the sole calcite phase is monitored (Baglioni et al. 2014).

Recently, Rodriguez-Navarro et al. highlighted that different results might in fact come from overlooking the role of precursor phases (e.g. amorphous calcium carbonate and vaterite) (Rodriguez-Navarro et al. 2016b); the authors monitored the formation of both amorphous and crystalline $CaCO_3$ phases through thermal analysis, and fitted the results to the solid-state deceleratory kinetic models summarized in a review by Khawam and Flanagan (Khawam and Flanagan 2006). Among the different deceleratory models, the best fitting was obtained using a first order model (Rodriguez-Navarro et al. 2016b).

In the present contribution, the carbonation kinetics of four different formulations of $Ca(OH)_2$ nanoparticles' dispersions was investigated, inquiring for the first time the applicability to these systems of the mathematical "Boundary Nucleation and Growth" model (BNGM), originally developed by Cahn (Cahn 1956), and later used by Thomas to describe the hydration of tricalcium silicate (C_3S) grains (Thomas 2007). The carbonation of $Ca(OH)_2$ nanoparticles is a water-mediated process that takes place at the solid-liquid interface (Beruto and Botter 2000; Dheilly et al. 2002; Yang et al. 2003; Nikulshina et al. 2007; Rodriguez-Navarro et al. 2016b); therefore, the BNGM was evaluated considering that the process is expected to preferentially occur via nucleation at the grain boundaries, followed by growth along the particles surface, and then outward into the pore space between the particles, until the products regions coalesce. Namely, this model accounts for the effect of the surface area of the particles on the carbonation kinetics.

After selecting the BNGM based on the aforementioned rationale, a rigorous approach was followed, by evaluating separately the contributions of nucleation and growth of $CaCO_3$ during the carbonation process. Thus, it was evaluated the

possible application of limit cases of the model, where one of the two contributions (*i.e.* either boundary nucleation or growth) prevails over the other.
The selected four $Ca(OH)_2$ nanoparticles dispersions were chosen as they are an inclusive set of widely used standards in the consolidation of carbonate-based materials, obtained via different synthetic pathways. The systems exhibit different characteristics, such as the used liquid medium (ethanol, 2-propanol), and the specific surface area of the particles. The kinetic behavior of the four systems was thus compared, calculating the rate constants, the activation energies and the linear growth rate of the carbonation process.
Fourier Transform Infrared Spectroscopy (FTIR) was selected to investigate the carbonation process, as it feasibly allowed to monitor over time the transformation of calcium hydroxide into both amorphous and crystalline calcium carbonate phases (Andersen and Brečević 1991; Vagenas 2003). The hydroxide to carbonate conversion was followed under strictly controlled environmental conditions (T, RH, CO_2 concentration), evaluating the effect of the temperature on the process. Finally, an evaluation of the stable (calcite) and metastable (vaterite, aragonite) crystalline $CaCO_3$ phases was given for the different systems.

PART III

Experimental

Chapter 4 – Materials

4.1. Nanocomposite formulations for adobe consolidation

The first step of the research was dedicated to the selection of suitable materials, in terms of compatibility (both with the substrate and mutual, in case of composite systems), applicability and efficacy. As described in Chapter 2, silica nanoparticles, calcium hydroxide nanoparticles, and a cellulose derivative were selected for the formulation of a stable and effective dispersion for the consolidation of water-sensitive powdery substrate, *i.e.* adobe, via the *in situ* formation of calcium silicate hydrate (CSH) cementing phases.
The selected components are described below and showed in Figure 4.1.

Nanosilica

A nanosilica aqueous dispersion was prepared diluting to 10 g/L the commercial product Levasil CS40-213 (Akzo Nobel Chemicals GmbH), *i.e.* monodisperse spheres of amorphous SiO_2 (original concentration of 40 wt% in water, 0.2 wt% of Na_2O as stabilizer), declared particle size of 25 nm, specific surface area of 130 m^2/g, pH 9, hereinafter reported as *SiO_2*.

Nanolime

An ethanol dispersion of $Ca(OH)_2$ nanoparticles (hereinafter reported as *lime*) produced via solvothermal reaction as reported in the literature (Poggi et al. 2016) was used. The synthesis yields hexagonal platelets of portlandite of ca. 100-200 nm, at a concentration of 35 g/L, which was diluted to 5 g/L.

Cellulose derivative

An ethanol solution of a commercial hydroxypropyl cellulose (or HPC, specifically Klucel®-G, 300 mPas, Phase Restauro) was prepared at a concentration of 20 g/L (hereinafter reported as *HPC*. The product has a viscosity of 150-450 cP (2 wt% solution, 25 °C) and a molecular weight of 370,000 Da. Hydroxypropyl cellulose is a non-ionic cellulose ether, whose structure is reported in Figure 4.2. Klucel HPC is manufactured by reacting alkali cellulose with propylene oxide at elevated temperatures and pressures. The propylene oxide can be substituted on the cellulose through an ether linkage at the three reactive hydroxyls present on each anhydroglucose monomer unit of the cellulose chain (substitution degree, SD, of 1-3) (Ashland Inc. Klucel).

Figure 4.1 - Aqueous dispersion of silica nanoparticles, SiO_2 component (left); ethanol dispersion of calcium hydroxide nanoparticles, *lime* component (center); ethanol solution of hydroxyropyl cellulose, *HPC* component (right)

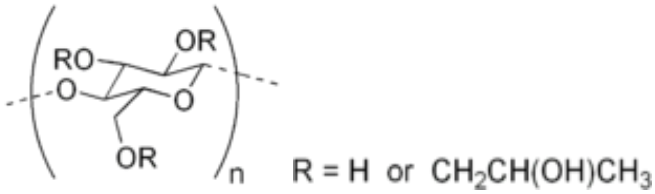

Figure 4.2 - Structure of hydroxypropyl cellulose

Ethanol (ACS grade) was purchased by Fluka. Water was purified by a Millipore Milli-Q UV system (resistivity >18 MΩ cm).

4.2. Study of the carbonation kinetics of nanolimes

Four alcoholic dispersions of $Ca(OH)_2$ nanoparticles were selected as commonly used for the consolidation of carbonate-based materials, and representative of two of the main synthetic routes commonly adopted for the formulation of $Ca(OH)_2$ nanoparticles' dispersions, *i.e.* the treatment of slaked lime and sol-gel solvothermal processes (see Chapter 1).

The system's name, solvent, concentration, synthesis procedure, mean particle size and specific surface area are summarized in Table 4.1.

CaLoSiL®E5 and CaLoSiL®IP5 are $Ca(OH)_2$ nanoparticles alcohol dispersions (5 g/L) prepared via alkoxide route (Ziegenbalg 2005; Rodriguez-Navarro and Ruiz-Agudo 2018) and commercialized by IBZ-Salzchemie GmbH & Co. KG (Germany). The systems were labeled as CE and CIP, where the letters E and IP indicate that the particles are dispersed respectively in ethanol and 2-propanol. The other two investigated nanolimes are Nanorestore Plus® (labeled as LE) and Nanorestore® (labeled as LIP). Nanorestore Plus® is a concentrated (35 g/L) dispersion in ethanol, obtained by following a solvothermal route starting from metallic calcium (Poggi et al. 2014, 2016), which was diluted to 5 g/L and labeled

as LE. Nanorestore® is a dispersion (5 g/L) of $Ca(OH)_2$ nanoparticles prepared by treatment of slaked lime (Giorgi et al. 2000b).

SYSTEM NAME	**SOLVENT**	**CONC.** ($g \cdot L^{-1}$)	**PREPARATION**	**PART. SIZE** (nm)	**SPEC. SURF. AREA** ($m^2 \cdot g^{-1}$)
CE	ethanol	5	Solvo-thermal process from Ca	50-250	38
LE	ethanol	5		100-200	36
CIP	2-propanol	5		50-250	38
LIP	2-propanol	5	Break-down method from slaked lime	300-500 (with few micron-sized aggregates)	20

Table 4.1 - Properties of the four considered $Ca(OH)_2$ alcohol dispersions: system name, alcohol, concentration, preparation, particle size and surface area

The particles' size for the commercial systems CE and CIP is extracted from the literature (Technical Leaflet CaLoSiL®); the particles' size distribution of the LE and LIP systems was measured through Dynamic Light Scattering (DLS) measurements, as described in the following chapter. The mean particle size of the LE system, is ca. 100-200 nm; the LIP system shows a bimodal distribution, with primary particles of 300-500 nm and larger aggregates of about 1 μm.
The specific surface area of nanoparticles was obtained via nitrogen sorption porosimetry, as described in the following chapter.

Chapter 5 – Analytical Methods

5.1 Nanocomposite formulations for adobe consolidation

This paragraph is dedicated to the description of the analytical methods employed for the characterization of the composite formulations and for the assessment of the consolidation effect produced by treatments of the adobe samples.

5.1.1. Formulations characterization

The formulations were characterized to gain information on the kinetic stability, particles size distribution and ζ- potential, morphology and composition on the components, and formation of new phases.

5.1.1.1. UV−VIS spectrometry: turbidimetric analysis

The kinetic stability of the dispersions (*SiO_2*, *lime*, all the binary systems and the ternary system) was investigated via turbidimetric analysis, performed with a Cary Bio 100 UV−VIS spectrophotometer (Varian). The absorbance at λ = 600 nm (spectral band width = 1 nm) was recorded at 25 °C as a function of time, at regular time intervals, over a total period of 1 month, using sealed quartz cuvettes with an optical path of 1 cm. Decreases in the absorbance were ascribed to the formation of aggregates and sedimentation. The values reported are the average of five measurements.

5.1.1.2. pH measurements

The pH of the SiO_2 aqueous dispersion was measured using a glass electrode pH-meter (Crison-Basic20): the reported value is the average of three measurements.

5.1.1.3. Dynamic light scattering (DLS): particle size and ζ- potential

The particle size distribution and ζ-potential were determined using a 90Plus Particle Size Analyzer (Brookhaven Instrument Corporation), with incident 659 nm laser light radiation and collection at 90°. The measurements were recorded at 25 °C. For the particle size measurements, the systems were diluted 1:10. The values reported are the average of three measurements consisting of 5 runs of 30 seconds. The refractive index of the liquid medium (ethanol:water blend 4:1) is 1.36 (Nowakowska 1939; Scott 1946); the presence of the highly diluted cellulose derivative dissolved in the blend (Klucel®-G, 0.5 g/L) was not considered as relevant for the measurements. For the solid content of the dispersions, the average of the indexes of the components (SiO_2, $Ca(OH)_2$) was used. The CONTIN method was used for fitting the autocorrelation functions, to obtain the particle size distributions. The data are intensity-weighted. For the ζ-potential measurements, the Smoluchowski equation was used for the fitting of the autocorrelation function.

5.1.1.4. Transmission electron microscopy (TEM)

The systems were also observed using Transmission Electron Microscopy (TEM), with a STEM CM12 Philips electron microscope. The samples were cast onto a carbon-coated copper grid sample holder, followed by evaporation of the solvent at room temperature.

5.1.1.5. Attenuated Total Reflectance Fourier Transform Infrared Spectroscopy (ATR-FTIR)

ATR-FTIR was performed using a Thermo Nicolet Nexus 870 spectrometer equipped with a liquid nitrogen-cooled Mercury Cadmium Telluride detector, a single reflection diamond crystal ATR unit and a Golden Gate diamond cell. The spectra were acquired in the 650−4000 cm^{-1} range with a spectral resolution of 4 cm^{-1}. The samples were air-dried and grinded prior to measurement.

5.1.1.6. X-ray diffraction (XRD)

XRD was carried out using a D8 Bruker "Da Vinci" diffractometer equipped with a primary Ge monochromator using for Cu Kα1 radiation (λ = 1.54 Å) and a Sol-X solid state detector in Debye-Scherrer geometry (2θ range of 5 - 60°, step size of 0.02°, time/step of 0.3 s, voltage of 40 kV and current of 40 mA). The samples were air-dried and grinded prior to measurement.

5.1.1.7. Scanning electron microscopy (SEM)

For SEM investigations, the dispersions were deposited on the stab and let dried prior to measurement with a field emission gun scanning electron microscope (FEG-SEM), ΣIGMA (Carl Zeiss, Germany) with acceleration potential of 25 kV.

5.1.2. Adobe soil characterization

Before treatment, the adobe soil (Figure 5.1) was characterized by determining the grain size distribution, the Atterberg Limits, the carbonate content, and the

organic content. XRD measurements were also carried out to investigate the soil mineralogical composition.

Figure 5.1 - Grinding of adobe soil prior to characterization

5.1.2.1. Grain size distribution

The grain size distribution of the adobe soil was characterized according to the Standard Test Method for particle-size analysis of soils (ASTM D422-63) and the Standard Test Method for particle-size distribution of fine-grained soils using sedimentation analysis (ASTM D7928-16).

5.1.2.2. Atterberg Limits

The Atterberg Limits were also obtained (Liquid Limit - BS 1377:1975 and Plastic Limit - ASTM D 4318-93), and the Plastic Index was then calculated.

5.1.2.3. Carbonates content and organic content

The carbonates content was determined using a Dietrich-Fruhling calcimeter, and the organic content was determined by the C-N-H determination method.

5.1.3. Adobe mock-ups characterization

Two months after the treatment, the treated (T) and non-treated (NT) adobe specimens were characterized to assess the consolidation efficacy by colorimetric analyses, ATR-FTIR, XRD, phenolphtalein test, peeling tape test, abrasion test, wet-dry cycles, water sorption measurements, and drilling test.

5.1.3.1. Colorimetric measurements

Colorimetric analyses were performed using an X-Rite SP60 portable colorimeter, (D65/10°, 8 mm diameter circular measuring spot), to evaluate the possible color changes produced by the application of the formulation. The experiment was performed on four areas of three different samples. The color difference between the treated and non-treated samples was calculated using the formula $\Delta E^* = \sqrt{\Delta L^{*2} + \Delta a^{*2} + \Delta b^{*2}}$, where L*, a* and b* are the coordinates of the CIE 1976 color space (Figure 5.2).

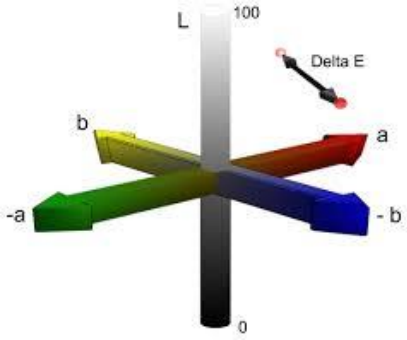

Figure 5.2 - CIE 1976 color space

5.1.3.2. Attenuated Total Reflectance Fourier Transform Infrared Spectroscopy (ATR-FTIR) and X-ray diffraction (XRD)

ATR-FTIR, XRD (described above) were used to assess the penetration and distribution of the applied product, and to verify the occurrence of consolidation reactions within the substrate.

5.1.3.3. Phenolphthalein test

The phenolphthalein test was also used to assess the penetration of the calcium hydroxide nanoparticles found in the ternary system, as an indication of the depth reached by the whole formulation. The penetration depth is visually measured thanks to the intense purple color assumed by phenolphthalein at alkaline pH. A 0.1% solution of phenolphtalein was sprayed onto the surface of samples right after treatment and cross sections of the samples were then cut to visualize the penetration depth (Lanzón et al. 2017).

5.1.3.4. Peeling test

The peeling test (or scotch tape test) is a common method used conservation practice for the evaluation of the efficacy of consolidating treatments in terms of restoration of the surface cohesion properties (Drdacky et al. 2012). The test consists in pressing pieces of adhesive tapes of known weight and area on the sample surface and peel them off after a few minutes (Figure 5.3). The decohesion index, DI (mg/cm^2), is the weight of the material loss per unit area, and it is inversely proportional to the grains' cohesion forces. The data reported are the average of measurements performed on four areas of the sample, for three different samples.The experiment was conducted three times on each area, in

order to obtain the decohesion index following the progressive removal of surface layers. The total removed mass over the three experiments was also calculated.

Figure 5.3 - Peeling test (or scotch tape test)

5.1.3.5. Abrasion test

The abrasion test (AFNOR PR XP P13-901 2001; Izemmouren et al. 2015) consists in subjecting the sample to mechanical erosion by brushing with a metal brush at a constant pressure (3 kg mass on the top center of the brush) for a given number of cycles (in this case three cycles, each consisting of 60 rounds of brushing in one minute) on the entire length of the specimen (Figure 5.4). The abrasion coefficient, Ac (cm^2/mg), expresses the ratio of the surface to the quantity of the material removed by brushing and is proportional to the abrasive strength. The data reported in the graph are the average of tests performed on three samples; the total value after the three cycles was also calculated.

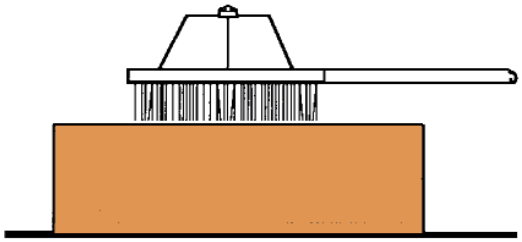

Figure 5.4 - Abrasion test

5.1.3.6. Wet-dry cycles

Wet-dry cycles were performed to assess the resistance to exposure to harsh environment cycles (ASTM D559/D559M 2015; Izemmouren et al. 2015) by immersing the samples in distilled water for 5 hours and drying at 60° C for 48h (Figure 5.5). Seven cycles were performed, and the weight loss is expressed as the percentage of dry mass reduction relative to the original mass, as average of the data obtained from two samples. The total value after the seven cycles was also calculated.

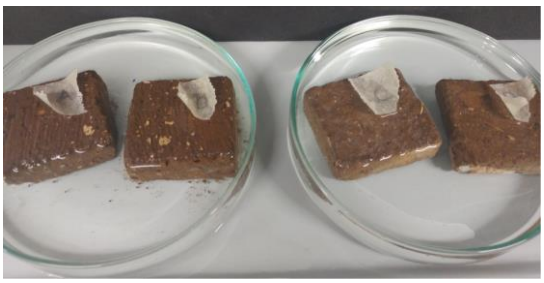

immersion (5h) → oven (48h)

Figure 5.5 - Wet/dry cycles

5.1.3.7. Water sorption measurements

For the water sorption measurements, the samples were oven-dried at 60 °C to constant mass, weighted and put on a porous support in contact with distilled water. The water intake is measured indirectly by weighting the samples at regular time intervals (Figure 5.6). The capillary water absorption coefficient, A_w ($mg/cm^2 \cdot s^{1/2}$), of the treated and untreated samples was obtained using the 'one tangent method', *i.e.* calculating the gradient of the straight line obtained by plotting the cumulative mass of water absorbed per unit area against the square root of time (BS EN 1925 1999; Karagiannis et al. 2016). The experiment was repeated twice.

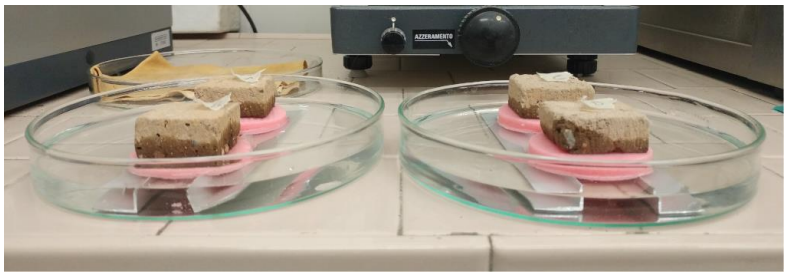

Figure 5.6 - Water sorption measurements

5.1.3.8. Drilling test

The drilling test (Pamplona et al. 2007) was carried out with a drilling resistance measurement system (Sint Technology, Italy), using a 5 mm diameter drill bit (maximum depth=10 mm, penetration rate=20 mm/min, revolution speed= 200 rpm) (Figure 5.7). Each result is the average of three holes produced on two different samples.

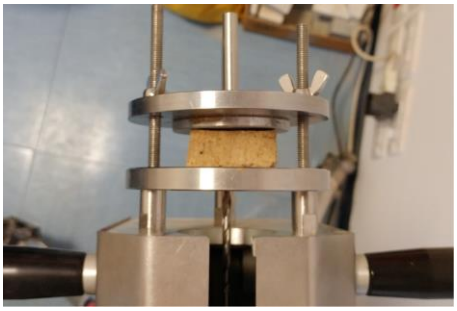

Figure 5.7 - Drilling test

5.2. Carbonation kinetics of nanolimes

This paragraph is dedicated to the description of the analytical methods employed for the study of the carbonation kinetics of nanolimes. The four commercial $Ca(OH)_2$ nanoparticles alcohol dispersions were first characterized via dynamic light scattering (DLS) (as described in section 5.1.1.3), and nitrogen sorption porosimetry, in order to obtain their specific surface areas, as described below. Then a systematic and compared study on their carbonation kinetics was carried out in controlled environmental conditions (T°C, RH%, CO_2 concentration) by means of FTIR spectroscopy (KBr pellet method).

5.2.1. Nitrogen sorption porosimetry

Nitrogen sorption is the most common and accurate method for total surface area measurements. Nitrogen sorption porosimetry measurements were performed using a Beckman Coulter SA-3100 Surface area analyzer. This gives access to the value of the surface area with an error of about 5%. The particle surface area of the four selected systems was determined by Brunauer-Emmett-Teller (BET)

measurement. The samples were previously dried under N_2 flow in order to avoid carbonation of portlandite particles.

5.2.2. Experimental procedure

5.2.2.1. Accelerated carbonation

Accelerated carbonation of nanoparticles was performed to study the carbonation kinetics of the four $Ca(OH)_2$ alcohol dispersions, in a home-made sealed climatic chamber set at RH = 75 (±2) % and T = 14, 22, 30 (±1.5) °C.
RH and T were controlled using NaCl saturated solutions and a thermostat, and continuously monitored using a data logger (Easylog EL-USB-2-LCD, 1 reading every 5 minutes). It is known that carbonation rate is fastened at RH ≥ 75% (Beruto and Botter 2000); and the temperature range was selected since they are representative of standard conditions typically found in case studies where the particles' dispersions are applied (e.g. consolidation of stone and mortars). Environmental CO_2 concentration in the chamber was 450 ppm, consistently with previous studies on the carbonation of $Ca(OH)_2$ (Gomez-Villalba et al. 2011; Cizer et al. 2012a). A fan was used to prevent carbon dioxide deposition on the bottom of the climatic chamber.

5.2.2.2. Fourier Transform Infrared Spectroscopy (FTIR)

The carbonation of the four $Ca(OH)_2$ alcohol dispersions was investigated via Fourier Transform Infrared (FTIR) analysis (Andersen and Brečević 1991; Vagenas 2003). Nanoparticle thin films were cast on KBr pellets and stored under controlled relative humidity, temperature and CO_2 pressure conditions in

the climatic chamber. The decrease of the calcium hydroxide characteristic peak (3645 cm^{-1} OH stretching) was monitored over time (Figure 5.8).

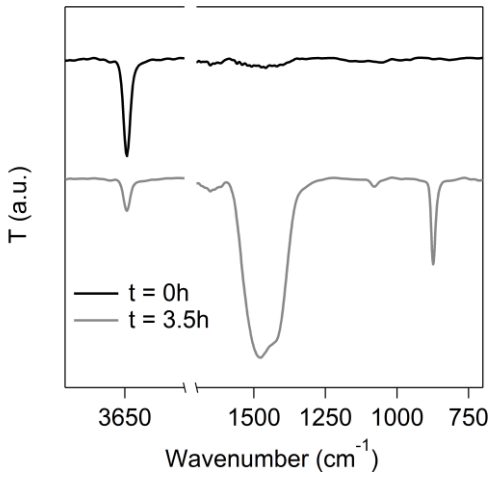

Figure 5.8 - FTIR spectra of the system CIP at 14 °C: the decrease of the calcium hydroxide characteristic peak (3645 cm^{-1} OH stretching) was monitored over time for the four systems at the three temperatures

Each pellet was prepared using 200 mg of dried KBr. For each measurement, the pellet was placed on a pellet holder, and 40 µL of the selected dispersion (4 x 10 µL) were deposited and dried under N_2 flow to ensure complete solvent evaporation without triggering the carbonation reaction. The same number of KBr pellets were left bare and used as backgrounds.

A spectrum was acquired on the pellet (t = 0), which was then placed into the chamber using the sample holder. At chosen time, the pellet was extracted from the chamber and another spectrum was acquired (t = x). As the extraction of the pellet and its short permanence in laboratory conditions (23°C, 50% RH) alter the carbonation process, each pellet was discarded after the measurement, *i.e.* different pellets were used for inquiring different carbonation times.

The FTIR spectra were acquired using a BIO-RAD FTS-40 spectrometer. Each sample spectrum was recorded in transmission mode, after collecting the background spectrum, which was subtracted afterwards. The spectral range investigated was 4000-400 cm^{-1}, acquiring 64 scans for each spectrum, and using a delay time of 30 s between the placement of the KBr pellet in the sample holder and the acquisition of the spectrum. In the obtained spectra, the transmittance (%) is reported as a function of wave number (cm^{-1}).

5.2.2.3. Data elaboration

The Win-Ir software was used to calculate the area of the absorption peak of $Ca(OH)_2$ centered at 3645 cm^{-1} (OH stretching (Carretti et al. 2013)), using a linear baseline. The evolution over time of this peak, during the carbonation process, was calculated as follows:

$$\alpha = \frac{(Area_{t0} - Area_{tx})}{Area_{t0}}$$

where $Area_{t0}$ is the area of the peak at $t = 0$, and $Area_{tx}$ is the area of the peak at a generic time $t = x$, measured for the same KBr pellet, on the same spot. Thus, α is defined as the carbonation degree, increasing from 0 to 1 upon completion of the carbonation process.

The software was also used to calculate the area of the characteristic absorption bands of calcium carbonate polymorphs.

5.2.2.4. Fitting of the experimental curves: Boundary Nucleation and Growth Model (BNGM)

The reaction degrees (α) of the four systems at the three temperatures were plotted against time, and the carbonation curves were fitted to the Boundary Nucleation and Growth Model (BNGM).

According to the generalized BNGM, the volume fraction of transformed phase originating from nuclei on the same grain boundary, X, can be expressed as follows:

$$X = 1 - exp[-2O_V^B \int_0^{Gt}(1 - exp(-Y^e))dy] \qquad \text{Eq. 5.1}$$

Where O_V^B is the total area of the grain boundaries (randomly distributed in the original untransformed volume) per unit volume, *G* is the linear growth rate, *t* is the time since the start of the transformation; *y* is the perpendicular distance of a plane parallel to the boundary from the transforming boundary (*i.e. Gt*), Y^e is the extended area fraction of the intersection between a plane at distance *y* from the boundary and all regions nucleated on the grain boundary. Y^e can be mathematically described as:

$$Y^e = \frac{\pi I_B}{3} G^2 t^3 \left[1 - \frac{3y^2}{G^2 t^2} + \frac{2y^3}{G^3 t^3}\right] \qquad if \;\; t > y/G \qquad \text{Eq. 5.2}$$

$$Y^e = 0 \qquad if \;\; t < y/G$$

where I_B is the nucleation rate per unit area of untransformed boundary.

The volume of the transformed phase depends on three covariant parameters, *G*, I_B, and O_V^B, while only two degrees of freedom exist, named k_B and k_G, which are

defined by Thomas respectively as the rate at which the nucleated boundary area transforms, and the rate at which the non-nucleated grains between the boundaries transform (*i.e.* at which the porosities are filled with reaction products) (Thomas 2007; Del Buffa et al. 2016). The linear growth rate, *G*, and the nucleation rate I_B, are obtained from the rate constants k_B and k_G, by the following relationships:

$$k_B = (I_B O_V^B)^{1/4} G^{3/4} \qquad \text{Eq. 5.3}$$

$$k_G = O_V^B G \qquad \text{Eq. 5.4}$$

To achieve a numerically solvable equation, a change of variable from $y = Gt$ to $z = y/G$ is performed:

$$Y^e = \frac{\pi}{3}\frac{{k_B}^4}{k_G} t^3 \left[1 - \frac{3z^2}{t^2} + \frac{2z^3}{t^3}\right] \qquad if \;\; t > z \qquad \text{Eq. 5.5}$$

and hence:

$$X = 1 - exp[-2k_G \int_0^t (1 - exp(-Y^e))dz] \qquad \text{Eq. 5.6}$$

In this way, the parameters k_B and k_G are directly accessed by the fitting procedure described. The monitoring of the disappearance of hydroxide gives direct access to the progress of the carbonation. The reaction degree α versus time can be directly fitted using the generalized BNGM by explicitly introducing α into Eq. 5.6:

$$\alpha_t = \alpha_i \cdot \alpha_f \{1 - ex\,p[-2k_G \int_0^t (1 - exp(-Y^e))dz]\} \qquad \text{Eq. 5.7}$$

where α_t is the fraction of converted calcium hydroxide at time *t*, and α_i and α_f are the fractions at initial and final time, respectively. The fitting of the time evolution of α using Eq. 5.7 and Eq. 5.5 returns the two independent parameters k_B and k_G. The values of the linear growth rate, *G*, and of the nucleation rate, I_B, can be then calculated by Eq. 5.3 using k_B, k_G, and O_V^B. The latter parameter, O_V^B, is 76, 72, 76, 40 μm^{-1} for the systems CE, LE, CIP, LIP respectively, as reported in Table 5.1. O_V^B was obtained dividing the surface area of the dry $Ca(OH)_2$ powder (see Table 5.1) by the volume occupied by the carbonation products after complete carbonation (per gram of reacting hydroxide, 0.5 cm^3/g). This value was calculated from the stoichiometry of the reaction (see Eq. 5.8), using the density of the stable $CaCO_3$ polymorph, calcite, *i.e.* 2.71 g/cm^3 (which is close to the average of the densities of the three crystalline polymorphs).
The BNGM equations have been solved in Igor Pro, version 6.2.

$$Ca(OH)_2 + CO_2 \rightarrow CaCO_3 + H_2O \qquad \text{Eq. 5.8}$$

SYSTEM NAME	**SPEC. SURF. AREA** ($m^2 \cdot g^{-1}$)	$\mathbf{O_V^B}$ (μm^{-1})
CE	38	76
LE	36	72
CIP	38	76
LIP	20	40

Table 5.1 - Surface area and calculated O_V^B of the four considered $Ca(OH)_2$ alcohol dispersions

Chapter 6 – Nanocomposite formulation and application on adobe

6.1. Preparation of the composite formulation

The three components - silica nanoparticles, $Ca(OH)_2$ nanoparticles and hydroxypropyl cellulose - were combined in various proportions and concentrations, to obtain a hydro-alcoholic dispersion with the components in the desired amounts, keeping a low water content, in the right balance between the need of limit the use of aqueous media on water-sensitive substrates, and the necessity of some water content to trigger the alkaline activation of nanosilica and form CSH phases. Ethanol was selected as it is an optimal solvent in terms of volatility, surface tension, and boiling point, for the application of nanoparticles to mortars and stone (Baglioni et al. 2015).

A first approach involved the use of mesoporous silica nanoparticles (MSNPs), as their porous structure could improve the interaction with the cellulose chains in the composite system. Particularly, a one-pot synthesis (Gao and Zharov 2014) was reproduced to obtain large-pore mesoporous silica nanoparticles using a non-surfactant template, tannic acid. After dissolution of tannic acid in ethanol, ammonium hydroxide was added under vigorous stirring, then the silica precursor (TEOS) was added, and the system was kept under stirring for 3 hours. The product was purified by centrifugation and calcination. As summarized in Figure 6.1, uniform silica nanospheres of ca. 200 nm with interconnected pores of 9-11 nm were obtained. The figure shows the synthesis mechanism, a SEM and a TEM image of the particles, and the results obtained by porosimetric measurements and dynamic light scattering (DLS).

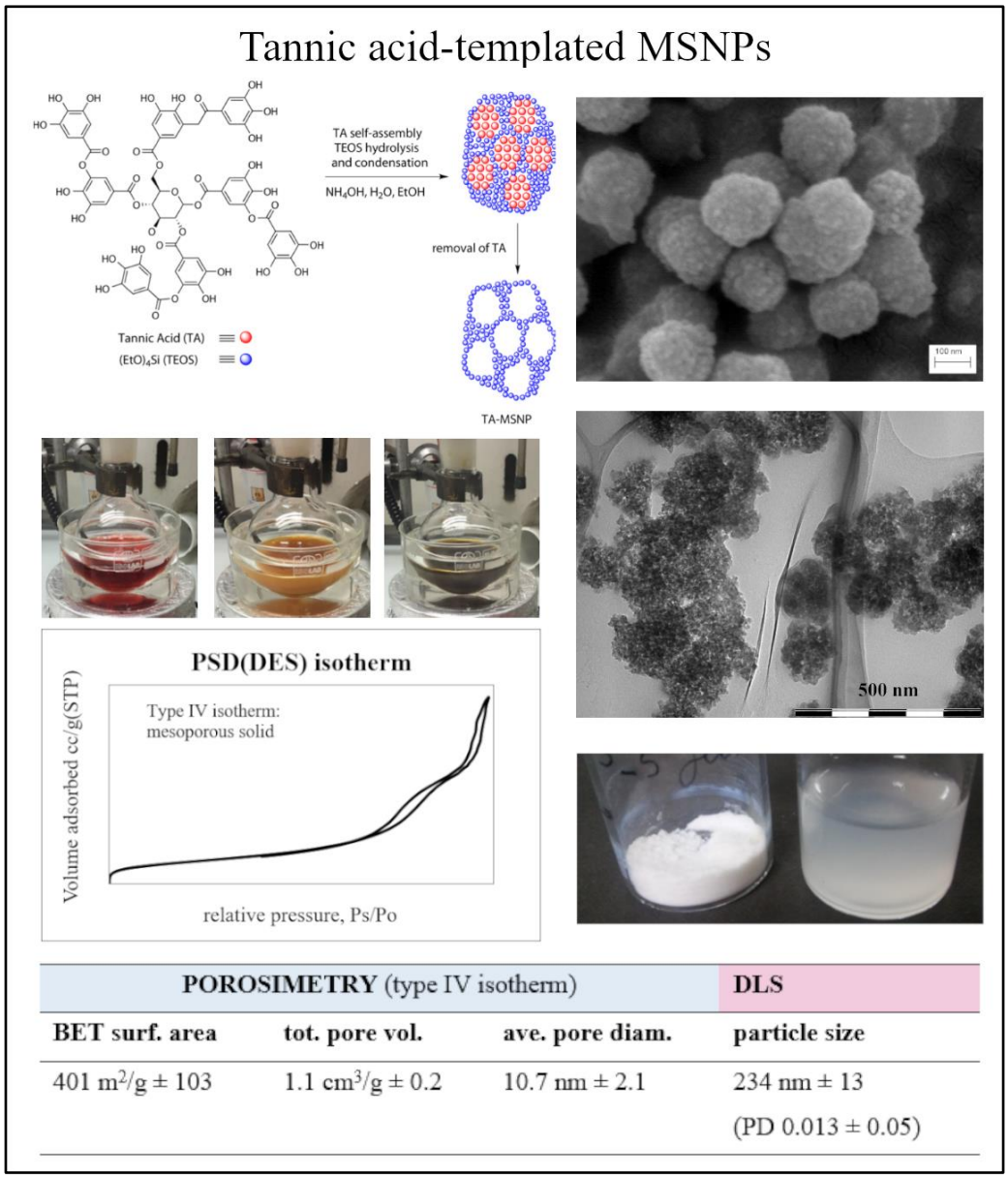

POROSIMETRY (type IV isotherm)			**DLS**
BET surf. area	**tot. pore vol.**	**ave. pore diam.**	**particle size**
401 $m^2/g \pm 103$	1.1 $cm^3/g \pm 0.2$	10.7 nm ± 2.1	234 nm ± 13 (PD 0.013 ± 0.05)

Figure 6.1 - Tannic-acid templated large-pore silica nanoparticles (MSNPs), synthesized following a literature procedure (Gao and Zharov 2014) and characterized by SEM (magnitude of 250kX), TEM, DLS (particle size) and nitrogen sorption porosimetry

However, no evidence of better performances was observed in respect of non-porous silica nanoparticles in terms of components interaction and homogeneity of distribution within the dispersion; moreover, non-porous silica allowed for the use of smaller particles and hence more stable systems, key parameters during the application phase.

Once selected the starting materials, namely non-porous silica nanoparticles dispersion (*SiO_2*), calcium hydroxide nanoparticles dispersion (*lime*), and hydroxypropyl cellulose solution (*HPC*), described in Chapter 4, a series of preparations was realized, in order to adjust the solvents ratio and components concentrations, and formulate the ternary system to be tested for the consolidation of adobe.

During this phase, preliminary mascroscopic observations of as-prepared samples allowed to evaluate the components mutual compatibility, and to tailor their proportions for the formulation of the ternary system. For instance, the combination of silica nanoparticles and $Ca(OH)_2$ nanoparticles lead to flocculation and sedimentation phenomena in short times (hours); instead, the addition of hydroxypropyl cellulose in the system allowed for higher stability (Figure 6.2).

Figure 6.2 - Dispersion and air-dried drop of (left) a nanosilica-nanolime dispersion, showing evident sedimentation and flocculation, and (right) a ternary system including nanosilica, nanolime and HPC

The selected ternary formulation for application and assessment on adobe mock ups (Figure 6.3) is a 4:1 (v/v) ethanol:water dispersion with concentrations of 2.5, 2.5 and 5 g/L of *SiO_2*, *lime* and *HPC* respectively (*SiO_2* : *lime* : *HPC* = 1 : 1 : 2 wt%), and it will be indicated as *SiO_2_HPC_lime*.

The binary combinations were also prepared (Figure 6.3), as comparison: two of the three components were combined, and the solvent of the missing dispersion/solution was added (*SiO_2_lime*, *SiO_2_HPC* and *HPC_lime)*.

Because the mixing of *SiO_2* and *lime* without *HPC* lead to immediate flocculation, the ternary system preparation involved, first, the addition of the ethanol solution of hydroxypropyl cellulose to the silica aqueous dispersion, and then the ethanol dispersion of $Ca(OH)_2$ nanoparticles was added. The composite system was kept under stirring for 6 hours. Table 6.1 shows the composition of the selected ternary composite, the binary combinations and the single components.

System	**Medium**	**Concentration** (g/L)		
		SiO_2	***lime***	***HPC***
SiO_2	H_2O	10	-	-
lime	EtOH	-	5	-
HPC	EtOH	-	-	20
SiO_2 _lime	H_2O/EtOH (1:4)	2.5	2.5	-
SiO_2_HPC	H_2O/EtOH (1:4)	2.5	-	5
HPC_lime	H_2O/EtOH (1:4)	-	2.5	5
SiO_2_HPC_lime	H_2O/EtOH (1:4)	2.5	2.5	5

Table 6.1 - Composition of the selected ternary composite, the binary combinations and the single components

Figure 6.3 - Ternary system *SiO_2_HPC_lime*, and binary systems *SiO_2_HPC*, *HPC_lime*, *SiO_2_lime* (from left to right)

6.2. Treatment of the adobe mock-ups

As target material of the present study, adobe bricks from the Morelos state, Mexico, originally prepared using local soil and straw fibers, were used. The bricks (5 x 10 x 20 cm^3) were cut with an abrasive disc saw into smaller specimens (Figure 6.4) with dimensions of 4 x 4 x 2 cm^3 and average weight of ca. 40 g.

Figure 6.4 - Adobe mock-ups preparation: cutting

The treatment of adobe was performed by soaking each specimen with 20 ml of ternary formulation (*SiO_2_HPC_lime*). The specimens were placed in a container previously filled with the formulation, and kept there until complete absorption (ca. 1 day), as shown in Figure 6.5. Then, the specimens were stored under room conditions (T = 23°C, RH = 50%) until characterization. As comparison, the same treatment was performed using the single components and the binary combinations *SiO_2_HPC* and *HPC_lime*. The treatment with the binary *SiO_2_lime* was not performed due to immediate particle flocculation, as above mentioned.

Figure 6.5 - Treatment of adobe mock-ups

Chapter 7 – Results and discussion

7.1. Formulations characterization

After selecting the three components and preparing the ternary formulation with the components dispersed in the desired amount, various techniques were used to obtain a characterization of the system to be used for adobe consolidation, in terms of stability, particles' dimensions, components interaction and formation of new phases.
In the following paragraphs the results obtained from the characterization of the ternary system (*SiO_2_HPC_lime*), the binary systems (*SiO_2_HPC, HPC_lime, SiO_2_lime*) and the single components are described.

7.1.1. UV−VIS spectrometry: turbidimetric analysis

After 2 months of storage in closed glass bottle, the ternary system *SiO_2_HPC_lime* showed the formation of a gel-like phase (Figure 7.1). A similar behavior was observed to occur in shorter times in formulations where the hydro-alcoholic media is more rich in water, and in the *SiO_2_lime* system (but not in the other binary systems or single components in the hydro-alcoholic blend). It was hypothesised that the desired formation of a CSH phase occurred, and a more detailed characterization was performed, as shown in section 7.1.5-7.1.7.
Turbidimetric analyses were then performed to gain information on the kinetic stability of the dispersions (*i.e. SiO_2, lime, SiO_2_lime, SiO_2_HPC, HPC_lime* and *SiO_2_HPC_lime*) and the results are shown in Figure 7.2.

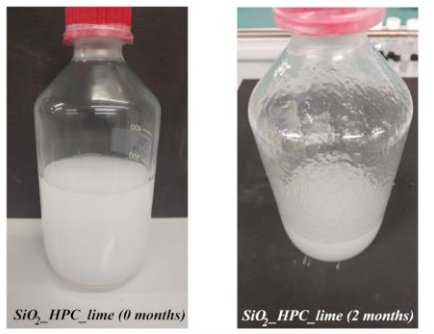

Figure 7.1 - Visual observation of a gel-like phase in the ternary system *SiO₂_HPC_lime* after two months from reparation

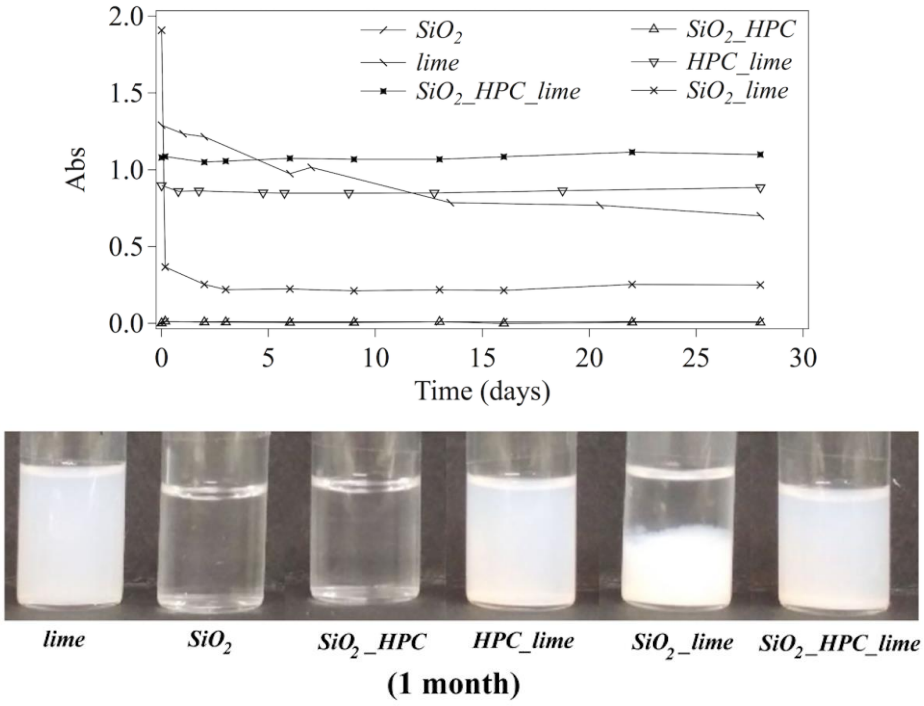

Figure 7.2 - Turbidimetric analyses performed on *lime*, *SiO₂*, *SiO₂_HPC*, *HPC_lime*, *SiO₂_lime*, and *SiO₂_HPC_lime*, over one month (top); visual inspections of the *SiO₂_HPC_lime* system as prepared, and after one month from preparation (bottom)

The small size of the silica nanoparticles makes both *SiO_2* and *SiO_2_HPC* appear transparent, hence no useful information could be obtained from the turbidimetry on those systems. However, in both cases no agglomeration or sedimentation of the particles was observed macroscopically over months (Figure 7.2).

Lime has a good turbidimetric stability over 4 weeks, and visual inspection showed that the particles dispersion does not settle even after months, confirming that nanoparticles of $Ca(OH)_2$ are stably dispersed in short chain alcohols, as largely reported in the literature (Poggi et al. 2016). The presence of hydroxypropyl cellulose in the dispersion increases its stability (*HPC_lime* > *lime*). This can be explained considering that HPC increases the system's viscosity, promoting the stability of the dispersed particles, despite the presence of larger agglomerates (highlighted by DLS, see below). As expected, for the poorly stable SiO2_lime system the absorbance drops from ca. 2 to 0.2 in less than one day.

The absorbance of the ternary system (*SiO_2_HPC_lime*) does not change over 4 weeks, as expected for systems containing HPC, confirming the stabilizing role of *Klucel*®-G in the formulation, which mediates the interaction between the silica and the lime through physical interposition of the fibers and by shielding the surface charges.

7.1.2. pH measurements

The pH of the *SiO_2* aqueous dispersion was measured using a glass electrode pH-meter, after dilution of the original product Levasil CS40-213, and the average of three measurements is ca. 7. The other systems are not reported as they are found in ethanol or ethanol-water blends. Measurements on the liquid medium of the ternary formulation gave values higher than 12.

7.1.3. Dynamic light scattering (DLS): particle size and ζ potential

To further investigate the components' behavior and their mutual interactions, the ζ-potential and particle size of the single components (*SiO_2, lime*), of the binary systems, and of the ternary system were then analyzed, and the results are reported in Table 7.1. The reported values are those of the as prepared samples. The CONTIN method was used to fit the autocorrelation functions, and the data are intensity-weighted. The mean particle size and relative variance (*i.e.* ratio of variance to the square of the mean, which is a measure of the polydispersity of diffusion coefficient, and is often represented as a polydispersity index) are reported. The main populations of multimodal distributions are also indicated.

In the case of *SiO_2* and *lime*, the data are in agreement with the literature (Graf et al. 2012; Poggi et al. 2014, 2016) and the information provided by producers: the silica nanoparticles (monodisperse spheres) exhibit in water a negative ζ-potential close to -30 mV, indicating a stable colloidal system due to electrostatic repulsion, and an average hydrodynamic diameter of 33 nm with a relative variance of 0.03.

The synthesized $Ca(OH)_2$ nanoparticles (hexagonal platelets) in ethanol have a positive ζ-potential of ca. 50 mV, consistent with the good stability of the system, and a mean particle size of 214 nm (relative variance of 0.16). This in agreement with the presence of two main populations centered at ca. 15 and 175 nm. According to the literature, the thickness of the platelets is 20-30 nm (Poggi et al. 2014).

When the components are in the (4:1) ethanol-water blend, some differences are noted in the ζ-potential and size of the particles, with respect to the systems in the pure media. Namely, the ζ-potential of silica nanoparticles in the blend (*SiO_{2T}*) has a slightly higher negative value, as expected from the fact that the dielectric constant of the dispersing medium (*i.e.* the blend) is lower than that of

water (Åkerlöf 1932; Moriyoshi et al. 1990). The particles' size is comparable with that of SiO_2, but the higher relative variance (0.19) indicates the presence of some aggregates. In the case of $Ca(OH)_2$ nanoparticles, passing from an ethanol dispersion to the blend ($lime_T$), the dielectric constant increases, and a lower positive ζ-potential is found. The particles' size increases, which can be explained considering that water molecules are known to bridge the hydroxide platelets, leading to the formation of aggregates (Gregory 1987; Baglioni et al. 2015).

The system *SiO_2_lime* could not be analyzed by DLS, as the interaction of the silica and $Ca(OH)_2$ nanoparticles, whose surface charge is of opposite sign, causes the formation of aggregates, and macroscopic phenomena of flocculation and sedimentation of the particles, which occur completely within 24 hours from the preparation of the binary system.

The binary systems *SiO_2_HPC* and *HPC_lime* have low ζ-potentials, conceivably related to the presence of hydroxypropyl cellulose. In the literature it is reported that surface adsorption of cellulose ethers (HPC; HEC) onto charged particles resulted in the decrease of ζ-potential, close to zero (Delgado 2001; Bouville and Deville 2014), and reduced the agglomeration of the particles due to the formation of a steric barrier. *SiO_2_HPC* shows two different size populations (ca. 35 and 160 nm), with mean particles' size of ca. 95 nm and relative variance of 0.46, which can be explained by the presence of a layer of HPC adsorbed on the surface of the silica particles (Berthier et al. 2011). In the case of *HPC_lime*, two population sizes are observed, with mean dimensions of 945 nm and relative variance of 0.25.

The ternary system *SiO_2_HPC_lime* exhibits a ζ-potential close to zero, as expected for the aforementioned considerations. The system shows two main populations with size of ca. 300 and 1050 nm, with a mean diameter of 941 nm and a relative variance of 0.16. This can be explained taking into account the

formation of agglomerates of silica and $Ca(OH)_2$ nanoparticles, and the adsorption of HPC on the agglomerates.

It is important to notice that the size of the agglomerates is compatible with the reported average pore size of adobe. In fact, adobe bricks have pore size of micrometric scale, up to a few mm, with porosity values of 20-40% (Brown et al. 1979; Hamiane et al. 2016).

System	**Medium**	**ζ-potential (mV ± SD)**	**Particle Size**		
			Mean size (nm)	**Rel. Var.**	**Distribution**
SiO_2	H_2O	-29 ± 7	33	0.03	Monomodal, narrow
lime	EtOH	53 ± 7	214	0.16	Multimodal, main populations at ca. 15 and 175 nm
SiO_{2T}	H_2O/EtOH (1:4)	-43 ± 12	38	0.19	Monomodal, narrow
$lime_T$	H_2O/EtOH (1:4)	41 ± 3	520	0.81	Monomodal, broad
SiO_2 _lime	H_2O/EtOH (1:4)	n/a	n/a	n/a	Formation of micron-sized aggregates
SiO_2_HPC	H_2O/EtOH (1:4)	-1 ± 11	95	0.46	Multimodal, main populations at ca. 35 and 160 nm
HPC_lime	H_2O/EtOH (1:4)	-1 ± 8	945	0.25	Multimodal, main populations at ca. 130 and 960
SiO_2_HPC_lime	H_2O/EtOH (1:4)	-3 ± 9	941	0.16	Multimodal, main populations at ca. 300 and 1050

Table 7.1 - ζ-potential and particle size data of the components and composite formulations, obtained by dynamic light scattering measurements

7.1.4. Transmission electron microscopy (TEM)

Transmission Electron Microscopy (TEM) was also used to observe the air-dried samples. Figure 7.3 (a and b) shows the two nanoparticles dispersions: the silica nanoparticles in the *SiO_2* system have dimensions of 25-35 nm, and the calcium hydroxide nanoparticles in the *lime* system have dimensions ranging from tens to a a few hundreds nanometers, consistently with the DLS data.

The *SiO_2_lime* system (Figure 7.3c) show the presence of spherical particles with size ranging from 20 to 100 nm corresponding to the SiO_2 component; some of the particles are surrounded by sub-spherical formations whose size ranges from 200 nm up to 1 μm. We hypothesised that such agglomerates (highlighted by arrows in Figure 7.3c) might indeed result from the initial interaction of silica and lime nanoparticles to possibily form CSH phases. The $Ca(OH)_2$ nanoparticles have undergone carbonation during the air-drying carried out prior to TEM analysis, hence the reaction between SiO_2 and $Ca(OH)_2$ might have been here arrested at early stages.

TEM observations of the *SiO_2_HPC* system (Figure 7.3d) show the presence of nanospheres of about 30 nm, which stack into chains or groups of 200-400 nm, in fair agreement with DLS data. The formation of bigger clusters (500 nm) of particles can be explained considering that the nanoparticles cluster during air-drying prior to TEM analysis.

Consistently with DLS, TEM analysis of the *HPC_lime* (Figure 7.3e) shows the presence of spherical sub-micron sized objects, which in some cases are neighboured by spherical or fibrous clusters. Moreover, the presence of some hexagonal or cubic shaped objects (ca.1 μm) suggests that carbonation of $Ca(OH)_2$ took place during air drying of the samples.

Figure 7.3 f, g shows nearly spherical or elongated agglomerates of about 1 μm, formed by the interaction of nanoparticles (less than 100 nm) and fibrous

structures, in the ternary system *SiO_2_HPC_lime*. The interaction results in tightly agglomerated structures, as opposed to those observed in the TEM analysis of the *SiO_2_lime* system.

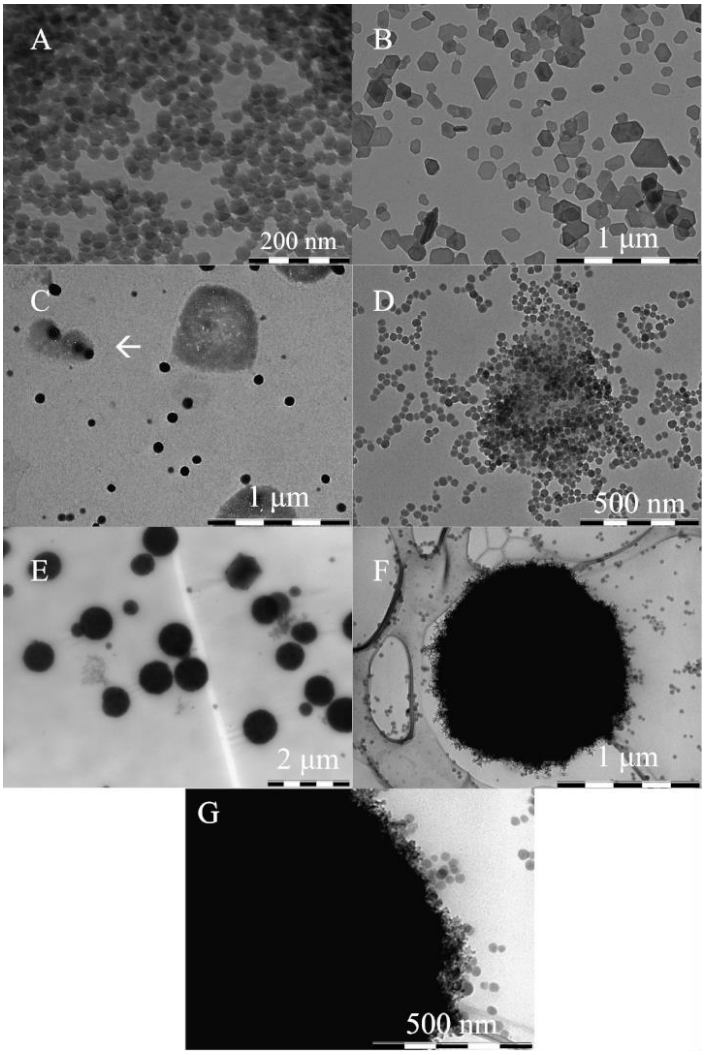

Figure 7.3 - TEM images of: (a) the silica nanoparticles (*SiO_2*), (b) the $Ca(OH)_2$ nanoparticles (*lime*), (c) the binary sistem *SiO_2_lime*, (d) the binary sistem *SiO_2_HPC*, (e) the binary sistem *HPC_lime*, and (f, g) the ternary system (*SiO_2_HPC_lime*)

7.1.5. Attenuated Total Reflectance Fourier Transform Infrared Spectroscopy (ATR-FTIR)

In order to gain information on the interaction between $Ca(OH)_2$ and silica nanoparticles, namely on the formation of CSH phases, ATR-FTIR and XRD analyses were performed on the ternary system *SiO_2_HPC_lime*.

ATR-FTIR analyses were performed on the formulation as prepared, and after 6 days, 9 days and 2 months from preparation (Figure 7.4), on air-dried and grinded samples.

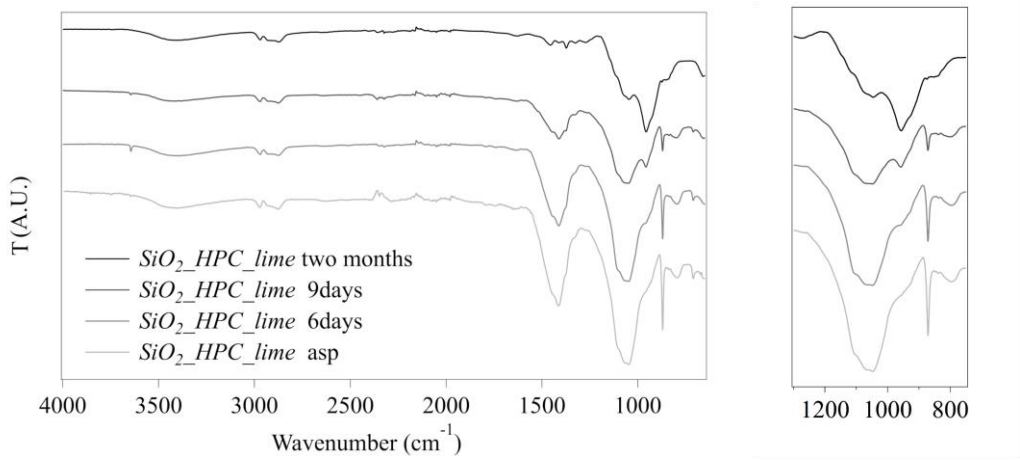

Figure 7.4 – ATR-FTIR spectra of air-dried ternary system *SiO_2_HPC_lime* as prepared ("asp"), and 6 days, 9 days and two months after preparation

The broad band centered at 3400 cm^{-1} and a small band at 1650 cm^{-1}, which are present in all the FTIR spectra of *SiO_2_HPC_lime*, are assigned to the stretching and bending of the hydroxyl groups of HPC, residual -OH groups in silica, and adsorbed water.

The characteristic peak around 3650 cm^{-1} (OH stretching) indicates the presence of calcium hydroxide. The latter is partially converted into calcium carbonate through reaction with atmospheric CO_2, during air-drying of the sample (Rodriguez-Navarro et al. 2013; Poggi et al. 2016; Samanta et al. 2016), as indicated by the presence of bands at 1400-1500 (ν_3 asymmetric CO_3 stretching), 876 (ν_2 asymmetric CO_3 bending), and 713 cm^{-1} (ν_4 symmetric CO_3 bending) (Plav et al. 1999; Gunasekaran et al. 2006), which are present in the spectra collected on the as-prepared formulation and after 6 and 9 days from preparation. Calcium hydroxide and also calcium carbonate signals are absent in the spectrum collected after two months from preparation.

The bands between 2970 and 2870 cm^{-1} (C–H stretching) in the four spectra can be ascribed to HPC. Bands between 1460-1270 cm^{-1} (C=C stretching) are also ascribable to HPC; while the band of HPC at 1075 cm^{-1} (C–O stretching) (Sudarsan Reddy, K., Prabhakar, M.N., Madhusudana Rao, K., Suhasini et al. 2013; Eguchi et al. 2017) overlaps with the absorption of silica at 1050 cm^{-1} (internal Si-O-Si asymmetric stretching), that also displays a band at 800 cm^{-1} (Si-O-Si symmetric stretching). The shoulder at 950 cm^{-1} is assigned to Si-O stretching of surface Si-OH groups (Marzouqa et al. 2012; Premaratne et al. 2013).

Interestingly, the spectra of *SiO_2_HPC_lime* collected after 9 days and, more evidently, after two months from preparation, show a marked increase of the band at 950 cm^{-1} and a correspondent decrease of the band at 1050 cm^{-1}, indicating the breakage of Si-O-Si bonds and the formation of silanol groups. The phenomenon was also observed in the binary system *SiO_2_lime*. This suggests the depolymerization of silica occurred, which is reported as finger-printing of calcium silicate hydrate (CSH) formation (Baltakys et al. 2007; Lin et al. 2010; Grangeon et al. 2016). Indeed, it is reported that the hydration reaction between $Ca(OH)_2$ and silica in water (Eq 7.1 and Figure 7.5a) starts with the dissolution

of $Ca(OH)_2$ (Figure 7.5b) followed by the breaking of the Si-O-Si covalent bonds by the released OH groups (Eq 7.2 and Figure 7.5c); then the Ca^{2+} ions bridge the depolymerized silica, forming the basic units of CSH (Eq 7.3 and Figure 7.5d) (Lin et al. 2011).

$$xCa(OH)_2 + xSiO_2 + zH_2O \rightarrow xCaOSiO_2 \cdot (x+z)H_2O(CSHgel) \quad \text{Eq. 7.1}$$

$$\equiv Si - O - Si \equiv + OH^- \rightarrow \equiv Si - O^- + HO - Si \equiv \quad \text{Eq. 7.2}$$

$$\equiv Si - O^- + HO - Si \equiv + Ca^{2+} + OH^- \rightarrow \equiv Si - O - Ca - O - Si \equiv + H_2O \quad \text{Eq. 7.3}$$

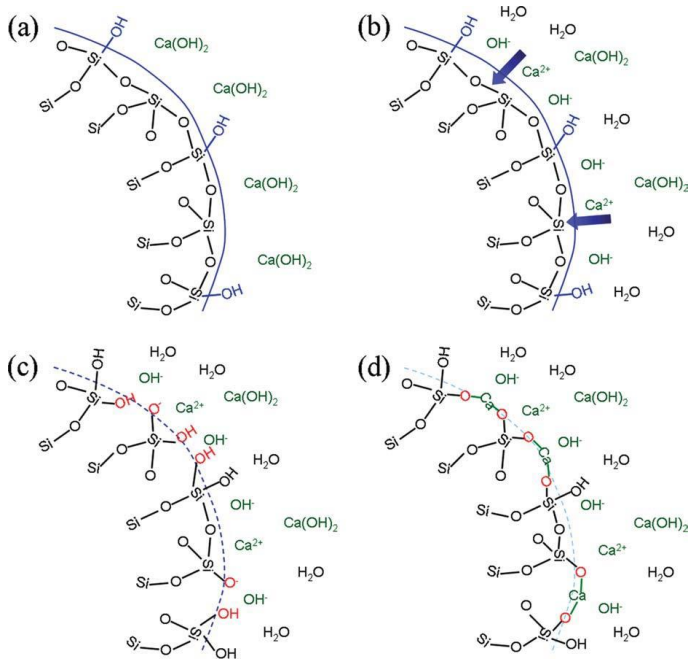

Figure 7.5 - Schematic illustration of the reaction between silica and calcium hydroxide in water

After two months, the absence of calcium hydroxide and carbonate bands in the spectrum indicates the complete reaction of calcium hydroxide and silica nanoparticles.

7.1.6. X-ray diffraction (XRD)

XRD analysis was carried on the ternary system as prepared, and two months after preparation (Figure 7.6).

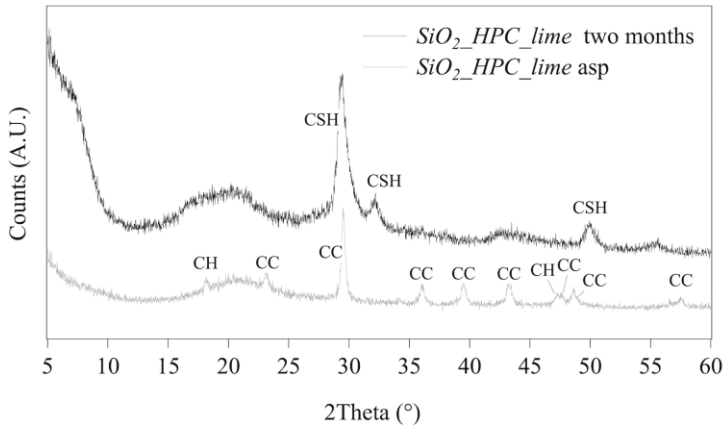

Figure 7.6 - XRD patterns of air-dried ternary system *SiO_2_HPC_lime* as-prepared (grey line) and two months after preparation (black line)

In the case of *SiO_2_HPC_lime* dried as-prepared (grey line), the peaks of calcium hydroxide (CH) and calcium carbonate (CC) are observed, along with a broad band centered around 20°, ascribable to the co-presence of amorphous silica (reported at 22° in the literature (Premaratne et al. 2013)) and HPC (band at 17° (Sudarsan Reddy, K., Prabhakar, M.N., Madhusudana Rao, K., Suhasini et al. 2013)). In *SiO_2_HPC_lime* dried two months after preparation (black line), three peaks are observed at 29.5°, 32° and 50°, indicating the formation of CSH

(Baltakys et al. 2007; Grangeon et al. 2013a, b); the broad band at 20° is ascribable to HPC or unreacted silica.

Basal peaks at less than 10° are reported in the literature for the calcium silicate hydrate mineral tobermorite, but their intensity can vary depending on the type of CSH phase, up to being barely or not observable (Wang et al. 2014; Guo et al. 2017).

7.1.7. Scanning electron microscopy coupled with energy dispersive X-ray spectroscopy (SEM)

SEM images of the *SiO_2* and *lime* components are reported in Figure 7.7.

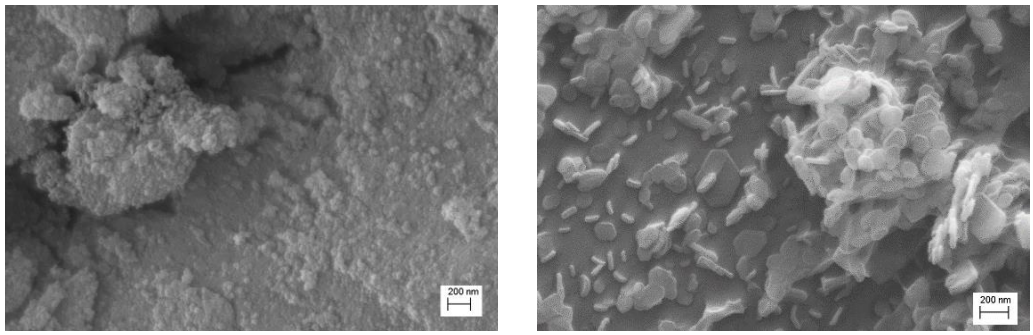

Figure 7.7 - SEM images of the air-dried single components SiO_2 and lime, (secondary electron images with magnitude of a) 69kX and b) 88kX)

The SEM investigation of the ternary system after two months from preparation, showed the presence of a homogeneous porous network of crumpled foils (Figure 7.8), a morphology typically produced by the formation of CSH from the alkaline activation of nanosilica (Lin et al. 2010; Tajuelo Rodriguez et al. 2015). The EDX analysis confirmed that calcium and silicon are homogeneously distributed across the foiled substrate.

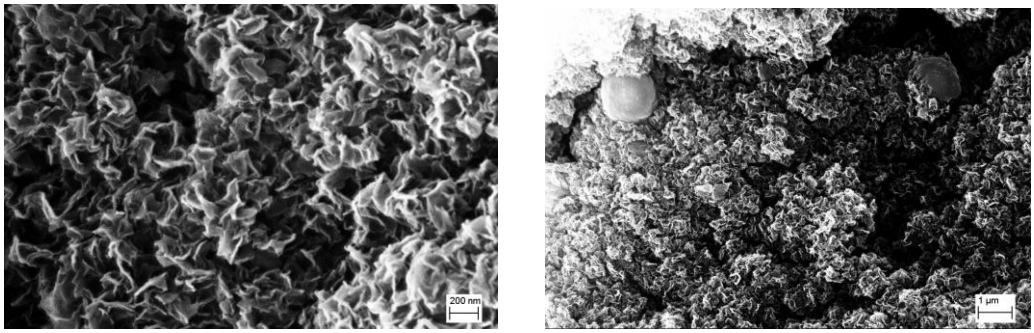

Figure 7.8 - SEM images of the ternary system *SiO_2_HPC_lime*, air-dried after two months from preparation (secondary electron images with magnitude of a) 21kX and b) 87Kx)

Overall, the compared analysis performed on the composite systems and single components, highlighted that the reaction of silica nanoparticles and calcium hydroxide in the presence of water leads to the desired formation of CSH in the ternary system (after ca. 1 week from the preparation). Therefore, it was hypothesize that this formulation could provide mechanical strengthening when applied onto the adobe samples.

After soil characterization, the ternary formulation was applied onto adobe mock-ups and the consolidating power was assessed by characterization of untreated and treated samples, as described below.

7.2. Adobe soil characterization

Before treatment, the soil of the adobe bricks was characterized, and the results are shown in Table 7.2. Figure 7.9 shows the grain size distribution of the adobe soil obtained by granulometric analysis. The soil was classified as silty sand (SM), according to the Unified Soil Classification System (USCS). The low clay percentage explains the poor mechanical properties of the samples, as expected

considering that the bricks were prepared using local soil from the construction area (Morelos region, Mexico), which has a high content of sand. The XRD analysis of the soil revealed a composition consisting predominantly of plagioclases (albite-anorthite) and, to a lesser extent, quartz and mica. Straw fibers were found included in the bricks. The organic content of the soil was found to be ca. 0.3%, and the carbonates content ca. 0.5%.

Granulometry				**Atterberg Limits**			**Org. content (%)**	**Carb. content (%)**
Clay (%) d<0.002 mm	**Silt (%) d 0.002-0.06mm**	**Sand (%) d 0.06-2mm**	**Gravel (%) d>2mm**	**LL (%)**	**PL (%)**	**PI (%)**		
0.1	23.5	74	2.5	33	26	7	0.3	0.5

Table 7.2 - Granulometric characterization of the soil, Atterberg limits (Liquid Limit, LL; Plastic Limit, PL; Plasticity Index, PI), organic content and carbonate content

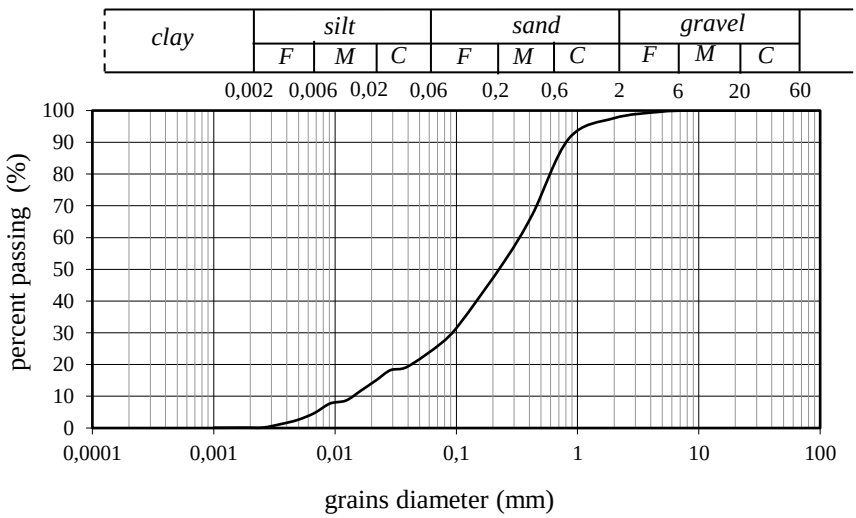

Figure 7.9 - Grain size distribution of the adobe soil

7.3. Adobe mock-ups characterization

7.3.1. Colorimetric measurements

Visual observations of the samples, up to two months after the treatment, did not highlight significant color variations produced by the application of the formulation *SiO_2_HPC_lime*, as compared to the non-treated samples (see Figure 7.15 in section 7.3.3). Colorimetry measurements were then performed, and the analyses showed an average color difference ΔE* of 2.5 ± 0.5, which is within the threshold generally adopted for the treatment of works of art, *i.e.* $\Delta E^* = 3$ (Berns and Reiman 2002).

7.3.2. Attenuated Total Reflectance Fourier Transform Infrared Spectroscopy (ATR-FTIR) and X-ray diffraction (XRD) and phenolphthalein test

The phenolphtalein test was used to assess the penetration of the calcium hydroxide nanoparticles found in the ternary system, as an indication of the depth reached by the whole formulation. The penetration depth is visually measured thanks to the intense purple color assumed by phenolphthalein at alkaline pH. A 0.1% solution of phenolphtalein was sprayed onto the surface of samples right after treatment. Cross sections of the samples were then cut, and a penetration of 3 mm was observed, which is consistent with that of nanolimes used elsewhere for the consolidation of stucco and adobe (Lanzón et al. 2017). The penetration depth can be affected by several factors including the type of dispersing solvent and the environmental conditions during the treatment, and both backmigration and aggregation of the particles have been discussed as possible issues limiting the penetration (Croveri et al. 2004; Dei and Salvadori 2006; Ziegenbalg 2008;

D'Armada and Hirst 2012; Daehne and Herm 2013; Natali et al. 2014). While enhancing the penetration of consolidant particles remains an open topic in stone conservation, it must be noticed that adobe bricks are mainly affected by environmental erosion of the exposed surface, leading to powdering and loss of grains cohesion; thus, the protection of the outer layers up to some mm from the surface was deemed as an acceptable result at this preliminary stage.

FTIR analyses were carried out on the treated samples at different depths from the surface, two months after treatment. Figure 7.10 shows the spectrum of a non-treated samples (grey line) and a treated sample (black line), that show similar profile, except for the bands at about 1500-1300 cm^{-1}, ascribable to HPC or calcium carbonate, and the small carbonate peak at 876 cm^{-1}. The characteristic peak of calcium hydroxide at ca. 3645 cm^{-1} is not detected in the treated adobe, suggesting that the hydroxide had completely reacted, possibly through formation of CSH and carbonation. However, owing to the intense bands of the silica originally found in the adobe samples, it was not possible to observe an intensity inversion between the band at 950 cm^{-1} (Si-O stretching of surface Si-OH groups) and that at 1050 cm^{-1} (stretching of Si-O-Si bonds), previously ascribed to the depolymerization of the nanosilica particles in *SiO_2_HPC_lime* and the formation of CSH.

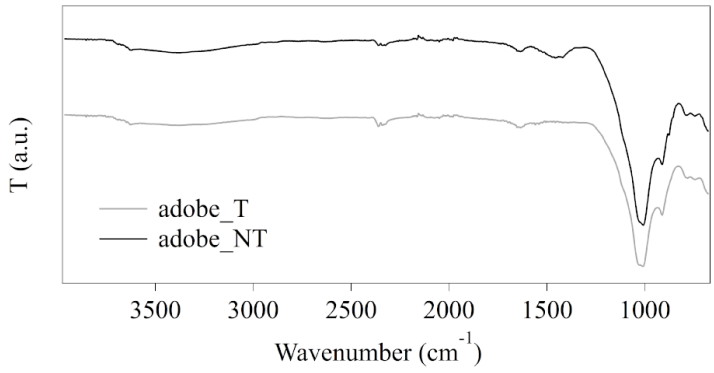

Figure 7.10 - FTIR pattern of untreated (NT, grey line)

and treated adobe (T, black line)

Instead, the XRD pattern of powders collected from the treated adobe samples up to 3 mm from the surface, showed peaks at 31.5°, 33.7° and 50.1° (Figure 7.11).

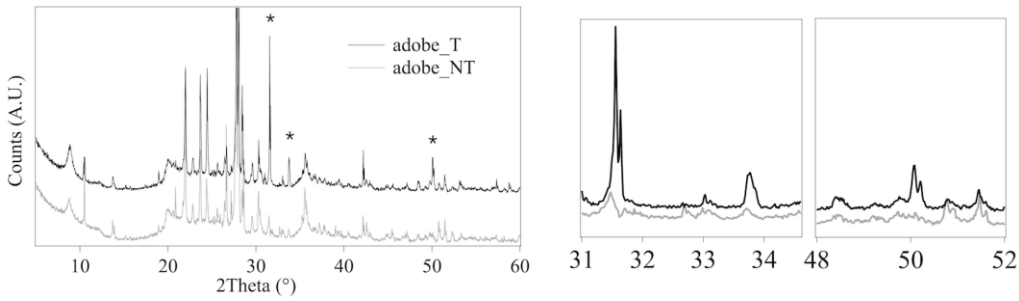

Figure 7.11 - XRD pattern of untreated (NT, grey line) and treated adobe (T, black line); the insets (31-34° and 48-52°) highlight the peaks at 31.5°, 33.7° and 50.1° found in the patterns of the treated adobe samples, which were assigned to CSH phases

Interestingly, these peaks exhibit a slight shift to higher angles, and are more resolved, as compared to those observed when CSH is formed in the ternary formulation (see Figure 7.6), which might suggest the formation of different calcium silicate hydrate phases, when the process takes place within the pores of the adobe samples. According to the literature, the calcium silicate hydrate minerals tobermorite ($Ca_5Si_6O_{16}(OH)_2 \cdot 4H_2O$) and jennite ($Ca_9Si_6O_{18}(OH)_6 \cdot 8H_2O$) show diffraction patterns with maxima in the 28.8-33.2° region and at 50.7°, with sharper or broader peaks depending on the degree of order of the phases and the size of the crystallites in the layer plane (Grangeon et al. 2013b). It must be noticed that when the formulation sets in the pores of adobe, the original silica component of adobe is present along with the SiO_2 nanoparticles, and a lower Ca/Si ratio is present than when CSH formation takes

place entirely in the formulation environment, which might play a role in the formation of CSH phases with different characteristics.

The reaction between SiO_2 and $Ca(OH)_2$ nanoparticles is known to depend on several factors, including the phase composition and size of the silica nanoparticles, the $Ca(OH)_2$ content, and the liquid to powder (L/P) ratio of the system (Lin et al. 2011). A key factor is the reactivity of the nanosilica with $Ca(OH)_2$, which is expected to be enhanced when the hydroxide particles have high surface area. In the presence of water, the SiO_2 nanoparticles come in contact with a saturated $Ca(OH)_2$ solution, which acts as an activator for the breakage of the Si-O-Si bonds, followed by the formation of the cementing phase. It has been shown that when the L/P is 1 mL/g, and for a Ca/Si ratio of 3 (using nanosilica and micron-sized lime particles), the setting of CSH takes place between 1 and 2 hours from activation (Lin et al. 2011). In our case, the ternary system was applied on the adobe samples 6 days after its preparation: the samples were soaked in the system for 1 day, and then left curing at room conditions (T = 23°C, RH = 50%). Drying of the samples took 2 more days. The permanence time of the formulation within the pores of adobe seemed to be enough to allow the formation of some CSH phases. HPC is expected to regulate water release, promoting CSH formation; in fact, water proton nuclear magnetic resonance relaxation experiments showed that cellulosic additives interact with water, determining its availability in the cement hydration process. It was found that cellulosic polymers delay the setting process while, on the other hand, they enhance the hydration efficiency. This was explained considering the hydrophilic character of the cellulose derivative, which is able to bind water, adsorb on silicate grains, and then distribute water homogeneously over the solid phase (Ridi et al. 2011, 2013; Del Buffa et al. 2016). The presence of the cellulosic polymers affects both the nucleation and growth rates of the hydrated phases; namely, the nucleation rate is reduced (even though the energy threshold to form

CSH nuclei remains unaltered), while the growth rate increases in the presence of the polymers (the energy threshold to start the growth of the nuclei is lowered)(Ridi et al. 2013).

7.3.3. Physico-mechanical tests

The Table 7.3 shows the result obtained with the peeling test, abrasion test, wet/dry cycles, capillary sorption measurements and drilling test on non-treated adobe (NT) and adobe treated with the ternary formulation *SiO_2_HPC_lime* (T).

	Total decohesion index after 3 peels (mg/cm^2)	**Total abrasion coefficient after 3 cycles (cm^2/g)**	**Total weight loss after 7 wet/dry cycles (%)**	**Capillary sorption coefficient ($mg/cm^2 \cdot s^{1/2}$)**	**Drilling resistance (N)**
Adobe_NT	3.1 ± 0.6	67 ± 3	4.41 ± 0.12	18.4 ± 0.2	0.88 ± 0.31
Adobe_T *SiO_2*_lime_*HPC*	1.2 ± 0.2	215 ± 7	0.74 ± 0.04	18.9 ± 0.4	1.07 ± 0.28

Table 7.3 - Characterization of adobe samples, untreated (NT), and treated with *SiO_2_HPC_lime* (T)

The peeling test or scotch tape test showed a remarkable decrease of the decohesion index for the adobe samples treated with *SiO_2_HPC_lime*. The positive effect was observed even when the peeling was repeated on the same portion of the sample's surface, up to three times. The average values of each of the three peeling cycles are shown in Figure 7.12; the total values after the three cycles are reported in Table 7.3.

Further proof of the consolidation effect was obtained with abrasion tests and wet/dry cycles, performed to check the response of the treated samples to harsh environmental conditions (wind and water erosion). The values reported in Table 7.3 and Figure 7.13 show a higher abrasion coefficient for the samples treated with *SiO_2_HPC_lime*, indicating an improved resistance to abrasion. The average values of each cycle, obtained from tests on three different samples, are shown in the graph; the total values after the three cycles are reported in the table.

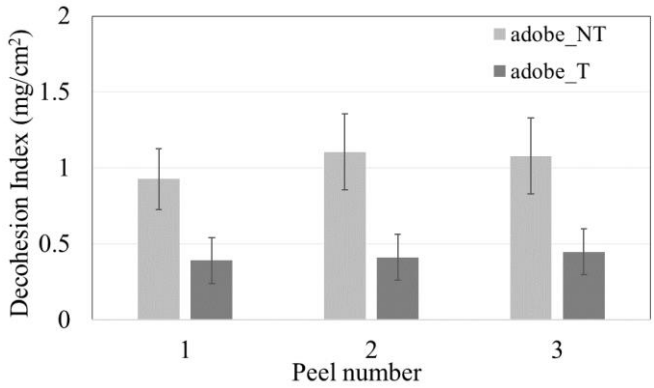

Figure 7.12 - Decohesion index (obtained with the scotch tape test) of adobe samples, untreated (NT), and treated with *SiO_2_HPC_lime* (T)

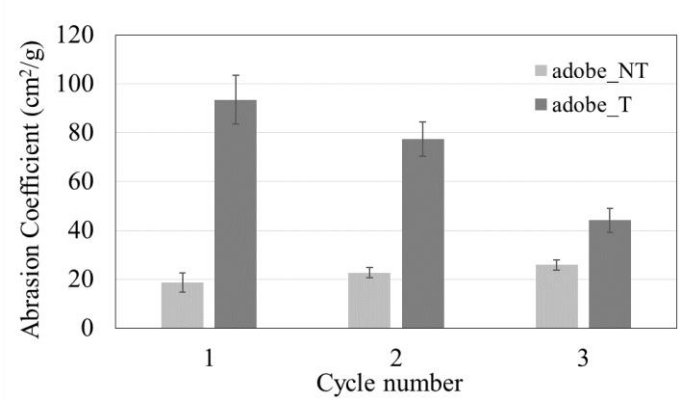

Figure 7.13 - Abrasion coefficient of adobe samples, untreated (NT), and treated with *SiO_2_HPC_lime* (T)

The average weight losses of untreated and treated samples caused by wet/dry cycles are shown in Figure 7.14 , and the total weight loss after the seven cycles is reported in Table 7.3. The results indicate that the application of the *SiO_2_HPC_lime* system resulted in a decrease of mass loss upon repeated immersions in water, indicating that consolidation took place. The capillary sorption coefficient obtained from water sorption measurements did not significantly change following the treatment of the samples (see Table 7.3), indicating that the internal porosity of adobe was not dramatically altered or blocked. Lastly, drilling resistance measurements showed only a slight increase of the resistance for the treated samples (see Table 7.3).

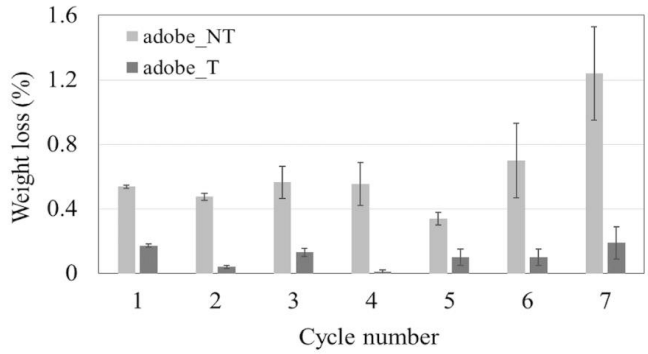

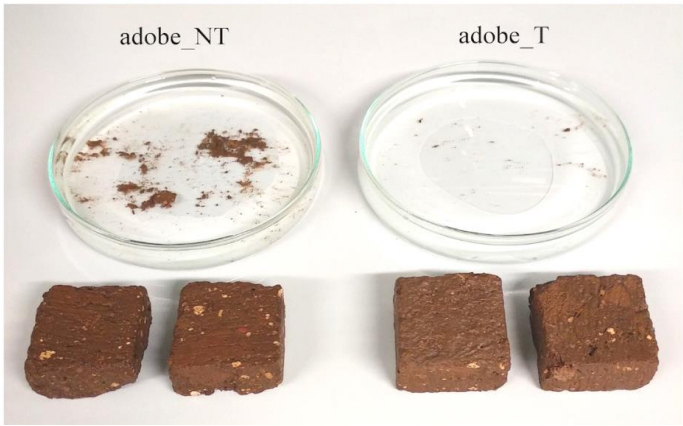

Figure 7.14 - Weight loss of adobe samples, untreated (NT), and treated with *SiO_2_HPC_lime* (T), during wet/dry cycles (top); the adobe after the seventh

wet/dry cycle: the untreated samples lost a significant amount of material, as opposed to those treated with the *SiO_2_HPC_lime* formulation (bottom)

It is important to notice that scotch tape test, abrasion test and wet/dry cycles revealed that some consolidation was obtained also applying only HPC (system *HPC_T*) or the two binary systems containing HPC (*HPC_lime* and *SiO_2_HPC* system), as reported in Table 7.4, while the application of only *SiO_2* and *lime* (system *SiO_{2T}* and *$lime_T$*), did not produce any significant consolidation effect. The system *SiO_2_lime* is not applicable, as the two components flocculate in short times when combined without HPC.

Namely, treatment with *HPC_T*, *HPC_lime* and *SiO_2_HPC* produced respectively total decohesion indexes of 1.9 ± 0.3, 1.9 ± 0.3 and 1.8 ± 0.3 mg/cm^2, and total abrasion coefficients of 152 ± 5, 137 ± 6 and 145 ± 5 cm^2/g. Besides, treatment with *HPC_T* produced a total weight loss after 7 wet/dry cycles of 2.02 ± 0.05 %. Moreover, in these cases, colorimetric analyses highlighted values of ΔE* higher then 3 (generally adopted threshold for the treatment of works of art), as reported in Table 7.4 and showed in Figure 7.15.

	Color Change ΔE* (in respect of NT)	**Total decohesion index after 3 peels (mg/cm^2)**	**Total abrasion coefficient after 3 cycles (cm^2/g)**	**Total weight loss after 7 wet/dry cycles (%)**
Adobe_NT		3.1 ± 0.6	67 ± 3	4.41 ± 0.12
Adobe_T *SiO_2*_lime_*HPC*	2.5 ± 0.5	1.2 ± 0.2	215 ± 7	0.74 ± 0.04
Adobe_T *SiO_2_HPC*	5 ± 1	1.8 ± 0.3	145 ± 5	NM
Adobe_T *HPC_lime*	13 ± 3	1.9 ± 0.3	137 ± 6	NM
Adobe_T *HPC_T*	4 ± 1	1.9 ± 0.3	152 ± 5	2.02 ± 0.05

Table 7.4 - Characterization of adobe samples, untreated (NT), and treated (T) with *SiO_2_HPC_lime*, *SiO_2_HPC*, *HPC_lime*, and *HPC_T*. (NM = not measured)

Figure 7.15 - Visual observations of the adobe samples

Therefore, it was concluded that the presence of hydroxypropyl cellulose led to some increase in surface cohesion, but further resistance was obtained by the application of the ternary system, without producing significant color variations, confirming the importance of combining the three components.

Chapter 8 – Results and discussion: carbonation kinetics of nanolimes

8.1. Study of the carbonation kinetics of nanolimes

Four alcoholic dispersions of $Ca(OH)_2$ nanoparticles were selected as widely used standards for stone consolidation, and their carbonation kinetics was investigated as a function of temperature, under strictly controlled environmental conditions. FTIR spectroscopy was used to monitor the decrease of calcium hydroxide characteristic peak (3645 cm^{-1} OH stretching) over time, and follow the calcium carbonate polymorphs evolution.
In the following paragraphs the applicability of the Boundary Nucleation and Growth Model to the carbonation kinetics of $Ca(OH)_2$ nanoparticles in air is discussed, and a description of the amorphous and crystalline carbonate phases is provided.

8.1.1. Generalized Boundary Nucleation and Growth Model

In order to select a kinetic model to describe the transformation of calcium hydroxide into calcium carbonate, we considered that the formation of ACC in the aqueous film reasonably occurs along the surface of the $Ca(OH)_2$ nanoparticles (at the solid-liquid interface); the products eventually cover the surface and fill the mesoporous structure formed by the particles' aggregation after alcohol evaporation. Overall, the process can be considered analogous to a phase transformation in a polycrystalline solid where nucleation occurs preferentially at the grain (particle) boundaries. Therefore, the generalized

Boundary Nucleation and Growth Model (BNGM) (Cahn 1956; Christian 2002) was adopted to describe the process kinetics. Previously, Thomas successfully applied this to the hydration kinetics of tricalcium silicate (C_3S), *i.e.* another process that involves dissolution-precipitation and the formation of hydration products on the surface of the C_3S particles, via boundary nucleation and growth (Taylor 1997; Garrault et al. 2006; Thomas 2007). Based on these considerations, a rigorous approach was followed, by first verifying the applicability of the generalized BNGM to describe the carbonation of the $Ca(OH)_2$ nanoparticles' dispersions: this enabled us evaluating the relevance of the single processes (nucleation, growth) on the overall kinetics; based on that, we could finally provide the best fit of the curves taking advantage of a "limiting case" of the BNG model. As described in Chapter 5, the reaction degree α versus time can be directly fitted using the generalized BNGM by using Eq. 8.1:

$$\alpha_t = \alpha_i \cdot \alpha_f \{1 - exp[-2k_G \int_0^t (1 - exp(-Y^e))dz]\} \qquad \text{Eq. 8.1}$$

Figure 8.1 shows a fitting obtained with the generalized BNGM (CE at 22˚C).

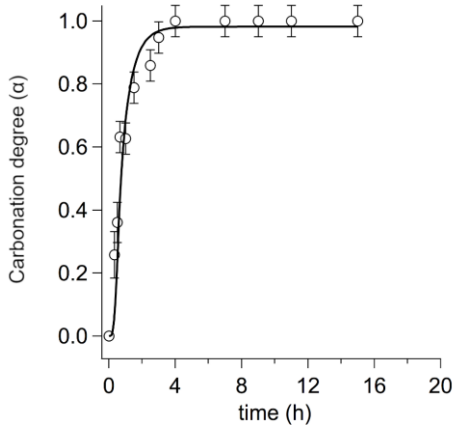

Figure 8.1 - Fitting of the carbonation curve of the CE system at 22°C, using the generalized BNGM

The fitting directly yields the two rate constants k_B and k_G, *i.e.* the rate at which the nucleated boundary area transforms, and the rate at which the porosities are filled with carbonation products (Thomas 2007; Del Buffa et al. 2016). Table 8.1 summarizes the values of k_B and k_G for CE, LE, CIP and LIP, at the three temperatures.

It is worth noting, though, that in many cases the fitting does not converge unless the k_B value is constrained (these cases are highlighted with a star in Table 8.1). In such cases we chose to constrain the kB value to the minimum necessary to make the fitting converge. These can be considered as the lowest possible estimations of kB. Nevertheless, kB is always higher than kG, indicating that nucleation proceeds at a faster pace with respect to growth.

SYSTEM NAME	**14ºC**		**22ºC**		**30ºC**	
	k_B	k_G	k_B	k_G	k_B	k_G
CE	0.66 ± 0.07	0.27 ± 0.03	1.58* ± 0.14	0.73 ±0.11	2.75 ± 0.45	0.74 ± 0.07
LE	0.96* ± 0.19	0.28 ± 0.03	1.4* ± 0.16	0.5 ± 0.04	1.46 ± 0.13	0.60 ± 0.07
CIP	0.90* ± 0.16	0.22 ± 0.03	1.66 ± 0.55	0.32 ± 0.03	2.10* ± 0.20	0.84 ± 0.09
LIP	0.74* ± 0.26	0.12 ± 0.01	1.05 ± 0.48	0.13 ± 0.01	1.55 ± 0.26	0.35 ± 0.03

*These values could be obtained only by constraining the k_B values to the minimum necessary to make the fitting converge

Table 8.1 - Rate constants (k_B [h^{-1}] and k_G [h^{-1}]) of the four systems at the three temperatures, directly obtained by fitting the experimental data to the generalized BNGM

The linear growth rate, G, and the nucleation rate I_B, can be calculated from k_B and k_G, using Eq. 8.2 and 8.3.

$$k_B = (I_B O_V^B)^{1/4} G^{3/4} \quad \text{Eq. 8.2}$$

$$k_G = O_V^B G \quad \text{Eq. 8.3}$$

The obtained I_B/G ratios are very large for all the considered systems and temperatures (e.g. ratios ranging from 10^4 to 10^7 $\mu m^{-1} h^{-2}$). According to Thomas, this indicates that the boundary regions are densely populated with nuclei, and transform completely early in the process. This means that the transformation does not depend on the nucleation rate, and mostly occurs by the subsequent thickening of slab-like regions of transformed product centered on the original boundaries (Thomas 2007). Under these conditions, a limiting case equation (Eq. 8.4) is used to describe the process kinetics, where the transformation rate decreases exponentially with time (Cahn 1956):

$$X = 1 - \exp[-2k_G t] \quad \text{Eq. 8.4}$$

8.1.2. Limiting case Boundary Nucleation and Growth Model

Therefore, the carbonation curves were fitted using Eq. 8.4.
Figure 8.2 shows a comparison between the generalized BNGM (A) and the BNGM limiting case (B) applied on CE system at 22°C.

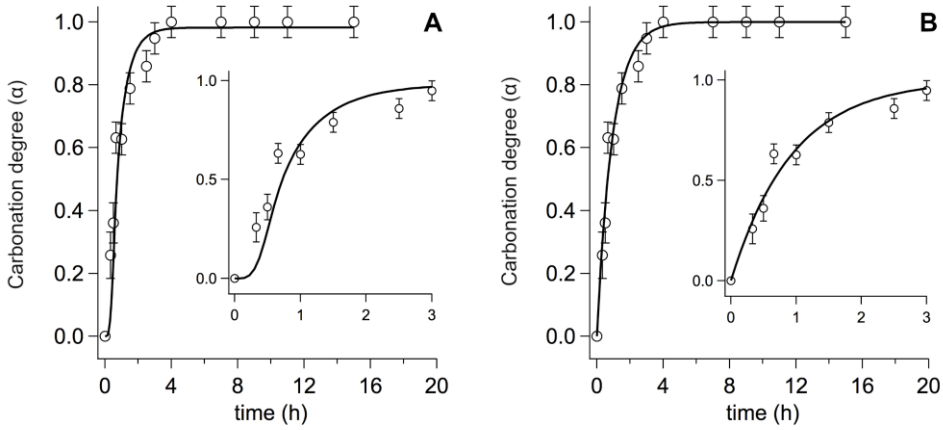

Figure 8.2 - Fitting of the carbonation curve of the CE system at 22°C, using (A) the generalized BNGM and (B) the limiting case BNGM. The insets highlight the different shape of the curves at the beginning of the kinetics (first 3 hours)

Indeed, the use of the BNGM limiting case allows for a good fitting of the data without using narrow constraints, differently from the application of the generalized model. As clearly shown in Figure 8.2 B, the fitting curve is exponential (independent on k_B), rather than sigmoidal (Figure 8.2 A). The demonstration provided here, *i.e.* that the kinetics is independent on the nucleation rate, corroborates and integrates the findings of other authors that employed either first order (Rodriguez-Navarro et al. 2016b) or pseudo-seond order (Montes-Hernandez et al. 2007, 2010; Rodriguez-Navarro et al. 2016b) deceleratory models to describe the carbonation kinetics of $Ca(OH)_2$ particles of different size (nano an sub-micro), in different environmental conditions. It must be noticed that none of these previous models addressed specifically the role of boundary nucleation and growth; namely, no values for the growth constant rate were provided in those works.

Fitting the curves under the limiting case BNGM directly yields the k_G values, which are reported in Table 8.2. The table also includes the *G* values (calculated from Eq. 4), and the ending time (t_f) of the $Ca(OH)_2$ transformation, *i.e.* when the absorption peak of $Ca(OH)_2$ centered at 3645 cm^{-1} (OH stretching) is no longer observable in the FTIR spectra of the nanoparticles' films.

	14°C			**22°C**			**30°C**		
	t_f	k_G	*G*	t_f	k_G	*G*	t_f	k_G	*G*
CE	5	0.23 ± 0.01	3.03 ± 0.28	4	0.53 ± 0.04	6.97 ± 0.88	3	0.67 ± 0.03	8.82 ± 0.84
LE	5	0.25 ± 0.01	3.47 ± 0.31	3	0.43 ± 0.02	5.97 ± 0.58	3	0.50 ± 0.03	6.94 ± 0.76
CIP	5	0.19 ± 0.01	2.50 ± 0.26	4	0.32 ± 0.02	4.21 ± 0.47	2.5	0.71 ± 0.03	9.34 ± 0.86
LIP	9	0.12 ± 0.01	3.00 ± 0.40	8	0.14 ± 0.01	3.50 ± 0.43	6	0.32 ± 0.01	8.00 ± 0.65

Table 8.2 - Parameters extracted from the limiting case BNGM fitting of the CE, LE, CIP, and LIP systems at the three considered temperatures (ending time (t_f) of the $Ca(OH)_2$ transformation, rate constant (k_G [h^{-1}]), and calculated linear growth rate (*G* [$nm \cdot h^{-1}$])), and from the Arrhenius plots for the four systems (activation energy, E_a [$kJ \cdot mol^{-1}$], and R^2)

As expected, for each system the conversion of $Ca(OH)_2$ nanoparticles into $CaCO_3$ is faster (*i.e.* higher k_G values) at higher temperatures. A representative example is shown in Figure 8.3, where the fitted carbonation curves of LIP display a higher slope passing from 14 to 22 and 30˚C (Figure 8.3 A-C).
Besides, increasing the temperature, the curves reach earlier the asymptotic plateau. At all temperatures, LIP exhibits k_G values lower than the other systems, and roughly double t_f values (see Table 8.3 and Figure 8.4). This was explained considering that the $Ca(OH)_2$ nanoparticles in LIP have larger dimensions (a bimodal distribution, with primary particles of 300-500 nm and larger aggregates

of about 1 μm) and lower surface area than the other systems; this results in a lower amount of boundaries available for the nucleation of $CaCO_3$, hence in a reduced reactivity during the carbonation process. At each temperature, CE, LE and CIP systems exhibit roughly the same t_f values, and the values of k_G of these systems are more similar to each other than to that of LIP. This highlights that the kinetic behavior is influenced by the preparation method of the particles' dispersions, as it determines the particles' size and surface area, which are comparable for the systems CE, LE and CIP (see Table 4.1 in Chapter 4).

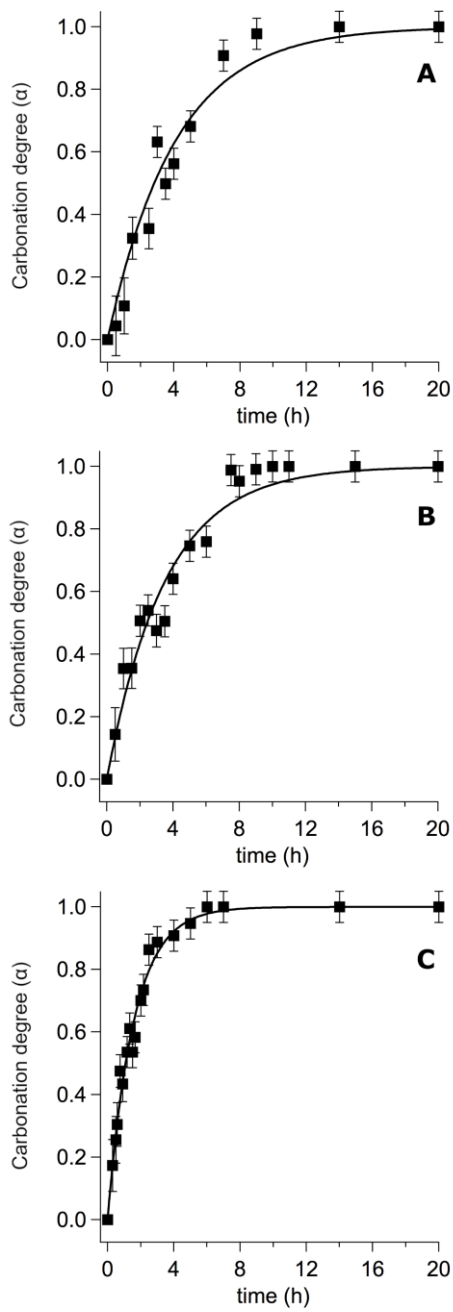

Figure 8.3 - Fitting of the carbonation curves of LIP at (A) 14°C, (B) 22°C, (C) 30°C, using the limiting case BNGM

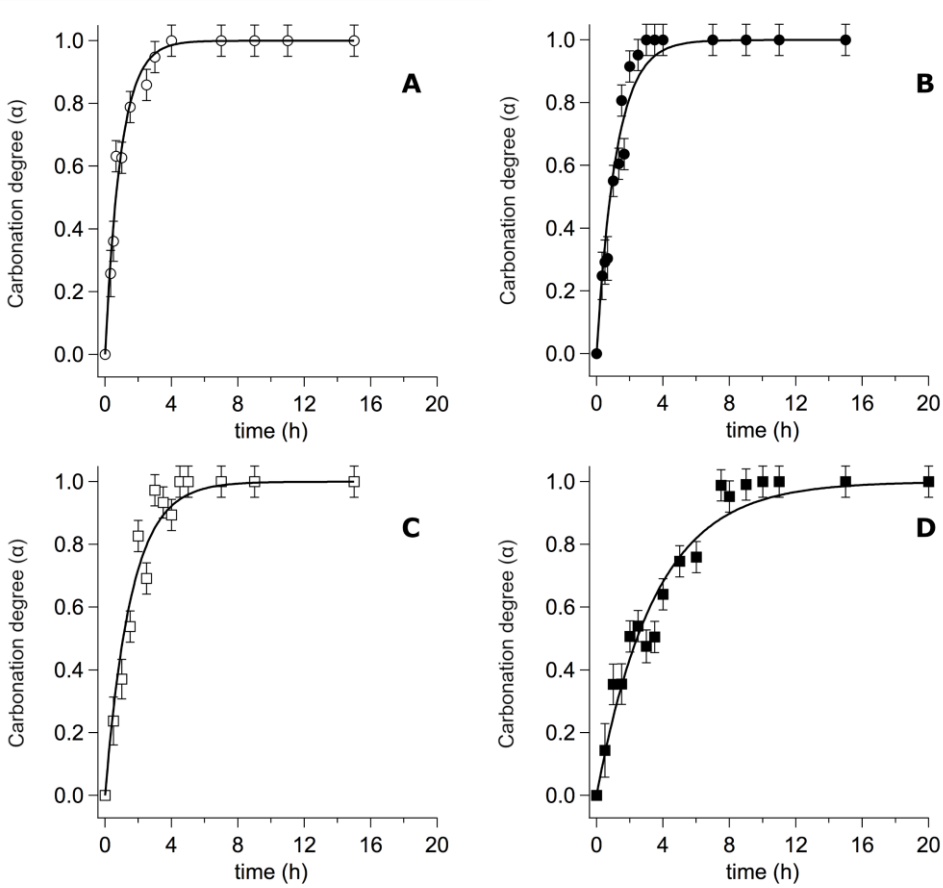

Figure 8.4 - Fitting of the carbonation curves at 22°C for (A) CE, (B) LE, (C) CIP, (D) LIP, using the limiting case BNGM

The linear growth rate (*G*) has comparable values for the four systems at 14˚C (*G* ~3 nm·h^{-1}) and 30˚C (*G* ~8 nm·h^{-1}), while at 22˚C the systems in ethanol have a *G* value that is 1.5-2 times higher than those in 2-propanol (*G* ~6-7 nm·h^{-1} for CE, LE; *G* ~4 nm·h^{-1} for CIP, LIP). The differences in *G*, observable at the intermediate temperature (22˚C), could be due to the role of the solvent in the formation of aggregates in the $Ca(OH)_2$ films. In fact, after the deposition of the nanoparticles' dispersions on the KBr pellets, alcohol evaporation leads to the formation of layers of stacked and aggregated particles. 2-propanol has a lower

dielectric constant than ethanol, which results in lower Debye lengths and reduced screening between the particles in dispersion. This trend might translate into differential aggregation of the particles during alcohol evaporation and in the dry films, with more pronounced aggregation (and lower *G* values) in the case of particles in 2-propanol. We thus hypothesized that the aggregation state of the particles have a different influence on the surface area of the dry $Ca(OH)_2$ films (which is similar for CE, LE, and CIP), and on k_G (which varies among the systems), *i.e.* the two factors that determine *G*. On the contrary, at 14˚C and 30˚C, the transformation of calcium hydroxide is respectively too slow or too fast in all systems to observe a significant difference in the linear growth rate of the transformation products; in other terms, in these conditions the influence of T on *G* is more significant than that of the solvent.

The activation energy of the $Ca(OH)_2$ transformation was calculated from Arrhenius plots (ln k_G versus 1/T) for the four systems (see Figure 8.5). Good R^2 values (0.86-0.98, see Table 8.3) were obtained from the linear fitting of the experimental data, indicating that the plots are linear across the considered temperature range. The slope of the linear fittings gives constant activation energies (E_a), which are reported in Table 8.3. Namely, it was found that the system LE exhibits the lowest dependence from temperature (E_a = 31.4 kJ·mol^{-1}), the system LIP has E_a = 43.9 kJ·mol^{-1}, and the two CaLoSiL® products showed different activation energies (E_a = 50.4 kJ·mol^{-1} for CE, and 59.6 kJ·mol^{-1} for CIP), possibly due to the different solvents used. To the best of our knowledge, this is the first time that activation energy values are provided for the carbonation of $Ca(OH)_2$ nanoparticles around room temperature and environmental CO_2 concentration.

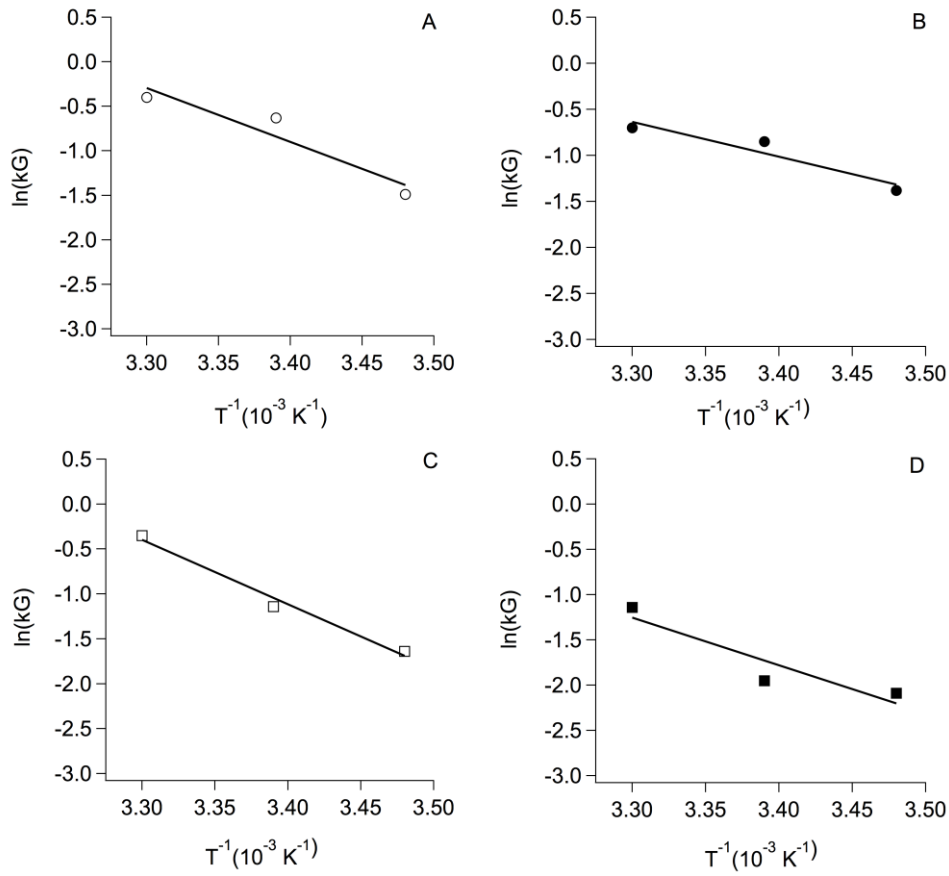

Figure 8.5 - Arrhenius plot (lnk_G versus 1/T) of the four systems: (A) CE system, (B) LE system, (C) CIP system, (D) LIP system

SYSTEM NAME	**E_a** (kJ·mol^{-1})	**R^2** of Arrhenius Plot
CE	50.4	0.90
LE	31.4	0.91
CIP	59.6	0.98
LIP	43.9	0.86

Table 8.3 - The activation energy (E_a) and the R^2 of the Arrhenius plots of the CE, LE, CIP, and LIP systems

Elsewhere, activation energy values of 6-12 kJ·mol^{-1} have been reported for the dry solid-gas carbonation of micrometric aggregates of $Ca(OH)_2$ nano-platelets or micron-sized particles at high temperature (> 250˚C) under non-isothermal conditions (Nikulshina et al. 2007; Montes-Hernandez et al. 2012), while values ranging from 20 to 200 kJ·mol^{-1} have been reported for the isothermal carbonation of CaO above 400˚C (Bhatia and Perlmutter 1983; Gupta and Fan 2002; Sun et al. 2008; Grasa et al. 2014; Ramezani et al. 2017). The fact that we found comparable activation energies for the room temperature (14-30˚C) carbonation of the $Ca(OH)_2$ nanoparticles' films, is explained considering that in our case the process takes place at high RH (75%), rather than in dry conditions. Vance et al. had previously reported an activation energy of 7.5 kJ·mol^{-1} for the carbonation of portlandite particles around room temperature, using liquid and supercritical CO_2 (Vance et al. 2015).

8.1.3. Calcium carbonate polymorphs

An important aspect of the carbonation process concerns the evolution of the calcium carbonate polymorphs. In this regard, FTIR spectroscopy was employed for monitoring both amorphous and crystalline phases over time. Namely, the time-evolution of the following absorption bands was monitored: calcite in-plane bending (v_4) at 713 cm^{-1}, vaterite in-plane bending (v_4) at 745 cm^{-1}, and aragonite out-of-plane bending (v_2) at 854 cm^{-1} (Andersen and Brečević 1991; Vagenas 2003). Besides, the presence of the broad band of ACC centered at 865 cm^{-1} (out-of-plane bending, v_2) was monitored, as well as its evolution and shift into a narrower band centered at 876 cm^{-1} (vaterite and calcite out-of-plane bending, v_2) (Andersen and Brečević 1991).

According to the literature, the carbonation of $Ca(OH)_2$ nanoparticles in humid air at room temperature involves the initial formation of ACC and its

transformation into metastable vaterite (and minor aragonite amounts), via a dissolution–precipitation process, followed by crystal growth (Beruto and Botter 2000; Montes-Hernandez et al. 2010; Gomez-Villalba et al. 2011, 2012; López-Arce et al. 2011; Rodriguez-Navarro et al. 2013, 2016b; Baglioni et al. 2014; Nielsen et al. 2014). As reported by Rodriguez-Navarro et al., building units of vaterite presumably form via heterogeneous nucleation onto ACC, and then aggregate by mesoscale assembly into nearly iso-oriented structures resembling mesocrystals. Aragonite spindle-like structures likely form after heterogeneous nucleation onto ACC; then aragonite dissolves and transforms either into calcite or into large prisms (by Ostwald ripening), and its presence is overall scarce. The stable phase, calcite, can directly nucleate and grow after dissolution of ACC/vaterite/aragonite, or nucleate on vaterite/aragonite and grow via non-classical particle-mediated aggregation or a classical ion-mediated mechanism (Rodriguez-Navarro et al. 2016b).

While ethanol seems to have no significant effect on ACC formation (Rodriguez-Navarro et al. 2016b), the presence of organic molecules (e.g. alcohols, alkoxides) on the surface of the $Ca(OH)_2$ particles (or grains) is known to favor the formation and kinetic stabilization of vaterite, delaying its transformation into calcite (Manoli and Dalas 2000; Seo et al. 2005; Zhang et al. 2008; Sand et al. 2012; Rodriguez-Navarro et al. 2016c). In few cases, the spectra of the CE, LE, CIP, and LIP systems recorded within the first hour of the carbonation process, exhibited weak bands at 2960-2830 cm^{-1} (CH stretching), 1075 and 1050 cm^{-1} (C-O stretching), ascribable both to residual alcohol (from the drying step) or to alkoxide (Liu et al. 2008). The latter can be due to untransformed reaction products in the case of nanoparticles obtained by solvothermal reaction, or can be formed by reaction of $Ca(OH)_2$ with short-chain alcohols during storage of the dispersions (Rodriguez-Navarro et al. 2016c). In any case, alkoxide is readily transformed into calcium hydroxide by hydrolysis in humid air.

The aforementioned polymorph evolution (ACC → vaterite → calcite) was observed for all the four systems at the three temperatures, in agreement with the trend reported in the literature (Ogino et al. 1987; Beruto and Botter 2000; Nielsen et al. 2014; De Yoreo et al. 2015; Rodriguez-Navarro et al. 2016b). Figure 8.6 shows a representative example (system CE at 14˚C) where the broad band centered at 865 cm^{-1} (ACC out-of-plane bending, v_2) becomes narrower and shifts over time to 876 cm^{-1} (vaterite and calcite out-of-plane bending, v_2).

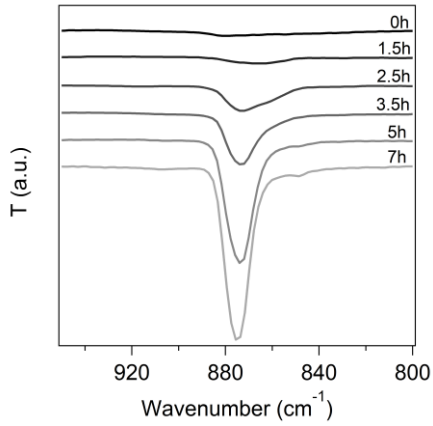

Figure 8.6 - Time-evolution of the carbonate out-of-plane bending absorption peak (v_2) for the CE system at 14°C: the broad band centered at 865 cm^{-1} (ACC out-of-plane bending, v_2) becomes narrower and shifts to 876 cm^{-1} (vaterite and calcite out-of-plane bending, v_2)

When temperature increases from 14 to 30˚C, the presence of ACC is observable up to progressively shorter times, *i.e.* until 2h from the beginning of the $Ca(OH)_2$ transformation at 14°C, and 0.5-2h at 22°C. At 30°C, ACC is detected in the system LIP in the first 20 minutes, while it is not detected in CE, LE and CIP, as it evolves into crystalline phases.

Both the vaterite band at 745 cm^{-1} and the calcite band at 713 cm^{-1} appear only after ACC disappearance, and both phases are detected at earlier times with increasing temperature. Calcite appeared after vaterite only in three cases (LE system at 14˚C and 22˚C, LIP system at 14˚C). Consistently with the literature (Chen et al. 2006; Nielsen et al. 2014; Rodriguez-Navarro et al. 2016b; Rodriguez-Navarro and Ruiz-Agudo 2018) traces of aragonite were detected in the four systems, always coexisting with vaterite.

At later stages, calcite prevails on vaterite, and disappearance of vaterite occurs at earlier times with increasing temperature. Calcite is the sole or dominant polymorph in CE, LE and CIP after 14h at 14˚C, 7h at 22˚C, and 4h at 30˚C. Figure 8.7 qualitatively shows the trends of the CE system at the three temperatures. For the LIP system, at 14˚C vaterite is present together with calcite after 14h. Calcite becomes the dominant phase after 14h at 22˚C, and after 7h at 30˚C. It is worth noting that the slower time evolution of $CaCO_3$ polymorphs in LIP is consistent with the slower $Ca(OH)_2$ transformation kinetics of this system as opposed to CE, LE, and CIP.

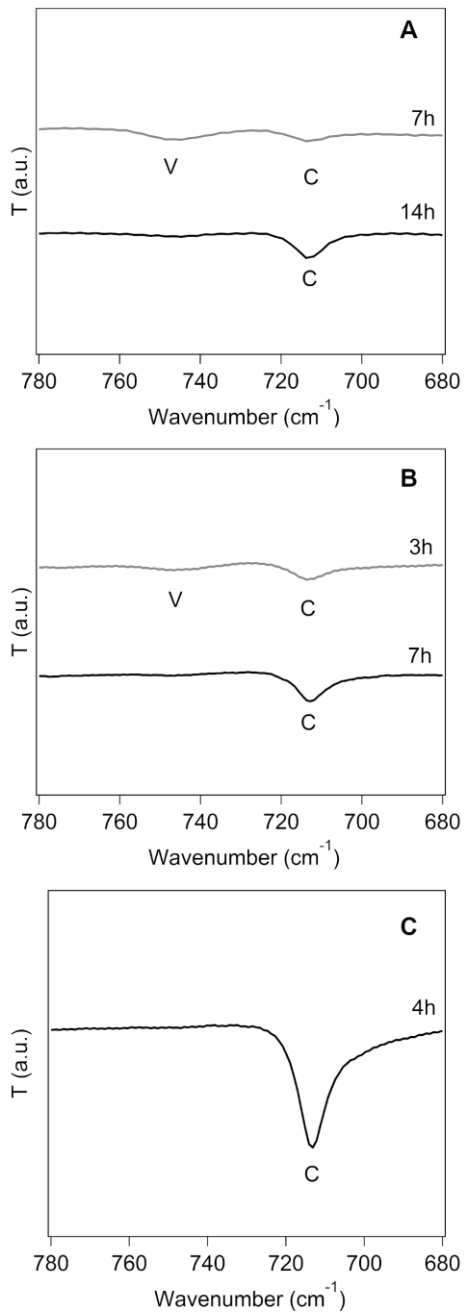

Figura 8.7 - FTIR spectra, showing the 780-680 cm^{-1} region, of the CE system at 14°C (A), 22°C (B) and 30°C (C), at different times through the carbonation process. The evolution of the in-plane bending absorption (v_4) of calcite ("C", 713 cm^{-1}) and vaterite ("V", 745 cm^{-1}) is highlighted

In order to evaluate semi-quantitatively the aforementioned trends for the formation of the crystalline polymorphs, we measured the absorbance of the vaterite peak at 745 cm^{-1} (Abs^{745}), and of the calcite peak at 713 cm^{-1} (Abs^{713}). The concentration of each polymorph (c_{VAT} and c_{CALC}) was then calculated using the following formula (Vagenas 2003):

$$c_{VAT} = (Abs^{745}/\alpha_{VAT}^{745})$$
$$c_{CALC} = (Abs^{713}/\alpha_{CALC}^{713})$$

where α_{VAT}^{745} and α_{CALC}^{713} are respectively the values of the absorption coefficients of vaterite and calcite, which were calculated by Vagenas et al. (α_{VAT}^{745} = 21.8 mm^{2}mg^{-1}; α_{CALC}^{713} = 63.4 mm^{2}mg^{-1}) (Vagenas 2003). The concentrations were then weighted by the initial amount of available calcium hydroxide for each considered sample (*i.e.* KBr pellet). The weighted concentration was labeled C*. Figure 8.8 shows the evolution of the vaterite and calcite C* values for the CE system at all the considered temperatures. Such trends are representative of all the systems, even though the LIP system has a slower time evolution of the two phases, as mentioned above. The quantitative evaluation confirmed that in most cases calcite coexists with vaterite starting from the first stages of the formation of crystalline phases. It has been shown that the formation of calcite takes place in solution through either direct (nucleation from solution) or indirect pathways (nucleation on vaterite and aragonite) (Rodriguez-Navarro et al. 2016b).

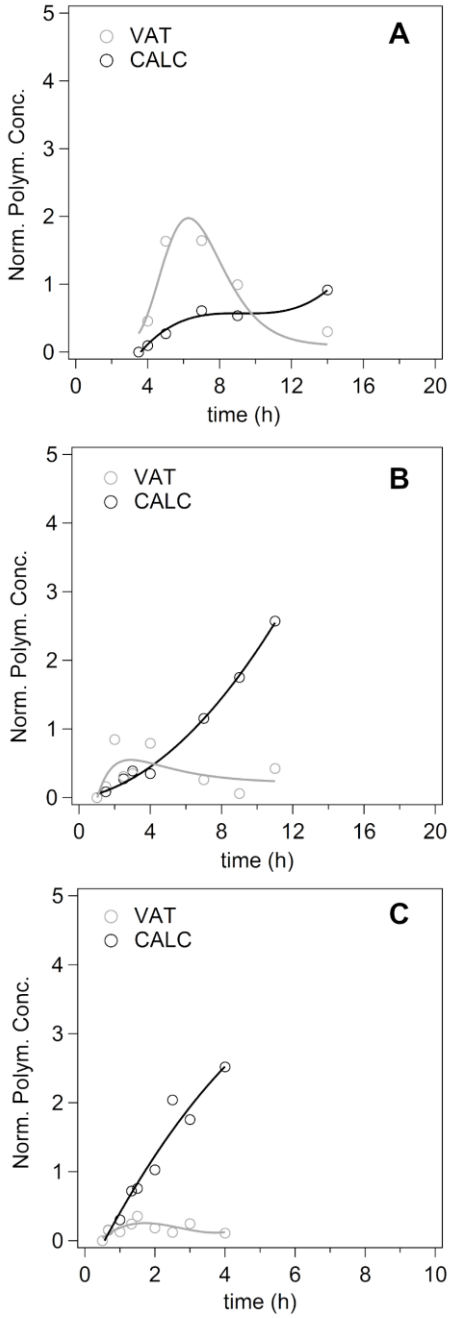

Figure 8.8 - Time-evolution of the vaterite and calcite weighted concentrations for the CE systems 14°C (A), 22°C (B), and 30°C (C). The solid lines were added as guides to better visualize the trend of the experimental data

PART IV

Conclusions

Conclusions and future perspectives

The present dissertation focused on the consolidation of stone materials, as the wide variety of the architectural and artistic patrimony makes its preservation a challenging issue for restorers and conservator scientists.

Adobe earth bricks are one of the most ancient building materials, and are still largely in use worldwide, but often exhibit lack of cohesion and loss of superficial grains. The present research reports the first evidence of the use of hybrid nano-composite materials for the consolidation of adobe. The materials selected for preparation of the ternary system (*SiO_2_HPC_lime*) have full physico-chemical compatibility with those of adobe, and each component was shown to play a role in the consolidation process, or in the stability of the formulation.

The physico-chemical characterization of the composite (by dynamic light scattering, electron microscopy, X-ray diffraction, and infrared spectroscopy) allowed to picture the interaction of the components. Namely, the interaction of highly reactive silica nanoparticles and calcium hydroxide nanoparticles led to the formation of calcium silicate hydrate (CSH), mimicking the chemistry of cement. Moreover, the use of nano-sized particles allowed the possibility to prepare stable and concentrated dispersions in water-solvent blends (without using surfactants as stabilizers). The choice of an ethanol-water blend with ratio 4:1 allowed to obtain stable dispersion of the components in the desired amounts (ethanol prevents bridging and aggregation of the hydroxide platelets), and represents a balance between the need of avoiding aqueous media on water-sensitive substrates and the necessity of some water content to trigger the alkaline activation of nanosilica and form CSH.

The nanoparticles were combined with a traditional consolidant and adhesive in conservation practice, *Klucel*®-G, as cellulose derivatives are known to act as water regulators, binding water and then distributing it homogenously over the solid phase, and overall enhancing the formation of CSH. The introduction of HPC in the formulation was also essential in that it limited the aggregation of the nanoparticles, and prevented the sedimentation of the aggregates by increasing the viscosity of the dispersion, without affecting its applicability.

After the formulation preparation and characterization, it was applied on real adobe samples, exhibiting high porosity and surface powdering mainly caused by wind and water erosion, to assess the effective consolidating power.

First, the desired formation of CSH within the pores of the treated adobe samples was evidenced by XRD measurements. Improvement of the mechanical properties of treated adobe was shown through representative tests of exposure to environmental erosion (*i.e.* resistance to peeling, abrasion, and wet-dry cycles). The obtained consolidation was ascribed to the combination of silica and lime nanoparticles in presence of water (forming CSH), and partially to the presence of the HPC component, as the ternary system was shown to grant better consolidation than the binary systems or single components.

A homogeneous penetration of composite particles up to few millimeters from the surface was assessed by XRD and the phenolphtalein test, granting protection of the outer layers, mostly degraded by erosion. Moreover, the treatment did not induce discoloration of adobe, and left the water permeability unaltered, both of which are essential requirements in stone consolidation, as opposed to conventional polymeric adhesives that are known to alter stone porosity and induce discoloration and flaking.

Overall, the ternary formulation was deemed as promising for the consolidation of earthen masonry, opening new perspectives in the use of nano-composites for immovable works of art. As future perspectives, applicatve protocols for real case

studies schould be developed, as immersion of adobe building units is unfeasable (e.g. application by brushing or spraying), and sufficient water content should be maintained after the treatment so to grant CSH formation even in dry and hot environments (e.g. humid cellulose pulp application onto the treated surface).

The tools necessary to perform good conservation interventions include the knowledge of the substrate to be treated, but also of the product to be applied for the purpose.

In this view, a compared physico-chemical study on the carbonation kinetics of four $Ca(OH)_2$ nanoparticles alcohol dispersions was performed, emerging materials for the consolidation of stone, thanks to their effectiveness, stability and compatibility. Despite their diffused adoption, the necessity to detail their carbonation process is a challenging issue.

In the present contribution, a rigorous approach was followed, by means of FTIR and accelerated carbonation under controlled T and RH conditions, assessing the applicability of the generalized Boundary Nucleation and Growth Model (BNGM) to the carbonation kinetics, and then evaluating limiting cases of the model. The four selected commercial nanolimes are represent standard products in term of particles preparation and dimensions, and alcohol used.

The carbonation of films of nanoparticles was studied at different temperatures, representative of applicative conditions, such as the use of the particles for the consolidation of movable and immovable cultural heritage.

The choice of the BNGM over Avrami-type or deceleratory models previously reported in the literature was due to the necessity of taking into account the effect of the surface area of the particles on the transformation of $Ca(OH)_2$ into amorphous and crystalline $CaCO_3$ in humid air. The process is assumed to take place on the surface boundaries of the particles, in the presence of a solution

(water film), where $Ca(OH)_2$ and atmospheric CO_2 can dissolve. The carbonation products then grow to fill the porosities in the nanoparticles' layers.

It was found that fitting the time evolution of the $Ca(OH)_2$ carbonation degree (obtained by FTIR) to the generalized model was possible only using narrow constraints on the value of the k_B (the rate at which the nucleated boundary area transforms). For all the systems, at all the considered temperatures (14˚C, 22˚C, 30˚C), the value of k_B is larger than that of k_G (the rate at which the porosities are filled with carbonation products). Moreover, the ratio between the nucleation rate, I_B, and the linear growth rate, G, are in all cases very large. Such conditions indicate that the boundary regions, densely populated with nuclei, transform early in the process with subsequent thickening of slab-like regions centered on the original boundaries. A BNGM limiting case equation was thus used to fit the process kinetics, where the transformation rate decreases exponentially with time.

The obtained k_G and the calculated G values and activation energies were then compared. It was found that particles with lower surface area exhibit a slower carbonation kinetics at all temperatures, which is to be considered in real cases applications. Contrarily to general expectations, size reduction is not the only valid criterion for consolidation treatments. Indeed, best consolidating effects are obtained when the particles size distribution matches that of the substrate's pores, which has to be evaluated in real cases study. It was also found that differences in linear growth rate and dependence from temperature can be ascribed to the dispersing alcohol used.

The time-evolution of $CaCO_3$ polymorphs described in the literature (ACC $\rightarrow$ vaterite/aragonite $\rightarrow$ calcite), and the role of alcohol in the stabilization of metastable carbonate phases (vaterite and minor aragonite) was confirmed. The polymorphs evolve with a rate depending on temperature, and, again, the process is slower in system with BET surface area of 20 m^2/g and particle size of 300-

500 nm, than in the three systems with BET surface area of 36-38 m^2/g, and particle size of 100-200 nm. Calcite coexists with vaterite starting from the initial formation of both phases, indicating that the former (stable polymorph) can form through either direct (nucleation after dissolution of ACC/vaterite/aragonite) or indirect pathways (nucleation on vaterite and aragonite). At later stages, calcite is the sole or dominant polymorph in most of the considered cases, but at low temperatures vaterite is still present in the system with the slowestf kinetic. This fact can also play a role in real cases applications, as the formation of vaterite can affects the bond formation with calcite-based substrates and the treatment performances. Nevertheless, on the long term, it converts to calcite, and some effectiveness in consolidating stone by vaterite was observed.

PART V

Annex

Bibliography

Achenza M, Atzeni C, Mocci S, Ulrico S (2008) Il manuale tematico della terra cruda. Regione Autonoma della Sardegna

Adorni E, Coïsson E, Ferretti D (2013) In situ characterization of archaeological adobe bricks. Constr Build Mater 40:1–9. doi: 10.1016/j.conbuildmat.2012.11.004

AFNOR PR XP P13-901 (2001) Compressed Earth Blocks for Walls and Partitions: Definitions, Specifications, Test Methods, Conditions of Acceptance

Åkerlöf G (1932) Dielectric constants of some organic solvent-water mixtures at various temperatures. J Am Chem Soc 54:4125–4139. doi: 10.1021/ja01350a001

Ambrosi M, Dei L, Giorgi R, et al (2001a) Stable dispersions of Ca(OH)2 in aliphatic alcohols: properties and application in cultural heritage conservation. Prog Colloid Polym Sci 118:68–72. doi: 10.1007/3-540-45725-9_15

Ambrosi M, Dei L, Giorgi R, et al (2001b) Colloidal particles of Ca(OH)2: Properties and applications to restoration of frescoes. Langmuir 17:4251–4255. doi: 10.1021/la010269b

Andersen FA, Brečević L (1991) Infrared Spectra of Amorphous and Crystalline Calcium Carbonate. Acta Chem Scand 45:1018–1024. doi: 10.3891/acta.chem.scand.45-1018

Angela Calia, Maurizio Masieri, Giovanni Baldi CM (2012) The Evaluation of Nanosilica Performance for Consolidation Treatment of an Highly Porous Calcarenite. In: 12 th International Congress on the Deterioration and Conservation of Stone

Armelao L, Bassan A, Bertoncello R, et al (2000) Silica glass interaction with

calcium hydroxide: A surface chemistry approach. J Cult Herit 1:375–384. doi: 10.1016/S1296-2074(00)01093-1

Ashland Inc. Klucel Hydroxypropyl cellulose - Physical and chemical properties

ASTM D559/D559M (2015) Standard Test Methods for Wetting and Drying Compacted Soil-Cement Mixtures. ASTM Int West Conshohocken, Pa 1–6

Avrami E, Guillaud H, Hardy M (2008) Terra Literature Review - An Overview of Research in Earthen Architecture Conservation

Baglioni P, Chelazzi D, Giorgi R (2015) Nanotechnologies in the Conservation of Cultural Heritage: A Compendium of Materials and Techniques. Springer Dordrecht Heidelberg London New York

Baglioni P, Chelazzi D, Giorgi R, et al (2014) Commercial Ca(OH)2 nanoparticles for the consolidation of immovable works of art. Appl Phys A 114:723–732. doi: DOI 10.1007/s00339-013-7942-6

Baglioni P, Chelazzi D, Giorgi R, Poggi G (2013) Colloid and Materials Science for the Conservation of Cultural Heritage: Cleaning, Consolidation, and Deacidification. Langmuir 29:5110–5122. doi: 10.1021/la304456n

Baglioni P, Giorgi R (2006) Soft and hard nanomaterials for restoration and conservation of cultural heritage. Soft Matter 2:293–303. doi: 10.1039/b516442g

Baglioni P, Vargas RC, Chelazzi D, et al (2006) The Maya Site of Calakmul: In Situ Preservation of Wall Paintings and Limestone Using Nanotechnology. In: The Object in Context: Crossing Conservation Boundaries: Contributions to the Munich

Baltakys K, Jauberthie R, Siauciunas R, Kaminskas R (2007) Influence of modification of SiO2 on the formation of calcium silicate hydrate. Mater Sci 25:663–670

Berns RS, Reiman DM (2002) Color managing the third edition of Billmeyer and Saltzman's Principles of Color Technology. Color Res Appl 27:360–373.

doi: 10.1002/col.10083

Berthier DL, Herrmann A, Ouali L (2011) Synthesis of hydroxypropyl cellulose derivatives modified with amphiphilic diblock copolymer side-chains for the slow release of volatile molecules. Polym Chem 2:2093–2101. doi: 10.1039/c1py00195g

Beruto DT, Botter R (2000) Liquid-like H2O adsorption layers to catalyze the Ca(OH)2/CO2solid-gas reaction and to form a non-protective solid product layer at 20°C. J Eur Ceram Soc 20:497–503. doi: 10.1016/S0955-2219(99)00185-5

Bhatia SK, Perlmutter DD (1983) Effect of the product layer on the kinetics of the CO2-lime reaction. AIChE J 29:79–86. doi: 10.1002/aic.690290111

Borsoi G, Lubelli BL, Van Heesa R, et al (2016) Understanding the transport of nanolime consolidants within Maastricht limestone. J Cult Herit 18:242–249. doi: http://dx.doi.org/10.1016/j.culher.2015.07.014

Bouhicha M, Aouissi F, Kenai S (2005) Performance of composite soil reinforced with barley straw. Cem Concr Compos 27:617–621. doi: 10.1016/j.cemconcomp.2004.09.013

Bouville F, Deville S (2014) Dispersion of boron nitride powders in aqueous suspensions with cellulose. J Am Ceram Soc 97:394–398. doi: 10.1111/jace.12653

Brown PW, Clifton JR (1978) Adobe I: The properties of adobe. Stud Conserv. doi: 10.2307/1505842

Brown PW, Robbins CR., Clifton JR (1979) Adobe II: Factors Affecting the Durability of Adobe Structures. Stud Conserv 24:23–39. doi: 10.1179/sic.1979.003

BS EN 1925 (1999) Natural Stone Test Methods - Determination Of Water Absorption Coefficient By Capillarity. 1–10

Cahn JW (1956) The kinetics of grain boundary nucleated reactions. Acta Metall

4:449–459. doi: 10.1016/0001-6160(56)90041-4

Caporale A, Parisi F, Asprone D, et al (2014) Critical surfaces for adobe masonry: Micromechanical approach. Compos Part B Eng 56:790–796. doi: 10.1016/j.compositesb.2013.08.087

Carretti E, Chelazzi D, Rocchigiani G, et al (2013) Interactions between nanostructured calcium hydroxide and acrylate copolymers: Implications in cultural heritage conservation. Langmuir 29:9881–9890. doi: 10.1021/la401883g

Chan C-M (2011) Effect of Natural Fibres Inclusion in Clay Bricks: Physico-Mechanical Properties. Int J Civ Environ Eng 5:7–13

Chelazzi D, Camerini R, Giorgi R, Baglioni P (2018) Nanomaterials for the consolidation of stone artifacts. In: Advanced Materials for the Conservation of Stone

Chelazzi D, Poggi G, Jaidar Y, et al (2013) Hydroxide nanoparticles for cultural heritage: Consolidation and protection of wall paintings and carbonate materials. J Colloid Interface Sci 392:42–49. doi: 10.1016/j.jcis.2012.09.069

Chen SF, Yu SH, Hang J, et al (2006) Polymorph discrimination of CaCO3 mineral in an ethanol/water solution: Formation of complex vaterite superstructures and aragonite rods. Chem Mater 18:115–122. doi: 10.1021/cm0519028

Christian JW (2002) The theory of transformations in metals and alloys, 3rd edition. Pergamon Press, Oxford, 2002.

Cizer Ö, Rodriguez-Navarro C, Ruiz-Agudo E, et al (2012a) Phase and morphology evolution of calcium carbonate precipitated by carbonation of hydrated lime. J Mater Sci 47:6151–6165. doi: 10.1007/s10853-012-6535-7

Cizer Ö, Van Balen K, Elsen J, Van Gemert D (2012b) Real-time investigation

of reaction rate and mineral phase modifications of lime carbonation. Constr Build Mater 35:741–751. doi: 10.1016/j.conbuildmat.2012.04.036

Clifton JR (1982) Stone Consolidating Materials - A Status Report. In: Conservation of Historic Stone Buildings and Monuments. The National Academies Press, Washington, DC, pp 287–311

Clifton JR (1977) Preservation o Historic Adobe Structures - A Status Report. National Bureau of Standards (U.S.), Washington, DC

Croveri P, Dei L, Giorgi R, Salvadori B (2004) Consolidation of Globigerina Limestone (Malta) by Means of Inorganic Treatments: Preliminary Results. In: Kwiatkowski D, Lofvendahl R (eds) Proceedings of the 10th international congress on deterioration and conservation of stone, vol 1, Stockholm. p 463

D'Armada P, Hirst E (2012) Nano-lime for consolidation of plaster and stone. J Archit Conserv 1:63–80. doi: 10.1080/13556207.2012.10785104

Daehne A, Herm C (2013) Calcium hydroxide nanosols for the consolidation of porous building materials - results from EU-STONECORE. Herit Sci 1:11–20. doi: 10.1186/2050-7445-1-11

Daniele V, Taglieri G (2010) Nanolime suspensions applied on natural lithotypes: The influence of concentration and residual water content on carbonatation process and on treatment effectiveness. J Cult Herit 11:102–106. doi: 10.1016/j.culher.2009.04.001

Daniele V, Taglieri G (2012) Synthesis of Ca(OH)2 nanoparticles with the addition of Triton X-100. Protective treatments on natural stones: Preliminary results. J Cult Herit 13:40–46. doi: 10.1016/j.culher.2011.05.007

Daniele V, Taglieri G, Gregori A (2013) Synthesis of Ca(OH)2 Nanoparticles Aqueous Suspensions and Interaction with Silica Fume. Adv Mater Res 629:482–487. doi: 10.4028/www.scientific.net/AMR.629.482

Daniele V, Taglieri G, Quaresima R (2008) The nanolimes in Cultural Heritage conservation: Characterisation and analysis of the carbonatation process. J Cult Herit 9:294–301. doi: 10.1016/j.culher.2007.10.007

De Rosario I, Elhaddad F, Pan A, et al (2015) Effectiveness of a novel consolidant on granite: Laboratory and in situ results. Constr Build Mater 76:140–149. doi: 10.1016/j.conbuildmat.2014.11.055

De Yoreo JJ, Gilbert PUPA, Sommerdijk NAJM, et al (2015) Crystallization by particle attachment in synthetic, biogenic, and geologic environments. Science (80-) 349:aaa6760. doi: 10.1126/science.aaa6760

De Zorzi C, Favaro M, Tomasin P, et al (2009) Consolidation of stone and wall paintings by calcium metallorganic precursors of calcite. In: Science and technology for the safeguard of Cultural Heritage in the Mediterranean basin. p 433

Dei L, Salvadori B (2006) Nanotechnology in cultural heritage conservation: nanometric slaked lime saves architectonic and artistic surfaces from decay. J Cult Herit 7:110–115. doi: 10.1016/j.culher.2006.02.001

Del Buffa S, Fratini E, Ridi F, et al (2016) State of Water in Hydrating Tricalcium Silicate Pastes: The Effect of a Cellulose Ether. J Phys Chem C 120:7612–7620. doi: 10.1021/acs.jpcc.6b00691

Delgado A V. (2001) Interfacial Electrokinetics and Electrophoresis. In: Surfactant Science series, volume 106. CRC Press, pp 1–1016

Dheilly RM, Tudo J, Sebaibi Y, Quéneudec M (2002) Influence of storage conditions on the carbonation of powdered Ca(OH)2. Constr Build Mater 16:155–161. doi: 10.1016/S0950-0618(02)00012-0

Doat P, CRATerre (1983) Costruire en terre

Drdacky M, Lesak J, Rescic S, et al (2012) Standardization of peeling tests for assessing the cohesion and consolidation characteristics of historic stone surfaces. Mater Struct (Dordrecht, Netherlands) 45:505–520. doi:

10.1617/s11527-011-9778-x

Eguchi N, Kawabata K, Goto H (2017) Electrochemical Polymerization of 4,4-Dimethyl-2,2'-Bithiophene in Concentrated Polymer Liquid Crystal Solution. J Mater Sci Chem Eng 05:64–70. doi: 10.4236/msce.2017.52007

Elert K, Pardo ES, Rodriguez-Navarro C (2015) Alkaline activation as an alternative method for the consolidation of earthen architecture. J Cult Herit 16:461–469. doi: 10.1016/j.culher.2014.09.012

Falchi L, Balliana E, Izzo FFC, et al (2013) Distribution of nanosilica dispersions in Lecce stone. Sci Ca' Foscari 1:40–46. doi: 10.7361/SciCF-441

Favaro M, Mendichi R, Ossola F, et al (2006) Evaluation of polymers for conservation treatments of outdoor exposed stone monuments. Part I: Photo-oxidative weathering. Polym Degrad Stab 91:3083–3096. doi: 10.1016/j.polymdegradstab.2006.08.012

Favaro M, Tomasin P, Ossola F, Vigato PA (2008) A novel approach to consolidation of historical limestone: The calcium alkoxides. Appl Organomet Chem 22:698–704. doi: 10.1002/aoc.1462

Fratini E, Page MG, Giorgi R, et al (2007) Competitive surface adsorption of solvent molecules and compactness of agglomeration in calcium hydroxide nanoparticles. Langmuir 23:2330–2338. doi: 10.1021/la062023i

Galán-Marín C, Rivera-Gómez C, Petric J (2010) Clay-based composite stabilized with natural polymer and fibre. Constr Build Mater 24:1462–1468. doi: 10.1016/j.conbuildmat.2010.01.008

Gao Z, Zharov I (2014) Large pore mesoporous silica nanoparticles by templating with a nonsurfactant molecule, tannic acid. Chem Mater 26:2030–2037. doi: 10.1021/cm4039945

García-Carmona J, Morales JG, Clemente RR (2003) Morphological control of precipitated calcite obtained by adjusting the electrical conductivity in the Ca(OH)2-H2O-CO2system. J Cryst Growth 249:561–571. doi:

10.1016/S0022-0248(02)02173-5

Garrault S, Behr T, Nonat A (2006) Formation of the C-S-H layer during early hydration of tricalcium silicate grains with different sizes. J Phys Chem B 110:270–275. doi: 10.1021/jp0547212

Giorgi R, Ambrosi M, Toccafondi N, Baglioni P (2010a) Nanoparticles for Cultural Heritage Conservation : Calcium and Barium Hydroxide Nanoparticles for Wall Painting Consolidation. Chem Eur J 16:9374–9382. doi: 10.1002/chem.201001443

Giorgi R, Baglioni M, Berti D, Baglioni P (2010b) New Methodologies for the conservation of cultural heritage: Micellar solutions, microemulsions, and hydroxide nanoparticles. Acc Chem Res 43:695–704. doi: 10.1021/ar900193h

Giorgi R, Dei L, Baglioni P (2000a) A New Method for Consolidating Wall Paintings Based on Dispersions of Lime in Alcohol. Stud Conserv 45:154–161. doi: 10.1179/sic.2000.45.3.154

Giorgi R, Dei L, Baglioni P (2000b) A New Method for Consolidating Wall Paintings Based on Dispersions of Lime in Alcohol. Stud Conserv 45:154–161. doi: 10.1179/sic.2000.45.3.154

Gomez-Villalba L, López-Arce P, Fort R (2012) Nucleation of CaCO3 polymorphs from a colloidal alcoholic solution of Ca(OH)2 nanocrystals exposed to low humidity conditions. Appl Phys A Mater Sci Process 106:213–217. doi: 10.1007/s00339-011-6550-6

Gomez-Villalba LS, López-Arce P, Alvarez de Buergo M, Fort R (2011) Structural stability of a colloidal solution of Ca(OH)2 nanocrystals exposed to high relative humidity conditions. Appl Phys A 104:1249–1254. doi: 10.1007/s00339-011-6457-2

Graf C, Gao Q, Schütz I, et al (2012) Surface functionalization of silica nanoparticles supports colloidal stability in physiological media and

facilitates internalization in cells. Langmuir 28:7598–7613. doi: 10.1021/la204913t

Grangeon S, Claret F, Lerouge C, et al (2013a) On the nature of structural disorder in calcium silicate hydrates with a calcium/silicon ratio similar to tobermorite. Cem Concr Res 52:31–37. doi: 10.1016/j.cemconres.2013.05.007

Grangeon S, Claret F, Linard Y, Chiaberge C (2013b) X-ray diffraction: A powerful tool to probe and understand the structure of nanocrystalline calcium silicate hydrates. Acta Crystallogr Sect B Struct Sci Cryst Eng Mater 69:465–473. doi: 10.1107/S2052519213021155

Grangeon S, Claret F, Roosz C, et al (2016) Structure of nanocrystalline calcium silicate hydrates: Insights from X-ray diffraction, synchrotron X-ray absorption and nuclear magnetic resonance. J Appl Crystallogr 49:771–783. doi: 10.1107/S1600576716003885

Grasa G, Martínez I, Diego ME, Abanades JC (2014) Determination of CaO carbonation kinetics under recarbonation conditions. Energy and Fuels 28:4033–4042. doi: 10.1021/ef500331t

Greenberg SA (1961) Reaction between silica and calcium hydroxide solutions. Kinetics in the temperature range 30 to 85°. J Phys Chem 65:12–16. doi: 10.1021/j100819a005

Gregory J (1987) Flocculation by polymers and polyelectrolytes. In: Tadros TF (ed) Solid/Liquid Dispersions. Academic Press, London, UK, pp 163–180

Grimaldi DM, Pérez NA, Porter JH (2012) The preservation of sandstone reliefs at the archeological site of Tajin, Mexico, using colloidal silica. In: 12th International Congress on the Deterioration and Conservation of Stone Columbia University, New York. pp 1–9

Guerrero Baca L (2007) Arquitectura en tierra. Hacia la recuperación de una cultura constructiva. Apuntes 20:182–201

Gunasekaran S, Anbalagan G, Pandi S (2006) Raman and infrared spectra of carbonates of calcite structure. J Raman Spectrosc 37:892–899. doi: 10.1002/jrs.1518

Guo X, Meng F, Shi H (2017) Microstructure and characterization of hydrothermal synthesis of Al-substituted tobermorite. Constr Build Mater 133:253–260. doi: 10.1016/j.conbuildmat.2016.12.059

Gupta H, Fan LS (2002) Carbonation-calcination cycle using high reactivity calcium oxide for carbon dioxide separation from flue gas. Ind Eng Chem Res 41:4035–4042. doi: 10.1021/ie010867l

Hamiane M, Djefour I, Merabet H, et al (2016) Design of Adobe Bricks of Local Raw Materials for Use in the Monuments of Earthen Architecture (Case of Adrar Hospital) Algeria. Civ Eng Archit 4:147–152. doi: 10.13189/cea.2016.040401

Illampas R, Ioannou I, Charmpis DC (2013) Overview of the pathology, repair and strengthening of adobe structures. Int. J. Archit. Herit. 165–188

Izemmouren O, Guettala A, Guettala S (2015) Mechanical Properties and Durability of Lime and Natural Pozzolana Stabilized Steam-Cured Compressed Earth Block Bricks. Geotech Geol Eng 33:1321–1333. doi: 10.1007/s10706-015-9904-6

Karagiannis N, Karoglou M, Bakolas A, Moropoulou A (2016) Building Materials Capillary Rise Coefficient: Concepts, Determination and Parameters Involved. In: J D (ed) New Approaches to Building Pathology and Durability. Building Pathology and Rehabilitation. Springer, Singapore, pp 27–44

Khawam A, Flanagan DR (2006) Solid-state kinetic models: Basics and mathematical fundamentals. J Phys Chem B 110:17315–17328. doi: 10.1021/jp062746a

Kim EK, Won J, Do J young, et al (2009) Effects of silica nanoparticle and

GPTMS addition on TEOS-based stone consolidants. J Cult Herit. doi: 10.1016/j.culher.2008.07.008

Kita Y (2013) The functions of vegetable mucilage in lime and earth mortars - A Review. In: 3rd Historic Mortars Conference. Glasgow, UK

Lanzón M, Madrid JA, Martínez-Arredondo A, Mónaco S (2017) Use of diluted Ca(OH)2 suspensions and their transformation into nanostructured CaCO3 coatings: A case study in strengthening heritage materials (stucco, adobe and stone). Appl Surf Sci 424:20–27. doi: 10.1016/j.apsusc.2017.02.248

Lin Q, Lan X, Li Y, et al (2010) Preparation and characterization of novel alkali-activated nano silica cements for biomedical application. J Biomed Mater Res - Part B Appl Biomater 95 B:347–356. doi: 10.1002/jbm.b.31722

Lin Q, Xu Z, Lan X, et al (2011) The reactivity of nano silica with calcium hydroxide. J Biomed Mater Res - Part B Appl Biomater 99 B:239–246. doi: 10.1002/jbm.b.31891

Liu X, Piao X, Wang Y, Zhu S (2008) Calcium Ethoxide as a Solid Base Catalyst for the Transesterification of Soybean Oil to Biodiesel. Energ Fuel 22:1313−1317

López-Arce P, Gómez-Villalba LS, Martínez-Ramírez S, et al (2011) Influence of relative humidity on the carbonation of calcium hydroxide nanoparticles and the formation of calcium carbonate polymorphs. Powder Technol 205:263–269. doi: 10.1016/j.powtec.2010.09.026

López-Arce P, Gomez-Villalba LS, Pinho L, et al (2010) Influence of porosity and relative humidity on consolidation of dolostone with calcium hydroxide nanoparticles: Effectiveness assessment with non-destructive techniques. Mater Charact 61:168–184. doi: 10.1016/j.matchar.2009.11.007

Manoli F, Dalas E (2000) Spontaneous precipitation of calcium carbonate in the presence of ethanol, isopropanol and diethylene glycol. J Cryst Growth 218:359−364. doi: 10.1016/S0022-0248(00)00560-1

Martínez-Camacho F (2009) El mucilago de nopal como alternativa para la consolidacion de adobe. estudio de un caso: el Templo de la Antigua Mision de Nuestra Senora del Pilar y Santiago de Cocospera, Sonora. Escuela Nacional de Conservacion, Restauracion y Museografia

Martínez-Camacho F, Vazquez-Negrete J, Lima E, et al (2008) Texture of nopal treated adobe: restoring Nuestra Señora del Pilar mission. J Archaeol Sci. doi: 10.1016/j.jas.2007.10.019

Marzouqa DM, Zughul MB, Taha MO, Hodali HA (2012) Effect of particle morphology and pore size on the release kinetics of ephedrine from mesoporous MCM-41 materials. J Porous Mater 19:825–833. doi: 10.1007/s10934-011-9537-y

Maskell D, Heath A, Walker P (2014) Inorganic stabilisation methods for extruded earth masonry units. Constr Build Mater 71:602–609. doi: 10.1016/j.conbuildmat.2014.08.094

Miliani C, Velo-Simpson ML, Scherer GW (2007) Particle-modified consolidants: A study on the effect of particles on sol-gel properties and consolidation effectiveness. J Cult Herit 8:1–6. doi: 10.1016/j.culher.2006.10.002

Mitchell DRG, Hinczak I, Day RA (1998) Interaction of silica fume with calcium hydroxide solutions and hydrated cement pastes. Cem Concr Res 28:1571–1584. doi: 10.1016/S0008-8846(98)00133-1

Montes-Hernandez G, Chiriac R, Toche F, Renard F (2012) Gas-solid carbonation of Ca(OH)2and CaO particles under non-isothermal and isothermal conditions by using a thermogravimetric analyzer: Implications for CO2capture. Int J Greenh Gas Control 11:172–180. doi: 10.1016/j.ijggc.2012.08.009

Montes-Hernandez G, Pommerol A, Renard F, et al (2010) In situ kinetic measurements of gas-solid carbonation of Ca(OH)2 by using an infrared

microscope coupled to a reaction cell. Chem Eng J 161:250–256. doi: 10.1016/j.cej.2010.04.041

Montes-Hernandez G, Renard F, Geoffroy N, et al (2007) Calcite precipitation from CO2-H2O-Ca(OH)2 slurry under high pressure of CO2. J Cryst Growth 308:228–236. doi: 10.1016/j.jcrysgro.2007.08.005

Moriyoshi T, Ishii T, Tamai Y, Tado M (1990) Static Dielectric Constants of Water + Ethanol and Water + 2-Methyl-2-propanol Mixtures from 0.1 to 300 MPa at 298.15 K. J Chem Eng Data 35:17–20. doi: 10.1021/je00059a005

Mosquera MJ, Bejarano M, De la Rosa-Fox N, Esquivias L (2003) Producing crack-free colloid-polymer hybrid gels by tailoring porosity. Langmuir 19:951–957. doi: 10.1021/la0265981

Mosquera MJ, De Los Santos DM, Montes A, Valdez-Castro L (2008) New nanomaterials for consolidating stone. Langmuir. doi: 10.1021/la703652y

Mosquera MJ, de los Santos DM, Rivas T, et al (2009) New Nanomaterials for Protecting and Consolidating Stone. J Nano Res 8:1–12. doi: 10.4028/www.scientific.net/JNanoR.8.1

Mosquera MJ, De Los Santos DM, Rivas T (2010) Surfactant-synthesized ormosils with application to stone restoration. Langmuir 26:67737–6745. doi: 10.1021/la9040979

Nanni A, Dei L (2003) Ca(OH)2 Nanoparticles from W/O Microemulsions. Langmuir 19:933–938. doi: 10.1021/la026428o

Natali I, Saladino ML, Andriulo F, et al (2014) Consolidation and protection by nanolime: Recent advances for the conservation of the graffiti, Carceri dello Steri Palermo and of the 18th century lunettes, SS. Giuda e Simone Cloister, Corniola (Empoli). J Cult Herit 15:151–158. doi: 10.1016/j.culher.2013.03.002

Nielsen MH, Aloni S, De Yoreo JJ (2014) In situ TEM imaging of CaCO3

nucleation reveals coexistence of direct and indirect pathways. Science (80-) 345:1158–1162. doi: 10.1126/science.1254051

Nikulshina V, Gálvez ME, Steinfeld A (2007) Kinetic analysis of the carbonation reactions for the capture of CO2from air via the Ca(OH)2-CaCO3-CaO solar thermochemical cycle. Chem Eng J 129:75–83. doi: 10.1016/j.cej.2006.11.003

Nowakowska J (1939) The refractive indices of ethyl alcohol and water mixtures. Loyola University Chicago

Ogino T, Suzuki T, Sawada K (1987) The formation and transformation mechanism of calcium carbonate in water. Geochim Cosmochim Acta 51:2757–2767. doi: 10.1016/0016-7037(87)90155-4

Oti JE, Kinuthia JM, Bai J (2009) Compressive strength and microstructural analysis of unfired clay masonry bricks. Eng Geol 109:230–240. doi: 10.1016/j.enggeo.2009.08.010

Pamplona M, Kocher M, Snethlage R, Barros LA (2007) Drilling resistance: overview and outlook. Zeitschrift der Dtsch Gesellschaft für Geowissenschaften 158:665–679. doi: 10.1127/1860-1804/2007/0158-0665

Pérez-Maqueda LA, Wang L, Matijević E (1998) Nanosize Indium Hydroxide by Peptization of Colloidal Precipitates. Langmuir 14:4397–4401. doi: 10.1021/la980149c

Pesce GL (2014) Study of carbonation in novel lime based materials. University of Bath

Pesce GL, Fletcher IW, Grant J, et al (2017) Carbonation of Hydrous Materials at the Molecular Level: A Time of Flight-Secondary Ion Mass Spectrometry, Raman and Density Functional Theory Study. Cryst Growth Des 17:1036−1044. doi: 10.1021/acs.cgd.6b01303

Pinto APF, Rodrigues JD (2008) Stone consolidation : The role of treatment procedures. J Cult Herit 9:38–53. doi: 10.1016/j.culher.2007.06.004

Plav B, Kobe S, Orel B (1999) Identification of crystallization forms of CaCO3 with FTIR spectroscopy. Kovine Zlitine Teh 33:517–521

Poggi G, Toccafondi N, Chelazzi D, et al (2016) Calcium hydroxide nanoparticles from solvothermal reaction for the deacidification of degraded waterlogged wood. J Colloid Interface Sci 473:1–8. doi: 10.1016/j.jcis.2016.03.038

Poggi G, Toccafondi N, Melita LN, et al (2014) Calcium hydroxide nanoparticles for the conservation of cultural heritage: New formulations for the deacidification of cellulose-based artifacts. Appl Phys A Mater Sci Process 114:685–693. doi: 10.1007/s00339-013-8172-7

Premaratne WAPJ, Priyadarshana WMGI, Gunawardena SHP, De Alwis AAP (2013) Synthesis of Nanosilica from Paddy Husk Ash and Their Surface Functionalization. J Sci Univ Kelaniya Sri Lanka 8:33–48. doi: 10.4038/josuk.v8i0.7238

Quagliarini E, Lenci S (2010) The influence of natural stabilizers and natural fibres on the mechanical properties of ancient Roman adobe bricks. J Cult Herit 11:309–314. doi: 10.1016/j.culher.2009.11.012

Ramezani M, Tremain P, Doroodchi E, Moghtaderi B (2017) Determination of Carbonation/Calcination Reaction Kinetics of a Limestone Sorbent in low CO2 Partial Pressures Using TGA Experiments. Energy Procedia 114:259–270. doi: 10.1016/j.egypro.2017.03.1168

Ridi F, Fratini E, Alfani R, Baglioni P (2013) Influence of acrylic superplasticizer and cellulose-ether on the kinetics of tricalcium silicate hydration reaction. J Colloid Interface Sci 395:68–74. doi: 10.1016/j.jcis.2012.12.048

Ridi F, Fratini E, Baglioni P (2011) Cement: A two thousand year old nano-colloid. J Colloid Interface Sci 357:255–264. doi: 10.1016/j.jcis.2011.02.026

Rodriguez-Navarro C, Burgos Cara A, Elert K, et al (2016a) Direct Nanoscale

Imaging Reveals the Growth of Calcite Crystals via Amorphous Nanoparticles. Cryst Growth Des 16:1850–1860. doi: 10.1021/acs.cgd.5b01180

Rodriguez-Navarro C, Elert K, Ševčík R (2016b) Amorphous and crystalline calcium carbonate phases during carbonation of nanolimes: implications in heritage conservation. CrystEngComm 18:6594–6607. doi: 10.1039/C6CE01202G

Rodriguez-Navarro C, Kudłacz K, Cizer Ö, Ruiz-Agudo E (2015) Formation of amorphous calcium carbonate and its transformation into mesostructured calcite. CrystEngComm 17:58–72. doi: 10.1039/c4ce01562b

Rodriguez-Navarro C, Ruiz-Agudo E (2018) Nanolimes: From synthesis to application. Pure Appl Chem 90:523–550. doi: 10.1515/pac-2017-0506

Rodriguez-Navarro C, Ruiz-agudo E, Burgos-cara A, et al (2017) Crystallization and Colloidal Stabilization of Ca(OH)2 in the Presence of Nopal Juice (Opuntia ficus indica): Implications in Architectural Heritage Conservation. Langmuir 33:10936–10950. doi: 10.1021/acs.langmuir.7b02423

Rodriguez-Navarro C, Suzuki A, Ruiz-Agudo E (2013) Alcohol dispersions of calcium hydroxide nanoparticles for stone conservation. Langmuir 29:11457–11470. doi: 10.1021/la4017728

Rodriguez-Navarro C, Vettori I, Ruiz-Agudo E (2016c) Kinetics and Mechanism of Calcium Hydroxide Conversion into Calcium Alkoxides: Implications in Heritage Conservation Using Nanolimes. Langmuir 32:5183–5194. doi: 10.1021/acs.langmuir.6b01065

Ruiz-Agudo E, Rodriguez-Navarro C (2010) Microstructure and rheology of lime putty. Langmuir 26:3868–3877. doi: 10.1021/la903430z

Sakka S, Petrykin V, Kakihana M (2005) Handbook of sol-gel science and technology. Volume 3. Applications of sol-gel technology. In: Inorganic–Organic Polymers with Barrier Properties Against Water Vapor, Oxygen

and Migrating Monomers

Salvadori B, Dei L (2001) Synthesis of Ca(OH)2 nanoparticles from diols. Langmuir 17:2371–2374. doi: 10.1021/la0015967

Samanta A, Chanda DK, Das PS, et al (2016) Synthesis of Nano Calcium Hydroxide in Aqueous Medium. J Am Ceram Soc 99:787–795. doi: 10.1111/jace.14023

Sand KK, Rodriguez-Blanco JD, Makovicky E, et al (2012) Crystallization of CaCO3 in water-Alcohol mixtures: Spherulitic growth, polymorph stabilization, and morphology change. Cryst Growth Des 12:842–853. doi: 10.1021/cg2012342

Scott TA (1946) Refractive index of ethanol-water mixtures and density and refractive index of ethanol-water-ethyl ether mixtures. J Phys Chem 50:406–412. doi: 10.1021/j150449a003

Seo KS, Han C, Wee JH, et al (2005) Synthesis of calcium carbonate in a pure ethanol and aqueous ethanol solution as the solvent. J Cryst Growth 276:680–687. doi: 10.1016/j.jcrysgro.2004.11.416

Sequeira S, Casanova C, Cabrita EJ (2006) Deacidification of paper using dispersions of Ca(OH)2 nanoparticles in isopropanol. Study of efficiency. J Cult Herit 7:264–272. doi: 10.1016/j.culher.2006.04.004

Shih S-M, Ho C-S, Song Y-S, Lin J-P (1999) Kinetics of the Reaction of Ca(OH)2 with CO2 at Low Temperature. Ind Eng Chem Res 38:1316–1322. doi: 10.1021/ie980508z

Sleater GA (1973) A Review of Natural Stone Preservation

Stefanis E, Panayiotou C (2007) Protection of lignocellulosic and cellulosic paper by deacidification with dispersions of micro- and nano-particles of Ca(OH)2 and Mg(OH)2 in alcohols. Restaurator 28:185–200. doi: 10.1515/REST.2007.185

Sudarsan Reddy, K., Prabhakar, M.N., Madhusudana Rao, K., Suhasini DM,

Naga Maheswara Reddy V, Kumara Babu P, et al (2013) Development and Characterization of Hydroxy Propyl Cellulose/Poly(vinyl alcohol) Blends and Their Physico-Chemical Studies. Indian J Adv Chem Sci 2 1:38–45

Sun P, Grace JR, Lim CJ, Anthony EJ (2008) Determination of intrinsic rate constants of the CaO-CO2reaction. Chem Eng Sci 63:47–56. doi: 10.1016/j.ces.2007.08.055

Tajuelo Rodriguez E, Richardson IG, Black L, et al (2015) Composition, silicate anion structure and morphology of calcium silicate hydrates (C-S-H) synthesised by silica-lime reaction and by controlled hydration of tricalcium silicate (C 3 S). Adv Appl Ceram 114:362–371. doi: 10.1179/1743676115Y.0000000038

Taylor H (1997) Cement Chemistry, Thomas Telford. 2nd ed. London: Thomas Telford Publishing

Technical Leaflet CaLoSiL® Colloidal nano-particles of lime for stone and plaster consolidation, IBZ-Salzchemie GmbH & Co.KG (Germany) https://ibz-freiberg.de/produkte

Thomas JJ (2007) A new approach to modeling the nucleation and growth kinetics of tricalcium silicate hydration. J Am Ceram Soc 90:3282–3288. doi: 10.1111/j.1551-2916.2007.01858.x

Vagenas N (2003) Quantitative analysis of synthetic calcium carbonate polymorphs using FT-IR spectroscopy. Talanta 59:831–836. doi: 10.1016/S0039-9140(02)00638-0

Vance K, Falzone G, Pignatelli I, et al (2015) Direct Carbonation of Ca(OH)<inf>2</inf> Using Liquid and Supercritical CO<inf>2</inf>: Implications for Carbon-Neutral Cementation. Ind Eng Chem Res 54:8908−8918. doi: 10.1021/acs.iecr.5b02356

Vazquez-negrete J, Lima E, Martı F, et al (2008) Texture of nopal treated adobe: restoring Nuestra Senora del Pilar mission. J Archaeol Sci 35:1125–1133.

doi: 10.1016/j.jas.2007.10.019

Wang S, Peng X, Tang L, et al (2014) Influence of inorganic admixtures on the 11 Å-tobermorite formation prepared from steel slags: XRD and FTIR analysis. Constr Build Mater 60:42–47. doi: 10.1016/j.conbuildmat.2014.03.002

Warren J (1999) Conservation of earth structures. Series in Conservation and Museology

Wheeler G (2005) Alkoxysilanes and the Consolidation of Stone. Research in Conservation. Los Angeles: Getty Conservation Institute.

Wihr R, Steenken G (1970) On the Preservation of Monuments and Works of Art with Silicates. In: London: International Institute for Conservation of Historic and Artistic Works (ed) New York Conference on Conservation of Stone and Wooden Objects. pp 71–75

Xu J, Chen QH, Qian QR (2004) Application of hydrosoluble polymers to preparation of nanoscale calcium hydroxide. Chem Res Chinese Univ 20:229–231

Yagi H, Iwazawa A, Sonobe R, et al (1984) Crystallization of calcium carbonate accompanying chemical absorption. Ind Eng Chem Fundamen 23:153–158

Yang T, Keller B, Magyari E, et al (2003) Direct observation of the carbonation process on the surface of calcium hydroxide crystals in hardened cement paste using an atomic force microscope. J Mater Sci 38:1909–1916. doi: 10.1023/A:1023544228319

Young SK (2006) Sol-Gel Science for Ceramic Materials. Mater Matters 1:8

Yura K, Fredrikson KC, Matijević E (1990) Preparation and properties of uniform colloidal indium compounds of different morphologies. Colloids and Surfaces 50:281–293. doi: 10.1016/0166-6622(90)80270-E

Zhang L, Yue LH, Wang F, Wang Q (2008) Divisive effect of alcohol-water mixed solvents on growth morphology of calcium carbonate crystals. J Phys

Chem B 112:10668–10674. doi: 10.1021/jp8034659

Ziegenbalg G (2005) Patent DE:10327514 B3

Ziegenbalg G (2008) Colloidal calcium hydroxide - a new material for consolidation and conservation of carbonatic stones. In: Proceedings of the 11th International Congress on Deterioration and Conservation of Stone, 15-20 September 2008, Torun, Poland

Zornoza-Indart A, Lopez-Arce P (2016) Silica nanoparticles (SiO2): Influence of relative humidity in stone consolidation. J Cult Herit 18:258–270. doi: 10.1016/j.culher.2015.06.002

(2008) Terra 2008: The 10th International Conference on the Study and Conservation of Earthen Architectural Heritage. The Getty Conservation Institute, Los Angeles, CA, Bamako, Mali

(2000) Terra 2000 Postprints: 8th International Conference on the Study and Conservation of Earthen Architecture. Torquay, Devon, UK

List of figures

List of tables

List of publications

- Chelazzi D, Camerini R, Giorgi R, Baglioni P, "*Nanomaterials for the consolidation of stone artifacts*", In Majid Hosseini and Ioannis Karapanagiotis (Eds): "*Advanced Materials for the Conservation of Stone*", Volume 1, Springer International Publishing

- Baglioni P, Camerini R, Chelazzi D, Giorgi R, *Nanotechnology applied to the conservation of cultural heritage: the consolidation and cleaning of mural paintings, stone and wood* - Proceedings of the IV International Workshop on Research, Conservation and Enhancement of Architectural Monuments: Preservation of Built Heritage, Book Editors: R. Shady, P. Novoa, C. Leyva, R. Peralta, Publisher: Zona Arqueológica Caral, Unidad Ejecutora 003, Ministerio de Cultura del Perú

- Camerini R, Chelazzi D, Giorgi R, Baglioni P, *Hybrid nano-composites for the consolidation of earthen masonry*, 2019 (539), 504-515

Acknowledgements

I would like to first thank my tutor, Prof. Rodorico Giorgi, who guided and supported me throught the past three years, which have been intense and rich in learnings.

I would also like to thank Prof. Piero Baglioni, Director of the CSGI, for his teachings and suggestions. The Director of the CSGI and the Head of the Chemistry Department of the University of Florence, where the present research project was performed, are acknowledged.

I wish to especially thank Giovanna Poggi and David Chelazzi, for their cooperation and inspiration, but also support, and friendship.

I wish to thank Dr. Yareli Jaidar (CNCPC-INAH and UNAM, Mexico City) for providing the adobe samples and the help in the matter of earthen materials, Dr. Francesca Ridi (CSGI, University of Florence) for helping me with the interpretation and fitting of the carbonation kinetics data, Dr. Costanza Montis (CSGI, University of Florence) for TEM experiments at Ce.M.E. (CNR, Florence), Dr. Laura Chelazzi and Dr. Samuele Ciattini (CRIST, University of Florence) for assistance on XRD experiments. Thanks to Prof. Giovanni Gigli, Dr. Pietro Vannocci, Dr. Massimiliano Nocentini, Dr. Guia Cecchini and Dr. Teresa Salvatici (Department of Earth Sciences, University of Florence) for preparation and tests on the adobe soil and samples, and Dr. Silvia Rescic (CNR, Florence) for drilling measurements at ICVBC.

I wish to thank all my friends and collegues, for making these years special.
Thanks to my family, and to my husband, for their love.

Publication: Hybrid nano-composites for the consolidation of earthen masonry

Journal of Colloid and Interface Science 539 (2019) 504–515

Contents lists available at ScienceDirect

Journal of Colloid and Interface Science

journal homepage: www.elsevier.com/locate/jcis

Regular Article

Hybrid nano-composites for the consolidation of earthen masonry

Rachel Camerini, David Chelazzi, Rodorico Giorgi *, Piero Baglioni *

CSGI and Department of Chemistry, University of Florence, via della Lastruccia 3-50019, Sesto Fiorentino, Italy

GRAPHICAL ABSTRACT

ARTICLE INFO

Article history:
Received 13 November 2018
Revised 20 December 2018
Accepted 21 December 2018
Available online 22 December 2018

Keywords:
Nano-composites
Calcium silicate hydrate
Silica
Calcium hydroxide
Hydroxypropyl cellulose
Earthen masonry
Adobe
Consolidation
Heritage preservation

ABSTRACT

Hypothesis: Earth is one of the oldest silicate-based materials in stone heritage, still largely used in architecture worldwide. Earthen materials are highly susceptible to wind and water erosion, leading to loss of cohesion and crumbling. Conventional consolidants (alkoxysilanes, synthetic or natural polymers) lack physico-chemical compatibility or effectiveness, and can promote degradation. We propose for the first time nano-composites for the surface consolidation of adobe, i.e. unbaked earth bricks often containing organic fibers and lime.

Experiments: We investigated, mimicking the setting of portland cement, the formation of calcium silicate hydrate (CSH) within adobe porosities, owing to the pozzolanic reaction between nanoparticles of silica and calcium hydroxide, to consolidate a powdery substrate. Different formulations were characterized by Fourier Transform Infrared spectroscopy (FTIR), X-ray diffraction (XRD), scanning and transmission electron microscopy (SEM, TEM), dynamic light scattering (DLS), and turbidimetry (UV–Vis spectroscopy).

Findings: A ternary composite made of SiO_2 nanoparticles, $Ca(OH)_2$ nanoparticles, and hydroxypropyl cellulose, dispersed in a (4:1) ethanol:water blend, was formulated. Each component is compatible with adobe, and plays a role in its consolidation. The treatment of adobe samples with the composite leads to the *in situ* formation of CSH, providing resistance to peeling, abrasion, and wet-dry cycles, with no aesthetic alteration. This opens new perpectives in the preservation of one of the most widely used construction materials.

* Corresponding authors.
E-mail addresses: camerini@csgi.unifi.it (R. Camerini), chelazzi@csgi.unifi.it (D. Chelazzi), giorgi@csgi.unifi.it (R. Giorgi), baglioni@csgi.unifi.it (P. Baglioni).

https://doi.org/10.1016/j.jcis.2018.12.082
0021-9797/

Publication: Hybrid nano-composites for the consolidation of earthen masonry

1. Introduction

Siliceous stones represent a wide and important material class in artistic and architectural heritage. These materials share a silicate-based matrix, but have extremely diversified compositions and structures, including both natural lithoids (from granite to sandstone) and artificial materials like ceramic products and cement. Among silicate-based substrates, earthen masonry (i.e. building materials obtained with an unfired mixture of soil and water) has been used since antiquity owing to its cheapness and availability, simple manufacturing process, good thermal and acoustic properties, and ecofriendliness. Nowadays, earthen masonry is diffusing in many industrialized countries (sustainable architecture). Currently, over half of the world's population lives in unbaked earth houses, as estimated by the United States Department of Energy [1]. The earthen architectural heritage includes immovable patrimony ranging from archaeological sites to modern buildings. The typical outdoor location of these artifacts requires continuous conservation interventions specifically addressed to the type of substrate and degradation.

Among earthen materials, adobe is of great archaeological and architectural interest [2,3]. Adobe bricks are handmade, obtained by mixing earth and water, and then sun drying the mixture. Recipes and mineralogical composition of soils are various, according to local traditions and materials availability. In order to avoid cracking during drying and optimize the bricks' strength, the mixture can be adjusted by re-proportioning the soil fractions, or by adding stabilizers, especially natural organic fibers (straw, dry grass) [4–6] or artificial products, often including lime in small percentages [7,8]. Adobe is particularly susceptible to wind and water erosion, and degrades easily. The prolonged circulation of water in the adobe pores induces washouts, freeze-thaw cycles, and swelling-shrinkage cycles of the clay fraction, leading to progressive reduction of the grains' cohesion, loss of mechanical properties, and eventually crumbling (Fig. 1). The availability of effective consolidants able to restore the cohesion of adobe artifacts, would help the preservation of an immense patrimony. However, conventional consolidants and adhesives, commonly used in restoration, exhibit several limitations and drawbacks [9]. Natural organic polymers have limited durability and effectiveness: plant mucilage (primarily cactus) is largely used in Mesoamerican regions, but it ages rapidly, requiring frequent treatments [1]; synthetic polymers are often physico-chemically and esthetically incompatible [10,11], and can undergo degradation and discoloration [12–14]. In most cases, polymers have to be removed with sophisticated methodologies [15–17], in order to protect the works of art from enhanced degradation. Alkoxysilanes solutions, commonly used on silicate stone, are known to form brittle xerogels susceptible to cracking, due to the high capillary pressures developed in the microporous network during drying [18,19]. Currently, valid alternatives to traditional consolidants for earthen materials, and in particular adobe, are still lacking.

Advancements in colloids and materials science have provided candidate materials to fill this gap. For instance, sols have been obtained using silica oligomers and surfactants, and applied to stone consolidation [20], and aqueous solutions of colloidal silica nanoparticles have been investigated as consolidants, inquiring the effect of relative humidity on the treatment of siliceous-carbonate stone [21]. Nanoparticles of $Ca(OH)_2$ have been successfully used for the consolidation of wall paintings, plaster and stone (not only carbonate); these nanoparticles can be stably dispersed in short chain alcohols up to high concentrations, and several approaches have been proposed in the last decades concerning their synthesis and application [22–25].

In the present contribution, we aimed to obtain consolidation of adobe by exploiting the *in situ* formation of calcium silicate hydrate (CSH), responsible for the hardening of cement, one of the most largely used construction materials [26]. The interaction of silica with calcium hydroxide, yielding CSH phases, has been widely studied in the past [27–31], and the alkaline activation of bulk silica with aqueous solutions of hydroxides was considered for the restoration of adobe [10]. However the effectiveness of the process was poor due to the micrometer size of the particles, i.e. the low surface area available for the CSH formation that could be enhanced when both silica and calcium hydroxide are in the form of nanoparticles. The possibility of preparing dispersions of nanoparticles in different solvents (besides water, short chain alcohols and water-alcohol blends) opens new perspectives for earthen materials consolidation. These systems are less prone than conventional water-based particles dispersions to sedimentation, aggregation, and detrimental effects caused by excessive wetting of earthen materials with water (freeze-thaw cycles, transport of soluble salts, growth of microorganisms [32]). Recently, Rodriguez-Navarro et al. observed the consolidation of sandstone after the application of nanolime dispersions, hypothesizing that the reaction between the dispersions and silica grains in the stone might lead to the formation of a gel similar to CSH phases [23]. Daniele et al. investigated the interaction of silica fume with $Ca(OH)_2$ aqueous suspensions stabilized by a non-ionic surfactant (Triton X-100) [33], reporting on the formation of CSH phases. However, the use of purely aqueous systems involves the aforementioned drawbacks in practical applications on stone, besides the use of surfactants as stabilizers is discouraged, as the long-term behavior of these additives on the stone substrate has not yet been investigated.

The aim of the present paper is to develop CSH *in situ* for the consolidation of adobe, starting from silica and $Ca(OH)_2$, two major

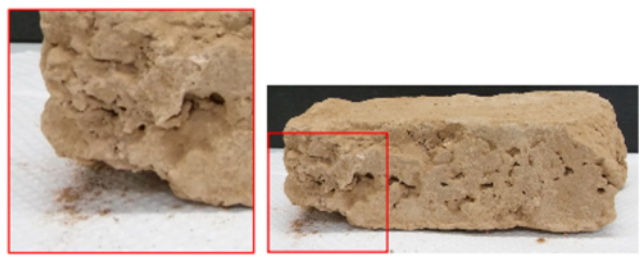

Fig. 1. An adobe brick from the Morelos state (Mexico) showing poor mechanical properties: crumbling and loss of grains occur just by touching.

components of the cement chemistry. The two components are in the form of nanoparticles to burst their reactivity. The formation of CSH is further enhanced by the addition of *Klucel*, hydroxypropyl cellulose, in the formulation. In fact, cellulose ethers (CEs) constitute an important class of organic polymers used in cement formulations. They are used in the cement industry as anti-washout or water-proofing admixtures, for the production of adhesive mortars, as viscosity-modifiers, and to control the workability of cement (i.e. the drying time). In this paper *Klucel* performs three main actions: (i) acts as a viscosity-modifier; (ii) cellulose based materials are typically used in adobe preparation to provide flexural strength and reduce hygrometric shrinkage during drying, and are commonly used in restoration practices as adhesives, densifiers, and additives for earthen grouts [4,34,35]; (iii) cellulose additives act as regulators of water release during the whole hydration reaction, increasing the hydration efficiency, and promoting the formation of CSH [26,36]. The three components were dispersed in a (4:1) ethanol:water blend. Ethanol was selected as it is an optimal solvent in terms of volatility, surface tension, and boiling point, for the application of nanoparticles to mortars and stone [37]. The amount of water was reduced, maintaining a water content suitable for the setting of CSH phases.

The composite system was characterized through Fourier Transform Infrared spectroscopy (FTIR), X-ray diffraction (XRD), scanning and transmission electron microscopy (SEM, TEM), dynamic light scattering (DLS), and turbidimetry (UV–Vis spectroscopy). The composite was then applied to adobe mock-ups, assessing the penetration depth of the formulation, the change in the color, mechanical properties and water sorption of the treated samples.

2. Materials and methods

2.1. Materials

Nanosilica dispersions were prepared diluting in water (down to 10 g/L) the commercial product Levasil CS40-213 (Akzo Nobel Chemicals), i.e. monodisperse spheres of amorphous SiO_2 (original concentration of 40 wt% in water, 0.2 wt% of Na_2O as stabilizer), particle size of 25 nm, specific surface area of 130 m^2/g, pH 9, hereinafter reported as *SiO_2*. The pH of the diluted nanosilica dispersion is 7. An ethanol dispersion of $Ca(OH)_2$ nanoparticles (hereinafter *lime*) was produced via solvothermal reaction as reported in the literature [38]. The synthesis yields hexagonal platelets of portlandite of ca. 200 nm, at a concentration of 35 g/L, which was diluted to 5 g/L. An ethanol solution of a commercial hydroxypropyl cellulose (hereinafter *HPC*) (*Klucel*®-G, 300 mPas, Phase Restauro) was prepared at a concentration of 20 g/L. Ethanol (ACS grade) was purchased by Fluka. Water was purified by a Millipore Milli-Q UV system (resistivity >18 MΩ cm).

2.2. Preparation of the ternary formulation

The ethanol dispersion of $Ca(OH)_2$ nanoparticles was added to a mixed ethanol solution of hydroxypropyl cellulose-silica aqueous dispersion. The mixed system (*SiO_2_HPC_lime*) was kept under stirring for 6 h. Different formulations were tested; the one selected for application and assessment on adobe mock ups is a hydro-alcoholic dispersion (ethanol:water = 4:1% v/v) with concentrations of 2.5, 2.5 and 5 g/L for *SiO_2*, *lime* and *HPC* respectively (*SiO_2* : *lime* : *HPC* = 1:1:2% w/w). These concentration values were selected to maximize the consolidation effect while maintaining the stability of the composite system (i.e. avoid sedimentation). The liquid medium of the ternary formulation is alkaline (the pH-meter gave values higher than 12).

2.3. Characterization of the components and the formulation

The possible formation of new phases in the ternary composite was investigated via morphological and compositional analyses, namely Attenuated Total Reflectance Fourier Transform Infrared Spectroscopy (ATR-FTIR), X-ray diffraction (XRD) and Scanning Electron Microscopy (SEM). ATR-FTIR was performed using a Thermo Nicolet Nexus 870 spectrometer equipped with a liquid nitrogen-cooled Mercury Cadmium Telluride detector, a single reflection diamond crystal ATR unit, and a Golden Gate diamond cell. The spectra were acquired in the 4000–650 cm^{-1} range with a spectral resolution of 4 cm^{-1}.

XRD was carried out using a D8 Bruker "Da Vinci" diffractometer equipped with a primary Ge monochromator using for Cu Kα1 radiation (λ = 1.54 Å) and a Sol-X solid state detector in Debye-Scherrer geometry (2θ range of 5–60°, step size of 0.02°, time/step of 0.3 s, voltage of 40 kV and current of 40 mA). For FTIR and XRD, the samples were air-dried and grinded prior to measurement.

For SEM investigations, the dispersions were deposited on the stab and let dry prior to measurement with a field emission gun scanning electron microscope (FEG-SEM), ΣIGMA (Carl Zeiss, Germany) with acceleration potential of 25 kV and a working distance of 8.6 mm.

In order to further investigate the mutual interaction of the components, the single dispersions/solutions (*SiO_2*, *lime*), their binary combinations (*SiO_2_lime*, *SiO_2_HPC* and *HPC_lime*) and the ternary system (*SiO_2_HPC_lime*) were characterized by dynamic light scattering (DLS). Measurements on the single components were also carried out at the same concentrations of the ternary composite system (e.g. *SiO_2* was diluted down to a concentration of 2.5 g/L in a 4:1 ethanol/water ratio); these samples are indicated as *SiO_{2T}*, and *$lime_T$*. The particle size distribution and ζ-potential were determined using a 90Plus Particle Size Analyzer (Brookhaven Instruments), with incident 659 nm laser light radiation, and collection at 90°. The measurements were recorded at 25 °C. For the particle size measurements, the systems were diluted 1:10. The values reported are the average of three measurements consisting of 5 runs of 30 s. The refractive index of the liquid medium (ethanol: water blend 4:1) is 1.36 [39,40]; the presence of the highly diluted cellulose derivative dissolved in the blend (*Klucel*®-G, 0.5 g/L) was not considered as relevant for the measurements. For the solid content of the dispersions, the average of the indexes of the components (SiO_2, $Ca(OH)_2$) was used. The CONTIN method was used for fitting the autocorrelation functions, to obtain the particle size distributions. The data are intensity-weighted. For the ζ-potential measurements, the Smoluchowski equation was used for the fitting of the autocorrelation function. The systems were also observed using Transmission Electron Microscopy (TEM), with a STEM CM12 Philips electron microscope. The samples were cast onto a carbon-coated copper grid sample holder, followed by evaporation of the solvent at room temperature.

The pH of the *SiO_2* aqueous dispersion was measured using a glass electrode pH-meter (Crison-Basic20): the reported value is the average of three measurements.

The kinetic stability of the dispersions (*SiO_2*, *lime*, all the binary systems and the ternary system) was investigated via turbidimetric analysis, performed with a Cary Bio 100 UV–VIS spectrophotometer (Varian). The absorbance at λ = 600 nm (spectral band width = 1 nm) was recorded at 25 °C as a function of time, at regular time intervals, over a total period of 1 month, using sealed quartz cuvettes with an optical path of 1 cm. Decreases in the absorbance were ascribed to the formation of aggregates and sedimentation. The values reported are the average of five measurements.

2.4. Treatment of the adobe samples

As target material of our study, we used adobe bricks from the Morelos state (Mexico), originally prepared using local soil and straw fibers. The bricks ($5 \times 10 \times 20$ cm^3) were cut with an abrasive disc saw into smaller specimens with dimensions of $4 \times 4 \times 2$ cm^3 and average weight of 40 g.

The treatment of adobe was performed by soaking each specimen with 20 mL of ternary formulation (*SiO2_HPC_lime*). The specimens were placed in a container previously filled with the formulation, and kept there until complete absorption (ca. 1 day). Then, the specimens were stored under room conditions (T = 23 °C, RH = 50%) until characterization. For comparison, the same treatment was performed using the single components and the binary combinations *SiO2_HPC* and *HPC_lime*. The treatment with the binary *SiO2_lime* was not performed due to immediate particle flocculation, see below.

2.5. Characterization of the adobe samples

Before treatment, the grain size distribution of the adobe soil was characterized according to the Standard Test Method for particle-size analysis of soils (ASTM D422-63) and the Standard Test Method for particle-size distribution of fine-grained soils, using sedimentation analysis (ASTM D7928-16). The Atterberg Limits were also obtained (Liquid Limit – BS 1377:1975 and Plastic Limit – ASTM D 4318-93), and the Plastic Index was then calculated. The carbonates content was determined using a Dietrich-Fruhling calcimeter, and the organic content was determined by the C—N—H determination method. XRD was also carried out to investigate the mineralogical composition of the soil.

Two months after the treatment, the treated (T) and non-treated (NT) adobe specimens were characterized to assess the consolidation efficacy. Colorimetric analyses were performed using an X-Rite SP60 portable colorimeter, (D65/10°, 8 mm diameter circular measuring spot), to evaluate the possible color changes produced by the application of the formulation. The experiment was performed on four areas of three different samples. The color difference between the treated and non-treated samples was calculated using the formula $\Delta E^* = \sqrt{\Delta L^{*2} + \Delta a^{*2} + \Delta b^{*2}}$, where L*, a* and b* are the coordinates of the CIE 1976 color space. ATR-FTIR, XRD, and the phenolphthalein test [24] were used to assess the penetration and distribution of the applied product, and to verify the occurrence of consolidation reactions within the substrate. Scotch tape tests, abrasion tests, wet-dry cycles, water sorption measurements, and drilling tests were carried out on the adobe samples.

The scotch tape test (or peeling test) is a common method used in conservation practice for the evaluation of the efficacy of consolidation treatments in terms of restoration of the surface cohesion properties [41]. The test consists in pressing pieces of adhesive tapes of known weight and area on the sample surface, and peel them off after few minutes. The decohesion index, DI (mg/cm^2), is the weight of the material lost per unit area, and is inversely proportional to the grains' cohesion forces. The data reported are the average of measurements performed on four areas of the sample, for three different samples. The experiment was conducted three times on each area, in order to obtain the decohesion index following the progressive removal of surface layers. The total removed mass over the three experiments was also calculated.

The abrasion test [42,43] consists in subjecting the sample to mechanical erosion by brushing with a metal brush at a constant pressure (3 kg mass on the top center of the brush), for a given number of cycles (in this case three cycles, each consisting of 60 rounds of brushing in one minute), over the entire length of the specimen. The abrasion coefficient, A_c (cm^2/mg), expresses the ratio of the surface to the quantity of the material removed by brushing, and is proportional to the abrasive strength. The data reported are the average of tests performed on three samples; the total value after the three cycles was also calculated.

Wet-dry cycles were performed to assess the resistance to exposure to harsh environmental cycles [43,44], by immersing the samples in distilled water for 5 h and drying at 60 °C for 48 h. Seven cycles were performed, and the weight loss was expressed as the percentage of dry mass reduction from the original mass, as the average of the data obtained from two samples. The total value after the seven cycles was also calculated.

For the water sorption measurements, the samples were oven-dried at 60 °C to constant mass, weighted and put on a porous support in contact with distilled water. The water intake is measured indirectly by weighting the samples at regular time intervals. The capillary water absorption coefficient, A_w (mg/cm^2·s$^{1/2}$), of the treated and untreated samples was obtained using the 'one tangent method', i.e. calculating the gradient of the straight line obtained by plotting the cumulative mass of water absorbed per unit area against the square root of time [45,46]. The experiment was repeated twice.

The drilling tests [47] were carried out with a drilling resistance measurement system (Sint Technology, Italy), using a 5 mm diameter drill bit (maximum depth = 10 mm, penetration rate = 20 mm/min, revolution speed = 200 rpm). Each result is the average of three holes produced on two different samples.

3. Results and discussion

3.1. Characterization of the components and formulation

In order to gain information on the interaction between Ca(OH)$_2$ and silica nanoparticles, namely on the formation of CSH phases, ATR-FTIR and XRD analyses were performed on the ternary system *SiO2_HPC_lime*.

ATR-FTIR analyses were performed on the formulation as prepared, and after 6 days, 9 days, and 2 months from preparation (Fig. 2), according to the procedure above reported. All the FTIR spectra of *SiO2_HPC_lime* show a broad band centered at 3400 cm^{-1} and a small band at 1650 cm^{-1} assigned to the stretching and bending of the hydroxyl groups of HPC, residual —OH groups in silica, and adsorbed water. The characteristic peak around 3640 cm^{-1} (OH stretching) indicates the presence of calcium hydroxide. The latter is partially converted into calcium carbonate through reaction (carbonation) with atmospheric CO_2, during air-drying of the sample [23,38,48], as indicated by the presence of bands at 1400–1500 (ν_3 asymmetric CO_3 stretching), 876 (ν_2 asymmetric CO_3 bending), and 713 cm^{-1} (ν_4 symmetric CO_3 bending) [49,50], which are present in the spectra collected on the formulation as prepared, and after 6 and 9 days from preparation. Calcium hydroxide and calcium carbonate bands are absent in the spectrum collected after two months from preparation. The bands between 2970 and 2870 cm^{-1} (C—H stretching) in the four spectra can be ascribed to HPC. Bands between 1460 and 1270 cm^{-1} (C=C stretching) are also ascribable to HPC; while the band of HPC at 1075 cm^{-1} (C—O stretching) [51,52] overlaps with the absorption at 1050 cm^{-1} of silica (internal Si—O—Si asymmetric stretching) that also displays a band at 800 cm^{-1} (Si—O—Si symmetric stretching). The shoulder at 950 cm^{-1} is assigned to the Si—O stretching of surface Si—OH groups [53,54]. Interestingly, the spectra of *SiO2_HPC_lime* collected after 9 days and, more evidently, after two months from preparation, show a marked increase of the band at 950 cm^{-1} and a correspondent decrease of the band at 1050 cm^{-1}, indicating the breakage of Si—O—Si

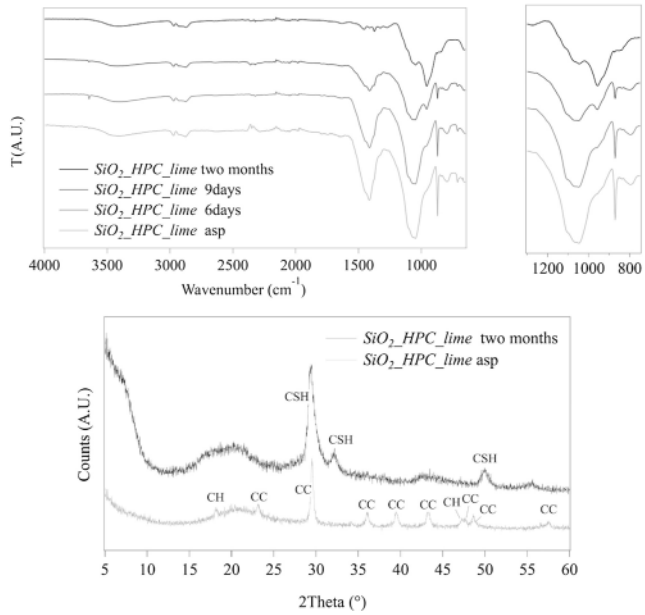

Fig. 2. (Top) ATR-FTIR spectra of air-dried ternary system *SiO2_HPC_lime* as prepared ("asp"), and 6 days, 9 days and two months after preparation; (bottom) XRD patterns of air-dried ternary system *SiO2_HPC_lime* as prepared and two months after preparation.

bonds and the formation of silanol groups. This suggests that silica depolymerization and the formation of calcium silicate hydrate (CSH) occurred [30,31,55]. In fact, it is reported that the hydration reaction between $Ca(OH)_2$ and silica in water starts with the dissolution of $Ca(OH)_2$ followed by the breaking of the Si—O—Si covalent bonds by the released OH groups; the Ca^{2+} ions then bridge the depolymerized silica, forming the basic units of CSH [56]. After two months, the absence of calcium hydroxide and carbonate bands in the spectrum indicates the complete reaction of calcium hydroxide and silica nanoparticles. Besides, after two months, the formation of a gel-like phase is macroscopically observed in the ternary formulation. A similar behavior was observed in the *SiO_2_lime* system, but not in the other binary systems or for single components in the hydro-alcoholic blend; thus, we concluded that the gel consisted of the newly formed CSH phase.

XRD analysis was carried on the ternary system as prepared, and two months after preparation. In the first case, the peaks of calcium hydroxide and calcium carbonate are observed, along with a broad band centered around 20°, ascribable to the co-presence of amorphous silica (reported at 22° in the literature [53]) and HPC (band at 17° [52]). After two months, three peaks are observed at 29.5°, 32° and 50°, indicating the formation of CSH [30,57,58]. Basal peaks at less than 10° are reported in the literature for tobermorite, but their intensity can vary depending on the type of CSH phase, up to being barely or not observable [59,60].

The SEM investigation of the ternary system after two months from preparation, showed the presence of a homogeneous porous network of crumpled foils (Fig. 3), a morphology typically produced by the formation of CSH from the alkaline activation of nanosilica [31,61]. The EDX analysis confirmed that calcium and silicon are homogeneously distributed across the foiled substrate.

To further investigate the components' behavior and their mutual interactions, the ζ-potential and particle size of the single components (*SiO_2*, *lime*, *HPC*), their binary systems, and the ternary system were then analyzed, and the results are reported in Table 1. The reported values are those of the as prepared samples. The CONTIN method was used to fit the autocorrelation functions, and the data are intensity-weighted. The mean particle size and relative variance (i.e. ratio of variance to the square of the mean, which is a measure of the polydispersity of diffusion coefficient, and is often represented as a polydispersity index) are reported. The main populations of multimodal distributions are also indicated. Transmission Electron Microscopy (TEM) was also used to observe the air-dried samples.

In the case of *SiO_2* and *lime*, the data are in agreement with the literature [38,62,63] and the information provided by producers: the silica nanoparticles (monodisperse spheres) exhibit in water a negative ζ-potential close to −30 mV, indicating a stable colloidal system due to electrostatic repulsion, and an average hydrodynamic diameter of 33 nm with a relative variance of 0.03, which is in agreement with the particles' size observed with TEM (25–35 nm, see Fig. 4). The pH of *SiO_2* system is 7, i.e. after dilution of the original product Levasil CS40-213.

The synthesized $Ca(OH)_2$ nanoparticles (hexagonal platelets) in ethanol have a positive ζ-potential of about 50 mV, consistent with the good stability of the system, and a mean particle size of 214 nm (relative variance of 0.16). This in agreement with the presence of two main populations centered at about 15 and 175 nm as also

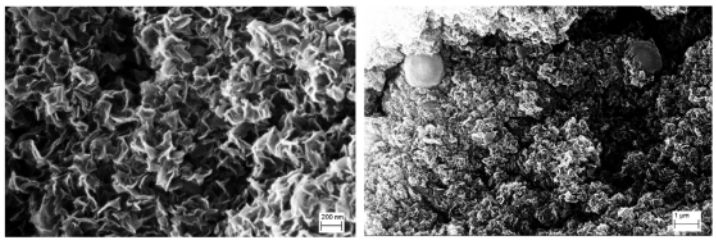

Fig. 3. SEM images of the ternary system *SiO₂_HPC_lime*, air-dried after two months from preparation (secondary electron images with magnitude of (a) 21kX and (b) 87kX).

Table 1
ζ-potential and particle size data of the different components and composite formulations, obtained by dynamic light scattering measurements.

System	Medium	ζ-potential (mV ± SD)	Particle size		
			Mean particles' size (nm)	Rel. Var.	Distribution
SiO_2	H_2O	−29 ± 7	33	0.03	Monomodal, narrow
lime	EtOH	53 ± 7	214	0.16	Multimodal, main populations at ca. 15 and 175 nm
SiO_{2T}	H_2O/EtOH (1:4)	−43 ± 12	38	0.19	Monomodal, narrow
$lime_T$	H_2O/EtOH (1:4)	41 ± 3	520	0.81	Monomodal, broad
SiO_2_lime	H_2O/EtOH (1:4)	n/a	n/a	n/a	Formation of micron-sized aggregates
SiO_2_HPC	H_2O/EtOH (1:4)	−1 ± 11	95	0.46	Multimodal, main populations at ca. 35 and 160 nm
HPC_lime	H_2O/EtOH (1:4)	−1 ± 8	945	0.25	Multimodal, main populations at ca. 130 and 960
SiO_2_HPC_lime	H_2O/EtOH (1:4)	−3 ± 9	941	0.16	Multimodal, main populations at ca. 300 and 1050

confirmed by TEM images (see Fig. 4b), with an average thickness of the platelets of 20–30 nm [63].

When the components are dispersed in the (4:1) ethanol-water solution, the ζ-potential and size of the particles change with respect to the systems in the pure media. In particular, the ζ-potential of silica nanoparticles in the blend (*SiO_{2T}*) has a slightly higher negative value, as expected from the fact that the dielectric constant of the dispersing medium (i.e. the blend) is lower than that of water [64,65]. The particles' size is comparable with that of *SiO_2*, but the higher variance (0.19) indicates the presence of some aggregates.

In the case of $Ca(OH)_2$ nanoparticles, passing from an ethanol dispersion to the blend (*$lime_T$*), the dielectric constant increases, and a lower positive ζ-potential is found. It is worth mentioning that the particles' size increases due to the water molecules bridging of the hydroxide platelets, leading to the formation of aggregates [37,66].

The system *SiO_2_lime* could not be analyzed by DLS, as the interaction of the silica and $Ca(OH)_2$ nanoparticles, whose surface charge is of opposite sign, leads to flocculation and sedimentation of the particles, which occur completely within 24 h from the preparation of the binary system. TEM observation of the system (Fig. 4c) shows the presence of spherical particles with size ranging from 20 to 100 nm corresponding to the SiO_2 component; some of the particles are surrounded by sub-spherical formations whose size ranges from 200 nm up to 1 μm. Such agglomerates (highlighted by arrows in Fig. 4c) might indeed result from the initial interaction of silica and lime nanoparticles.

The binary systems *SiO_2_HPC* and *HPC_lime* have low ζ-potentials, conceivably related to the presence of hydroxypropyl cellulose. In the literature it is reported that surface adsorption of cellulose ethers (HPC; HEC) onto charged particles resulted in the decrease of ζ-potential, close to zero [67,68], and reduced the agglomeration of the particles due to the formation of a steric barrier. *SiO_2_HPC* shows two different size populations (ca. 35 and 160 nm), with mean particles' size of ca. 95 nm and relative variance of 0.46, which can be explained by the presence of HPC adsorbed on the surface of the silica particles [69]. TEM observation of the system (Fig. 4d) shows the presence of nanospheres of about 30 nm, which stack into chains or groups of 200–400 nm, in fair agreement with DLS data. In the case of *HPC_lime*, two population sizes are observed with mean dimension of 945 nm and relative variance of 0.25.

The ternary system *SiO_2_HPC_lime* exhibits a ζ-potential close to zero, as expected for the aforementioned considerations. The system shows two main populations with size of ca. 300 and 1050 nm, with a mean size of 941 nm and a variance of 0.16. This can be explained taking into account the formation of agglomerates of silica and $Ca(OH)_2$ nanoparticles, and the adsorption of HPC on the agglomerates. TEM analysis (Fig. 4f, g) showed nearly spherical or elongated agglomerates of about 1 μm, formed by the interaction of nanoparticles (less than 100 nm) and fibrous structures.

It is important to notice that the size of the agglomerates is compatible with the average pore size of adobe. In fact, adobe bricks have pore size from micrometric scale up to a few mm, with porosity values of 20–40% [70,71].

Turbidimetric analyses were also performed to gain information on the kinetic stability of the dispersions (i.e. *SiO_2*, *lime*, *SiO_2_lime*, *SiO_2_HPC*, *HPC_lime* and *SiO_2_HPC_lime*), and the results are shown in Fig. 5. The small size of the silica nanoparticles makes both *SiO_2* and *SiO_2_HPC* appear transparent, hence no useful information could be obtained from turbidimetry on those systems. However, in both cases no agglomeration or sedimentation of the particles was observed macroscopically over months (Fig. 5).

Lime has a good turbidimetric stability over 4 weeks, and visual inspection showed that the particles dispersion does not settle even after months, confirming that nanoparticles of $Ca(OH)_2$ are stable in short chain alcohols, as already reported in the literature [38]. The presence of hydroxypropyl cellulose in the dispersion increases its stability (*HPC_lime* > *lime*). This can be explained considering that HPC increases the viscosity of the continuous phase, promoting the stability of the dispersed particles, despite the pres-

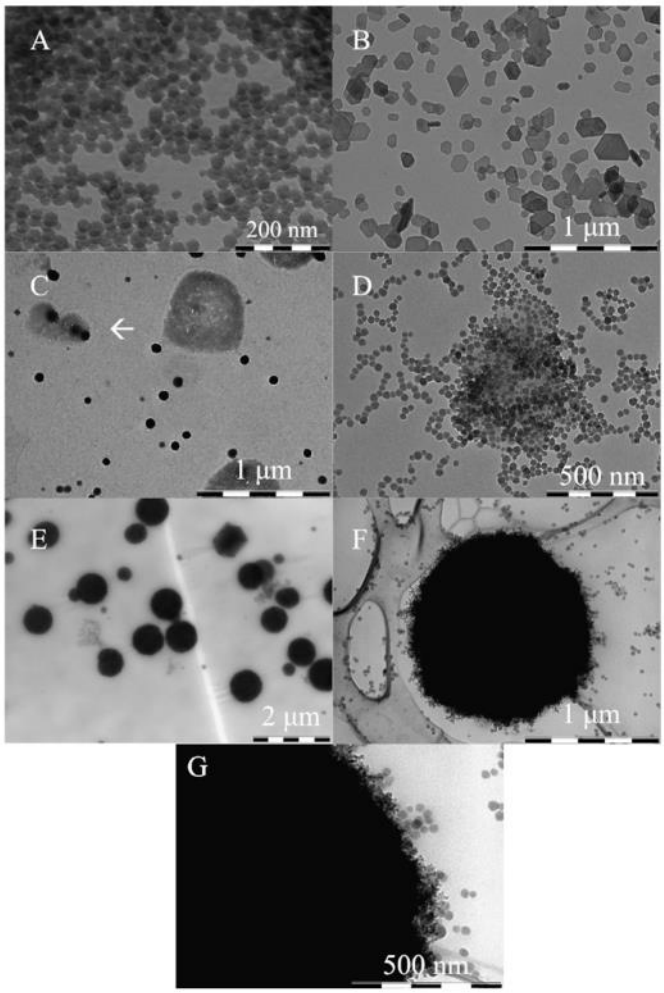

Fig. 4. TEM images of: (a) the silica nanoparticles (SiO_2), (b) the $Ca(OH)_2$ nanoparticles (*lime*), (c) the binary sistem SiO_2_*lime*, (d) the binary sistem SiO_2_*HPC*, (e) the binary sistem *HPC_lime*, and (f, g) the ternary system (SiO_2_*HPC_lime*).

ence of larger agglomerates (highlighted by DLS). As expected for the poorly stable SiO_2_*lime* system, the absorbance drops from ca. 2 to 0.2 in less than one day.

The absorbance of the ternary system (SiO_2_*HPC_lime*) does not change over 4 weeks, as expected for systems containing HPC, confirming the stabilizing role of *Klucel*®-G in the formulation, which mediates the interaction between the silica and the lime. After two months, the formation of gel-like phase (ascribed to CSH) occurred as described in the previous paragraphs.

Overall, it was possible to conclude that the formation of CSH takes place in the ternary system (starting about 1 week from the preparation).

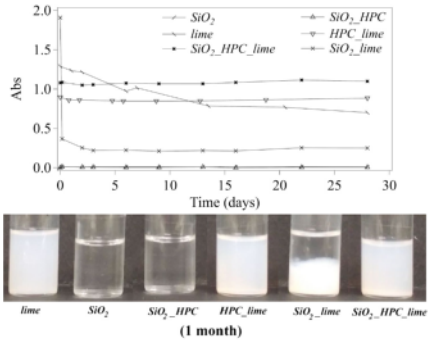

Fig. 5. (Top) turbidimetric analyses performed on *lime*, SiO_2, *SiO2_HPC*, *HPC_lime*, *SiO2_lime*, and *SiO2_HPC_lime*, over one month; (Bottom) visual inspections of the *SiO2_HPC_lime* system as prepared, and after one month from preparation.

3.2. Treatment of adobe samples

Before treatment, the soil of the adobe bricks was characterized, and the results are shown in Table 2. The soil was classified as silty sand (SM), according to the Unified Soil Classification System (USCS). The low clay percentage explains the poor mechanical properties of the samples, as expected considering that the bricks were prepared using local soil from the construction area (Morelos region, Mexico), which has a high content of sand. The XRD analysis of the soil (not shown) revealed a composition consisting predominantly of plagioclases (albite-anorthite) and, to a lesser extent, quartz and mica. Straw fibers were found included in the bricks. The organic content of the soil was found to be ca. 0.3%, and the carbonates content ca. 0.5%.

Visual observations of the samples, up to two months after the treatment, did not highlight significant color variations produced by the application of the formulation *SiO2_HPC_lime*, as compared to the non-treated samples. Colorimetry measurements were then performed, and the analyses showed an average color difference ΔE^* of 2.5 ± 0.5, which is within the threshold generally adopted for the treatment of works of art, i.e. $\Delta E^* = 3$ [72].

The phenolphtalein test was used to assess the penetration of the calcium hydroxide nanoparticles found in the ternary system, as an indication of the depth reached by the whole formulation. The penetration depth is visually measured thanks to the intense purple color assumed by phenolphthalein at alkaline pH. A 0.1% solution of phenolphtalein was sprayed onto the surface of samples right after treatment. Cross sections of the samples were then cut, and a penetration of 3 mm was observed, which is consistent with that of nanolimes used elsewhere for the consolidation of stucco and adobe [24]. The penetration depth can be affected by several factors including the type of dispersing solvent and the environmental conditions during the treatment, and both backmigration and aggregation of the particles have been discussed as possible issues limiting the penetration [73–78]. While enhancing the penetration of consolidant particles remains an open topic in stone conservation, it must be noticed that adobe bricks are mainly affected by environmental erosion of the exposed surface, leading to powdering and loss of grains cohesion; thus, the protection of the outer layers up to some mm from the surface was deemed as an acceptable result at this preliminary stage.

FTIR analyses (not shown) were carried out on the treated samples at different depths from the surface, two months after treatment. The characteristic band of calcium hydroxide at ca. 3640 cm^{-1} was not observed, suggesting that the hydroxide had completely reacted, possibly through formation of CSH and carbonation. Bands of calcium carbonate were indeed observed at 1400–1500, 876, and 713 cm^{-1}. However, owing to the intense bands of the silica originally found in the adobe samples, it was not possible to observe an intensity inversion between the band at 950 cm^{-1} (Si—O stretching of surface Si—OH groups) and that at 1050 cm^{-1} (stretching of Si—O—Si bonds), previously ascribed to the depolymerization of the nanosilica particles in *SiO2_HPC_lime* and the formation of CSH.

Instead, the XRD pattern of powders collected from the treated adobe samples up to 3 mm from the surface, showed peaks at 31.5°, 33.7° and 50.1° (Fig. 6). Interestingly, these peaks exhibit a slight shift to higher angles, and are more resolved, as compared to those observed when CSH is formed in the ternary formulation (see Fig. 2), which might suggest the formation of different calcium silicate hydrate phases, when the process takes place within the pores of the adobe samples. According to the literature, the calcium silicate hydrate minerals tobermorite ($Ca_5Si_6O_{16}(OH)_2{\cdot}4H_2O$) and jennite ($Ca_9Si_6O_{18}(OH)_6{\cdot}8H_2O$) show diffraction patterns with maxima in the 28.8–33.2° region and at 50.7°, with sharper or broader peaks depending on the degree of order of the phases and the size of the crystallites in the layer plane [58]. It must be noticed that when the formulation sets in the pores of adobe, the original silica component of adobe is present along with the SiO_2 nanoparticles, and a lower Ca/Si ratio is present than when CSH formation takes place entirely in the formulation environment, which might play a role in the formation of CSH phases with different characteristics.

The reaction between SiO_2 and $Ca(OH)_2$ nanoparticles is known to depend on several factors, including the phase composition and size of the silica nanoparticles, the $Ca(OH)_2$ content, and the liquid to powder (L/P) ratio of the system [56]. A key factor is the reactivity of the nanosilica with $Ca(OH)_2$, which is expected to be enhanced when the hydroxide particles have high surface area. In the presence of water, the SiO_2 nanoparticles come in contact with a saturated $Ca(OH)_2$ solution, which acts as an activator for the breakage of the Si—O—Si bonds, followed by the formation of the cementing phase. It has been shown that when the L/P is 1 mL/g, and for a Ca/Si ratio of 3 (using nanosilica and micron-sized lime particles), the setting of CSH takes place between 1 and 2 h from activation [56]. In our case, the ternary system was applied on the adobe samples 6 days after its preparation: the samples were soaked in the system for 1 day, and then left curing at room conditions (T = 23 °C, RH = 50%). Drying of the samples took 2 more days. The permanence time of the formulation within the pores of adobe seemed to be enough to allow the formation of some CSH phases. HPC is expected to regulate water release, promoting CSH formation; in fact, water proton nuclear magnetic

Table 2
Granulometric characterization of the soil, Atterberg limits (Liquid Limit, LL; Plastic Limit, PL; Plasticity Index, PI), organic content and carbonate content.

Granulometry				Atterberg limits			Organic content (%)	Carbonates content (%)
Clay (%) d < 0.002 mm	Silt (%) d 0.002–0.06 mm	Sand (%) d 0.06–2 mm	Gravel (%) d > 2 mm	LL (%)	PL (%)	PI (%)		
0.1	23.5	74	2.5	33	26	7	0.3	0.5

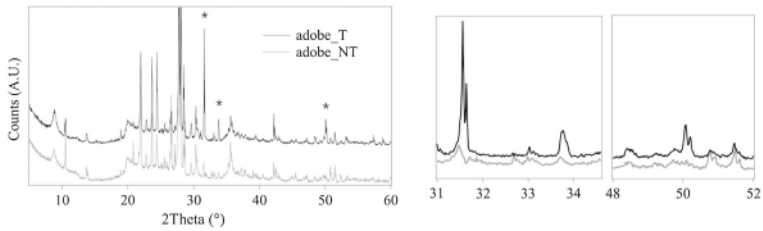

Fig. 6. XRD pattern of untreated (NT, grey line) and treated adobe (T, black line); the insets (31–34° and 48–52°) highlight the peaks at 31.5°, 33.7° and 50.1° found in the patterns of the treated adobe samples, which were assigned to CSH phases.

resonance relaxation experiments showed that cellulosic additives interact with water, determining its availability in the cement hydration process. It was found that cellulosic polymers delay the setting process while, on the other hand, they enhance the hydration efficiency. This was explained considering the hydrophilic character of the cellulose derivative, which is able to bind water, adsorb on silicate grains, and then distribute water homogeneously over the solid phase [26,36,79]. The presence of the cellulosic polymers affects both the nucleation and growth rates of the hydrated phases; namely, the nucleation rate is reduced (even though the energy threshold to form CSH nuclei remains unaltered), while the growth rate increases in the presence of the polymers (the energy threshold to start the growth of the nuclei is lowered) [36].

Applicative protocols should be developed for the treatment of adobe bricks in real case studies, carried out through spraying or brushing. Such protocols should guarantee that the amount of water necessary to trigger the formation of CSH is maintained within the stone pores after the treatment even in dry and hot environments. For instance, humid (not dripping) poultices (e.g. cellulose pulp) could be applied to the surface in order to keep humidity high enough, without loading large amounts of water in the pores [37].

The scotch tape test showed a remarkable increase of cohesion for the adobe samples treated with *SiO_2_HPC_lime*. The positive effect was observed even when the peeling was repeated on the same portion of the sample's surface, up to three times. The average values of each of the three peeling cycles are shown in Fig. 7; the total values after the three cycles are reported in Table 3.

Further proof of the consolidation effect was obtained with abrasion tests and wet/dry cycles, performed to assess the response of the treated samples to harsh environmental conditions (wind and water erosion). The values reported in Table 3 and Fig. 8 show a higher abrasion coefficient for the samples treated with *SiO_2_HPC_lime*, indicating improved resistance to abrasion. The average values of each cycle, obtained from tests on three different samples, are shown in the graph; the total values after the three cycles are reported in the table.

The average weight losses of untreated and treated samples caused by wet/dry cycles are shown in Fig. 9, and the total weight loss after the seven cycles is reported in Table 3. The results indicate that the application of the *SiO_2_HPC_lime* system resulted in a decrease of mass loss upon repeated immersions in water, indicating that consolidation took place. The capillary sorption coefficient obtained from water sorption measurements did not significantly change following the treatment of the samples

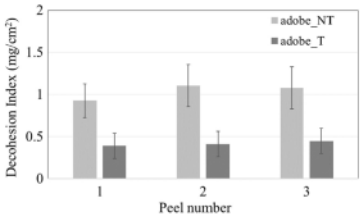

Fig. 7. Decohesion index (obtained with the scotch tape test) of adobe samples, untreated (NT), and treated with *SiO_2_HPC_lime* (T).

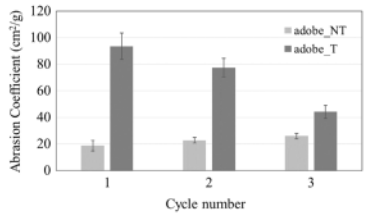

Fig. 8. Abrasion coefficient of adobe samples, untreated (NT), and treated with *SiO_2_HPC_lime* (T).

Table 3
Characterization of adobe samples, untreated (NT), and treated with *SiO_2_HPC_lime* (T).

	Total decohesion index after 3 peels (mg/cm²)	Total abrasion coefficient after 3 cycles (cm²/g)	Total weight loss after 7 wet/dry cycles (%)	Capillary sorption coefficient (mg/cm²·s^1/2)	Drilling resistance (N)
Adobe_NT	3.1 ± 0.6	67 ± 3	4.41 ± 0.12	18.4 ± 0.2	0.88 ± 0.31
Adobe_T(*SiO_2_HPC_lime*)	1.2 ± 0.2	215 ± 7	0.74 ± 0.04	18.9 ± 0.4	1.07 ± 0.28

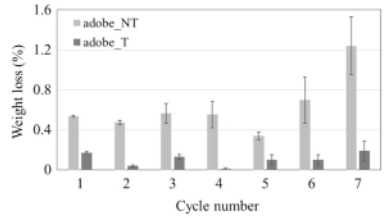

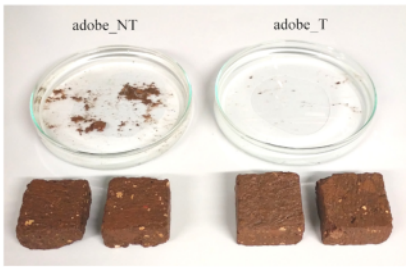

Fig. 9. (Top) Weight loss of adobe samples, untreated (NT), and treated with *SiO_2_HPC_lime* (T), during wet/dry cycles. (Bottom) The adobe samples (untreated and treated) after the seventh wet/dry cycle. The untreated samples lost a significant amount of material, as opposed to those treated with the *SiO_2_HPC_lime* formulation.

(see Table 3), indicating that the internal porosity of adobe was not altered, and the physico-chemical properties of the original material are preserved.

Lastly, drilling resistance measurements showed only a slight increase of the resistance for the treated samples (see Table 3).

It is important to notice that scotch tape tests, abrasion tests and wet/dry cycles revealed that some consolidation was obtained also applying only HPC (system HPC_T) or the two binary systems containing HPC (*HPC_lime* and *SiO_2_HPC* system) (see Table 4), while the application of only *SiO_2* or *lime* (system SiO_{2T} and $lime_T$) did not produce any significant consolidation effect. The system *SiO_2_lime* is not applicable, as the two components flocculate in short times when combined without HPC.

Namely, treatment with HPC_T, *HPC_lime* and *SiO_2_HPC* produced respectively total decohesion indexes of 1.9 ± 0.3, 1.9 ± 0.3 and 1.8 ± 0.3 mg/cm^2, and total abrasion coefficients of 152 ± 5, 137 ± 6 and 145 ± 5 cm^2/g. Besides, treatment with HPC_T produced a total weight loss after 7 wet/dry cycles of 2.02 ± 0.05%. Therefore, it was concluded that the presence of hydroxypropyl cellulose led to an increase in surface cohesion, but further resistance was obtained by the application of the ternary system, confirming the importance of combining the three components, which burst the CSH formation *in situ*.

4. Conclusions

This work reports the first evidence, to the best of our knowledge, of the use of hybrid nano-composite materials for the consolidation of adobe. Namely, a ternary system (*SiO_2_HPC_lime*) was formulated, composed of materials that have full physico-chemical compatibility with those of adobe (as opposed to scarcely compatible adhesives [10–14], used in the adobe restoration practice). Each component was shown to play a role in the consolidation process, or in the stability of the ternary formulation. The use of nano-sized particles allowed the possibility to prepare stable and concentrated dispersions in water-solvent blends, avoiding the use of surfactants as stabilizers [33]. Our starting hypothesis was that the *in situ* reaction of the hybrid's components (SiO_2 and $Ca(OH)_2$, in the presence of HPC) could lead to the formation of phases that consolidate the decohered adobe layers.

The physico-chemical characterization of the composite (by dynamic light scattering, electron microscopy, X-ray diffraction, and infrared spectroscopy) allowed to picture the interaction of the components. Namely, the interaction of highly reactive silica nanoparticles and calcium hydroxide nanoparticles led to the formation of calcium silicate hydrate (CSH), mimicking the chemistry of cement. The choice of an ethanol-water blend with ratio 4:1 allowed to obtain stable dispersions of the components in the desired amounts (ethanol prevents bridging and aggregation of the hydroxide platelets), and represented a balance between the need of avoiding aqueous media on water-sensitive substrates and the necessity of the presence of some water to trigger the alkaline activation of nanosilica and form CSH. To control and enhance the CSH reaction, nanoparticles were combined with a traditional consolidant and adhesive in conservation practice, *Klucel®-G*. In fact, cellulose derivatives are known to act as water regulators, binding water and then distributing it homogenously over the solid phase, leading to an enhancement of CSH formation. Moreover, HPC is also essential in promoting the stability of SiO_2 and $Ca(OH)_2$ nanoparticles, preventing the sedimentation of the aggregates by increasing the viscosity of the dispersion, without affecting its applicability.

Our findings on the mutual interaction of the hybrid's components were complemented by the assessment of the formulation for adobe consolidation. The ternary formulation was applied on real adobe samples, exhibiting high porosity and surface powdering caused by natural aging (wind and water erosion). XRD measurements evidenced the formation of CSH within the pores of the treated adobe samples. Representative tests of exposure to environmental erosion (i.e. resistance to peeling, abrasion, and wet-dry cycles) showed improvement of the mechanical properties of adobe treated with the *SiO_2_HPC_lime* formulation. In conclusion, consolidation was due to the formation of CSH, the main responsible for the setting process of cement, by reacting silica and lime nanoparticles in the presence of water and HPC. The ternary system was shown to grant better consolidation than the binary systems due to the presence of CSH promoted by the cellulose derivative. The composite particles penetrated homogeneously up to few millimeters from the surface, granting protection of the outer layers that are typically mostly degraded by erosion. Finally, the treatment did not induce discoloration of adobe, and left the

Table 4
Characterization of adobe samples, treated (T) with HPC_T, *HPC_lime*, and *SiO_2_HPC*. (NM = not measured).

	Total decohesion index after 3 peels (mg/cm^2)	Total abrasion coefficient after 3 cycles (cm^2/g)	Total weight loss after 7 wet/dry cycles (%)
Adobe_T(HPC_T)	1.9 ± 0.3	152 ± 5	2.02 ± 0.05
Adobe_T(*HPC_lime*)	1.9 ± 0.3	137 ± 6	NM
Adobe_T(*SiO_2_HPC*)	1.8 ± 0.3	145 ± 5	NM

water permeability unaltered, both of which are essential requirements in stone consolidation, as opposed to conventional polymeric adhesives that are known to alter stone porosity and induce discoloration and flaking [12–14].

Overall, the ternary formulation was deemed as promising for the consolidation of earthen masonry, opening new perspectives in the use of nano-composites for immovable works of art. Future work should explore the use of this formulation as an additive in the adobe preparation, so as to obtain bricks that are able to stand weathering and erosion better than traditional recipes. This would represent a novel acceptable, inexpensive, and sustainable construction material alternative to cement in underdeveloped countries, where adobe is largely used.

Acknowledgments

All the authors gratefully acknowledge Dr. Yareli Jaidar (CNCPC-INAH and UNAM, Mexico City) for providing the adobe samples, Dr. Laura Chelazzi and Dr. Samuele Ciattini (CRIST, University of Florence) for assistance on XRD experiments, Dr. Costanza Montis for TEM experiments at Ce.M.E. (CNR, Florence), Dr. Silvia Rescic (CNR, Florence) for drilling measurements at ICVBC, Prof. Giovanni Gigli, Dr. Pietro Vannocci, Dr. Massimiliano Nocentini, Dr. Guia Cecchini and Dr. Teresa Salvatici (Department of Earth Sciences, University of Florence) for the preparation of the adobe samples and providing assistance on soil and samples characterization. Michael Persson (AkzoNobel-Nouryon) is gratefully acknowledged for providing the silica particles, and for the useful discussions. CSGI and the European Union (NANORESTART project, Horizon 2020 research and innovation programme under grant agreement No 646063) are gratefully acknowledged for financial support.

References

[1] E. Avrami, H. Guillaud, M. Hardy, Terra literature review – an overview of research in earthen, Architect. Conserv. (2008).
[2] Terra 2008: The 10th International Conference on the Study and Conservation of Earthen Architectural Heritage, in: The Getty Conservation Institute, Los Angeles, CA, Bamako, Mali, 2008
[3] Terra 2000 Postprints: 8th International Conference on the Study and Conservation of Earthen Architecture, Torquay, Devon, UK, 2000.
[4] E. Quagliarini, S. Lenci, The influence of natural stabilizers and natural fibres on the mechanical properties of ancient Roman adobe bricks, J. Cult. Herit. 11 (2010) 309–314, https://doi.org/10.1016/j.culher.2009.11.012.
[5] C. Galán-Marín, C. Rivera-Gómez, J. Petric, Clay-based composite stabilized with natural polymer and fibre, Constr. Build. Mater. 24 (2010) 1462–1468, https://doi.org/10.1016/j.conbuildmat.2010.01.008.
[6] G. Calatan, A. Hegyi, C. Dico, C. Mircea, Determining the optimum addition of vegetable materials in adobe bricks, Procedia Technol. 22 (2016) 259–265, https://doi.org/10.1016/j.protcy.2016.01.077.
[7] D. Maskell, A. Heath, P. Walker, Inorganic stabilisation methods for extruded earth masonry units, Constr. Build. Mater. 71 (2014) 602–609, https://doi.org/10.1016/j.conbuildmat.2014.08.094.
[8] L. Guerrero Baca, Arquitectura en tierra. Hacia la recuperación de una cultura constructiva, Apuntes 20 (2007) 182–201.
[9] P. Baglioni, E. Carretti, D. Chelazzi, Nanomaterials in art conservation, Nat. Nanotech. 10 (2015) 287–290, https://doi.org/10.1038/nnano.2015.38.
[10] K. Elert, E.S. Pardo, C. Rodriguez-Navarro, Alkaline activation as an alternative method for the consolidation of earthen architecture, J. Cult. Herit. 16 (2015) 461–469, https://doi.org/10.1016/j.culher.2014.09.012.
[11] E. Doehne, C.A. Price, Stone Conservation: An Overview of Current Research, 2nd edition, 2011. https://doi.org//10.1016/0006-3207(70)90031-5.
[12] M. Favaro, R. Mendichi, F. Ossola, S. Simon, P. Tomasin, P.A. Vigato, Evaluation of polymers for conservation treatments of outdoor exposed stone monuments. Part II: photo-oxidative and salt-induced weathering of acrylic-silicone mixtures, Polym. Degrad. Stab. 92 (2007) 335–351, https://doi.org/10.1016/j.polymdegradstab.2006.12.008.
[13] O. Chiantore, M. Lazzari, Photo-oxidative stability of paraloid acrylic protective polymers, Polymer (Guildf). 42 (2001) 17–27, https://doi.org/10.1016/S0032-3861(00)00327-X.
[14] D. Chelazzi, A. Chevalier, G. Pizzorusso, R. Giorgi, M. Menu, P. Baglioni, Characterization and degradation of poly(vinyl acetate)-based adhesives for canvas paintings, Polym. Degrad. Stab. 107 (2014) 314–320.
[15] N. Bonelli, C. Montis, A. Mirabile, D. Berti, P. Baglioni, Restoration of paper artworks with microemulsions confined in hydrogels for safe and efficient removal of adhesive tapes, Proc. Natl. Acad. Sci. 115 (2018) 5932–5937, https://doi.org/10.1073/pnas.1801962115.
[16] M. Baglioni, C. Montis, D. Chelazzi, R. Giorgi, D. Berti, P. Baglioni, Polymer film dewetting by water/surfactant/good-solvent mixtures: a mechanistic insight and its implications for the conservation of cultural heritage, Angew. Chemie – Int. Ed. 57 (2018) 7355–7359, https://doi.org/10.1002/anie.201710930.
[17] D. Chelazzi, R. Giorgi, P. Baglioni, Microemulsions, micelles, and functional gels: how colloids and soft matter preserve works of art, Angew. Chemie – Int. Ed. 57 (2018) 7296–7303, https://doi.org/10.1002/anie.201710711.
[18] M.J. Mosquera, D.M. de los Santos, T. Rivas, P. Sanmartín, B. Silva, New nanomaterials for protecting and consolidating stone, J. Nano Res. 8 (2009) 1–12, https://doi.org/10.4028/www.scientific.net/JNanoR.8.1.
[19] M.A. Al-Dosari, S. Darwish, M.A. El-Hafez, N. Elmarzugi, N. Al-Mouallimi, S. Mansour, Effects of adding nanosilica on performance of ethylsilicat (TEOS) as consolidation and protection materials for highly porous artistic stone, J. Mater. Sci. Eng. A 6 (2016), https://doi.org/10.17265/2161-6213/2016.7-8.002.
[20] L. De Rosario, F. Elhaddad, A. Pan, R. Benavides, T. Rivas, M.J. Mosquera, Effectiveness of a novel consolidant on granite: laboratory and in situ results, Constr. Build. Mater. 76 (2015) 140–149, https://doi.org/10.1016/j.conbuildmat.2014.11.055.
[21] A. Zornoza-Indart, P. Lopez-Arce, Silica nanoparticles (SiO2): influence of relative humidity in stone consolidation, J. Cult. Herit. 18 (2016) 258–270, https://doi.org/10.1016/j.culher.2015.06.002.
[22] D. Chelazzi, G. Poggi, Y. Jaidar, N. Toccafondi, R. Giorgi, P. Baglioni, Hydroxide nanoparticles for cultural heritage: consolidation and protection of wall paintings and carbonate materials, J. Colloid Interface Sci. 392 (2013) 42–49, https://doi.org/10.1016/j.jcis.2012.09.069.
[23] C. Rodriguez-Navarro, A. Suzuki, E. Ruiz-Agudo, Alcohol dispersions of calcium hydroxide nanoparticles for stone conservation, Langmuir 29 (2013) 11457–11470, https://doi.org/10.1021/la4017728.
[24] M. Lanzón, J.A. Madrid, A. Martínez-Arredondo, S. Mónaco, Use of diluted Ca (OH)2 suspensions and their transformation into nanostructured CaCO3 coatings: a case study in strengthening heritage materials (stucco, adobe and stone), Appl. Surf. Sci. 424 (2017) 20–27, https://doi.org/10.1016/j.apsusc.2017.02.248.
[25] C. Rodriguez-Navarro, E. Ruiz-Agudo, Nanolimes: from synthesis to application, Pure Appl. Chem. 90 (2018) 523–550, https://doi.org/10.1515/pac-2017-0506.
[26] F. Ridi, E. Fratini, P. Baglioni, Cement: a two thousand year old nano-colloid, J. Colloid Interface Sci. 357 (2011) 255–264, https://doi.org/10.1016/j.jcis.2011.02.026.
[27] S.A. Greenberg, Reaction between silica and calcium hydroxide solutions. Kinetics in the temperature range 30 to 85°, J. Phys. Chem. 65 (1961) 12–16, https://doi.org/10.1021/j100819a005.
[28] D.R.G. Mitchell, I. Hinczak, R.A. Day, Interaction of silica fume with calcium hydroxide solutions and hydrated cement pastes, Cem. Concr. Res. 28 (1998) 1571–1584, https://doi.org/10.1016/S0008-8846(98)00133-1.
[29] L. Armelao, A. Bassan, R. Bertoncello, G. Biscontin, S. Daolio, A. Glisenti, Silica glass interaction with calcium hydroxide: a surface chemistry approach, J. Cult. Herit. 1 (2000) 375–384, https://doi.org/10.1016/S1296-2074(00)01093-1.
[30] K. Baltakys, R. Jauberthie, R. Siauciunas, R. Kaminskas, Influence of modification of SiO2 on the formation of calcium silicate hydrate, Mater. Sci. 25 (2007) 663–670.
[31] Q. Lin, X. Lan, Y. Li, Y. Ni, C. Lu, Y. Chen, Z. Xu, Preparation and characterization of novel alkali-activated nano silica cements for biomedical application, J. Biomed. Mater. Res. – Part B Appl. Biomater. 95 B (2010) 347–356, https://doi.org/10.1002/jbm.b.31722.
[32] P. Baglioni, D. Chelazzi, R. Giorgi, G. Poggi, Colloid and materials science for the conservation of cultural heritage: cleaning consolidation, and deacidification, Langmuir 29 (2013) 5110–5122, https://doi.org/10.1021/la304456n.
[33] V. Daniele, G. Taglieri, A. Gregori, Synthesis of Ca(OH)2 nanoparticles aqueous suspensions and interaction with silica fume, Adv. Mater. Res. 629 (2013) 482–487, https://doi.org/10.4028/www.scientific.net/AMR.629.482.
[34] M. Bouhicha, F. Aouissi, S. Kenai, Performance of composite soil reinforced with barley straw, Cem. Concr. Compos. 27 (2005) 617–621, https://doi.org/10.1016/j.cemconcomp.2004.09.013.
[35] C.-M. Chan, Effect of natural fibres inclusion in clay bricks: physico-mechanical properties, Int. J. Civ. Environ. Eng. 5 (2011) 7–13.
[36] F. Ridi, E. Fratini, R. Alfani, P. Baglioni, Influence of acrylic superplasticizer and cellulose-ether on the kinetics of tricalcium silicate hydration reaction, J. Colloid Interface Sci. 395 (2013) 68–74, https://doi.org/10.1016/j.jcis.2012.12.048.
[37] P. Baglioni, D. Chelazzi, R. Giorgi, Nanotechnologies in the Conservation of Cultural Heritage: A Compendium of Materials and Techniques, Springer, Dordrecht Heidelberg London New York, 2015. doi: 10.1007/978-94-017-9303-2.
[38] G. Poggi, N. Toccafondi, D. Chelazzi, P. Canton, R. Giorgi, P. Baglioni, Calcium hydroxide nanoparticles from solvothermal reaction for the deacidification of degraded waterlogged wood, J. Colloid Interface Sci. 473 (2016) 1–8, https://doi.org/10.1016/j.jcis.2016.03.038.
[39] J. Nowakowska, The Refractive Indices of Ethyl Alcohol and Water Mixtures, Loyola University, Chicago, 1939.
[40] T.A. Scott, Refractive index of ethanol-water mixtures and density and refractive index of ethanol-water-ethyl ether mixtures, J. Phys. Chem. 50 (1946) 406–412, https://doi.org/10.1021/j150449a003.
[41] M. Drdacky, J. Lesak, S. Rescic, Z. Slížková, P. Tiano, J. Valach, Standardization of peeling tests for assessing the cohesion and consolidation characteristics of

historic stone surfaces, Mater. Struct. (Dordrecht, Netherlands) 45 (2012) 505–520, https://doi.org/10.1617/s11527-011-9778-x.
[42] AFNOR PR XP P13-901, Compressed Earth Blocks for Walls and Partitions: Definitions, Specifications, Test Methods, Conditions of Acceptance (2001).
[43] O. Izemmouren, A. Guettala, S. Guettala, Mechanical properties and durability of lime and natural pozzolana stabilized steam-cured compressed earth block bricks, Geotech. Geol. Eng. 33 (2015) 1321–1333, https://doi.org/10.1007/s10706-015-9904-6.
[44] ASTM D559/D559M, Standard Test Methods for Wetting and Drying Compacted Soil-Cement Mixtures, ASTM Int., West Conshohocken, Pa, 2015, pp. 1–6.
[45] BS EN 1925, Natural Stone Test Methods – Determination Of Water Absorption Coefficient By Capillarity (1999) pp. 1–10.
[46] N. Karagiannis, M. Karoglou, A. Bakolas, A. Moropoulou, Building materials capillary rise coefficient: concepts, determination and parameters involved, in: D.J. (Ed.), New Approaches to Build. Pathol. Durability. Build. Pathol. Rehabil., Springer, Singapore, 2016, pp. 27–44, https://doi.org/10.1007/978-981-10-0648-7_2.
[47] M. Pamplona, M. Kocher, R. Snethlage, L.A. Barros, Drilling resistance: overview and outlook, Zeitschrift Der Dtsch. Gesellschaft Für Geowissenschaften 158 (2007) 665–679, https://doi.org/10.1127/1860-1804/2007/0158-0665.
[48] A. Samanta, D.K. Chanda, P.S. Das, J. Ghosh, A.K. Mukhopadhyay, A. Dey, Synthesis of nano calcium hydroxide in aqueous medium, J. Am. Ceram. Soc. 99 (2016) 787–795, https://doi.org/10.1111/jace.14023.
[49] S. Gunasekaran, G. Anbalagan, S. Pandi, Raman and infrared spectra of carbonates of calcite structure, J. Raman Spectrosc. 37 (2006) 892–899, https://doi.org/10.1002/jrs.1518.
[50] B. Plav, S. Kobe, B. Orel, Identification of crystallization forms of CaCO3 with FTIR spectroscopy, Kovine Zlitine Teh 33 (1999) 517–521.
[51] N. Eguchi, K. Kawabata, H. Goto, Electrochemical polymerization of 4,4-dimethyl-2,2'-bithiophene in concentrated polymer liquid crystal solution, J. Mater. Sci. Chem. Eng. 05 (2017) 64–70, https://doi.org/10.4236/msce.2017.52007.
[52] D.M. Sudarsan Reddy, K. Prabhakar, M.N. Madhusudana Rao, K. Suhasini, V. Naga Maheswara Reddy, P. Kumara Babu, K. Sudhakar, A. Chandra Babu, M.C.S. Subha, K. Chowdoji Rao, Development and characterization of hydroxy propyl cellulose/poly(vinyl alcohol) blends and their physico-chemical studies, Indian J. Adv. Chem. Sci. 2 (1) (2013) 38–45.
[53] W.A.P.J. Premaratne, W.M.G.I. Priyadarshana, S.H.P. Gunawardena, A.A.P. De Alwis, Synthesis of nanosilica from paddy husk ash and their surface functionalization, J. Sci. Univ. Kelaniya Sri Lanka 8 (2013) 33–48, https://doi.org/10.4038/josuk.v8i0.7238.
[54] D.M. Marzouqa, M.B. Zughul, M.O. Taha, H.A. Hodali, Effect of particle morphology and pore size on the release kinetics of ephedrine from mesoporous MCM-41 materials, J. Porous Mater. 19 (2012) 825–833, https://doi.org/10.1007/s10934-011-9537-y.
[55] S. Grangeon, F. Claret, C. Roosz, T. Sato, S. Gaboreau, Y. Linard, Structure of nanocrystalline calcium silicate hydrates: Insights from X-ray diffraction, synchrotron X-ray absorption and nuclear magnetic resonance, J. Appl. Crystallogr. 49 (2016) 771–783, https://doi.org/10.1107/S1600576716003885.
[56] Q. Lin, Z. Xu, X. Lan, Y. Ni, C. Lu, The reactivity of nano silica with calcium hydroxide, J. Biomed. Mater. Res. – Part B Appl. Biomater. 99 B (2011) 239–246, https://doi.org/10.1002/jbm.b.31891.
[57] S. Grangeon, F. Claret, C. Lerouge, F. Warmont, T. Sato, S. Anraku, C. Numako, Y. Linard, B. Lanson, On the nature of structural disorder in calcium silicate hydrates with a calcium/silicon ratio similar to tobermorite, Cem. Concr. Res. 52 (2013) 31–37, https://doi.org/10.1016/j.cemconres.2013.05.007.
[58] S. Grangeon, F. Claret, Y. Linard, C. Chiaberge, X-ray diffraction: a powerful tool to probe and understand the structure of nanocrystalline calcium silicate hydrates, Acta Crystallogr. Sect. B Struct. Sci. Cryst. Eng. Mater. 69 (2013) 465–473, https://doi.org/10.1107/S2052519213021155.
[59] S. Wang, X. Peng, L. Tang, L. Zeng, C. Lan, Influence of inorganic admixtures on the 11 Å-tobermorite formation prepared from steel slags: XRD and FTIR analysis, Constr. Build. Mater. 60 (2014) 42–47, https://doi.org/10.1016/j.conbuildmat.2014.03.002.
[60] X. Guo, F. Meng, H. Shi, Microstructure and characterization of hydrothermal synthesis of Al-substituted tobermorite, Constr. Build. Mater. 133 (2017) 253–260, https://doi.org/10.1016/j.conbuildmat.2016.12.059.
[61] E. Tajuelo Rodriguez, I.G. Richardson, L. Black, E. Boehm-Courjault, A. Nonat, J. Skibsted, Composition, silicate anion structure and morphology of calcium silicate hydrates (C-S-H) synthesised by silica-lime reaction and by controlled hydration of tricalcium silicate (C_3S), Adv. Appl. Ceram. 114 (2015) 362–371, https://doi.org/10.1179/1743676115Y.0000000038.
[62] C. Graf, Q. Gao, I. Schütz, C.N. Noufele, W. Ruan, U. Posselt, E. Korotianskiy, D. Nordmeyer, F. Rancan, S. Hadam, A. Vogt, J. Lademann, V. Haucke, E. Rühl, Surface functionalization of silica nanoparticles supports colloidal stability in physiological media and facilitates internalization in cells, Langmuir 28 (2012) 7598–7613, https://doi.org/10.1021/la204913t.
[63] G. Poggi, N. Toccafondi, L.N. Melita, J.C. Knowles, L. Bozec, R. Giorgi, P. Baglioni, Calcium hydroxide nanoparticles for the conservation of cultural heritage: new formulations for the deacidification of cellulose-based artifacts, Appl. Phys. A Mater. Sci. Process. 114 (2014) 685–693, https://doi.org/10.1007/s00339-013-8172-7.
[64] G. Åkerlöf, Dielectric constants of some organic solvent-water mixtures at various temperatures, J. Am. Chem. Soc. 54 (1932) 4125–4139, https://doi.org/10.1021/ja01350a001.
[65] T. Moriyoshi, T. Ishii, Y. Tamai, M. Tado, Static dielectric constants of water + ethanol and water + 2-methyl-2-propanol mixtures from 0.1 to 300 MPa at 298.15 K, J. Chem. Eng. Data. 35 (1990) 17–20, https://doi.org/10.1021/je00059a005.
[66] J. Gregory, Flocculation by polymers and polyelectrolytes, in: T.F. Tadros (Ed.), Solid/Liquid Dispersions, Academic Press, London, UK, 1987, pp. 163–180.
[67] A.V. Delgado, Interfacial electrokinetics and electrophoresis, in: Surfactant Sci. Ser., CRC Press, 2001, pp. 1–1016.
[68] F. Bouville, S. Deville, Dispersion of boron nitride powders in aqueous suspensions with cellulose, J. Am. Ceram. Soc. 97 (2014) 394–398, https://doi.org/10.1111/jace.12653.
[69] D.L. Berthier, A. Herrmann, L. Ouali, Synthesis of hydroxypropyl cellulose derivatives modified with amphiphilic diblock copolymer side-chains for the slow release of volatile molecules, Polym. Chem. 2 (2011) 2093–2101, https://doi.org/10.1039/c1py00195g.
[70] P.W. Brown, C.R. Robbins, J.R. Clifton, Adobe II: factors affecting the durability of adobe structures, Stud. Conserv. 24 (1979) 23–39, https://doi.org/10.1179/sic.1979.003.
[71] M. Hamiane, I. Djefour, H. Merabet, D. Bouallala, A. Zekagh, Y. Turki, M. Saidi, Design of adobe bricks of local raw materials for use in the monuments of earthen architecture (case of Adrar Hospital) Algeria, Civ. Eng. Archit. 4 (2016) 147–152, https://doi.org/10.13189/cea.2016.040401.
[72] R.S. Berns, D.M. Reiman, Color managing the third edition of Billmeyer and Saltzman's Principles of Color Technology, Color Res. Appl. 27 (2002) 360–373, https://doi.org/10.1002/col.10083.
[73] P. Croveri, L. Dei, R. Giorgi, B. Salvadori, Consolidation of globigerina limestone (Malta) by means of inorganic treatments: preliminary results, in: D. Kwiatkowski, R. Lofvendahl (Eds.), Proc. 10th Int. Congr. Deterior. Conserv. Stone 1, Stock, 2004, p. 463.
[74] L. Dei, B. Salvadori, Nanotechnology in cultural heritage conservation: nanometric slaked lime saves architectonic and artistic surfaces from decay, J. Cult. Herit. 7 (2006) 110–115, https://doi.org/10.1016/j.culher.2006.02.001.
[75] G. Ziegenbalg, Colloidal calcium hydroxide – a new material for consolidation and conservation of carbonatic stones, Proc. 1 1th Int. Congr. Deterior. Conserv. Stone, 15-20 Sept. 2008, Torun, Pol., 2008.
[76] P. D'Armada, E. Hirst, Nano-lime for consolidation of plaster and stone, J. Archit. Conserv. 1 (2012) 63–80, https://doi.org/10.1080/13556207.2012.10785104.
[77] A. Daehne, C. Herm, Calcium hydroxide nanosols for the consolidation of porous building materials – results from EU-STONECORE, Herit. Sci. 1 (2013) 11–20, https://doi.org/10.1186/2050-7445-1-11.
[78] I. Natali, M.L. Saladino, F. Andriulo, D. Chillura Martino, E. Caponetti, E. Carretti, L. Dei, Consolidation and protection by nanolime: recent advances for the conservation of the graffiti, Carceri dello Steri Palermo and of the 18th century lunettes, SS. Giuda e Simone Cloister, Corniola (Empoli), J. Cult. Herit. 1 (2014) 151–158, https://doi.org/10.1016/j.culher.2013.03.002.
[79] S. Del Buffa, E. Fratini, F. Ridi, A. Faraone, P. Baglioni, State of water in hydrating tricalcium silicate pastes: the effect of a cellulose ether, J. Phys. Chem. C 120 (2016) 7612–7620, https://doi.org/10.1021/acs.jpcc.6b00691.